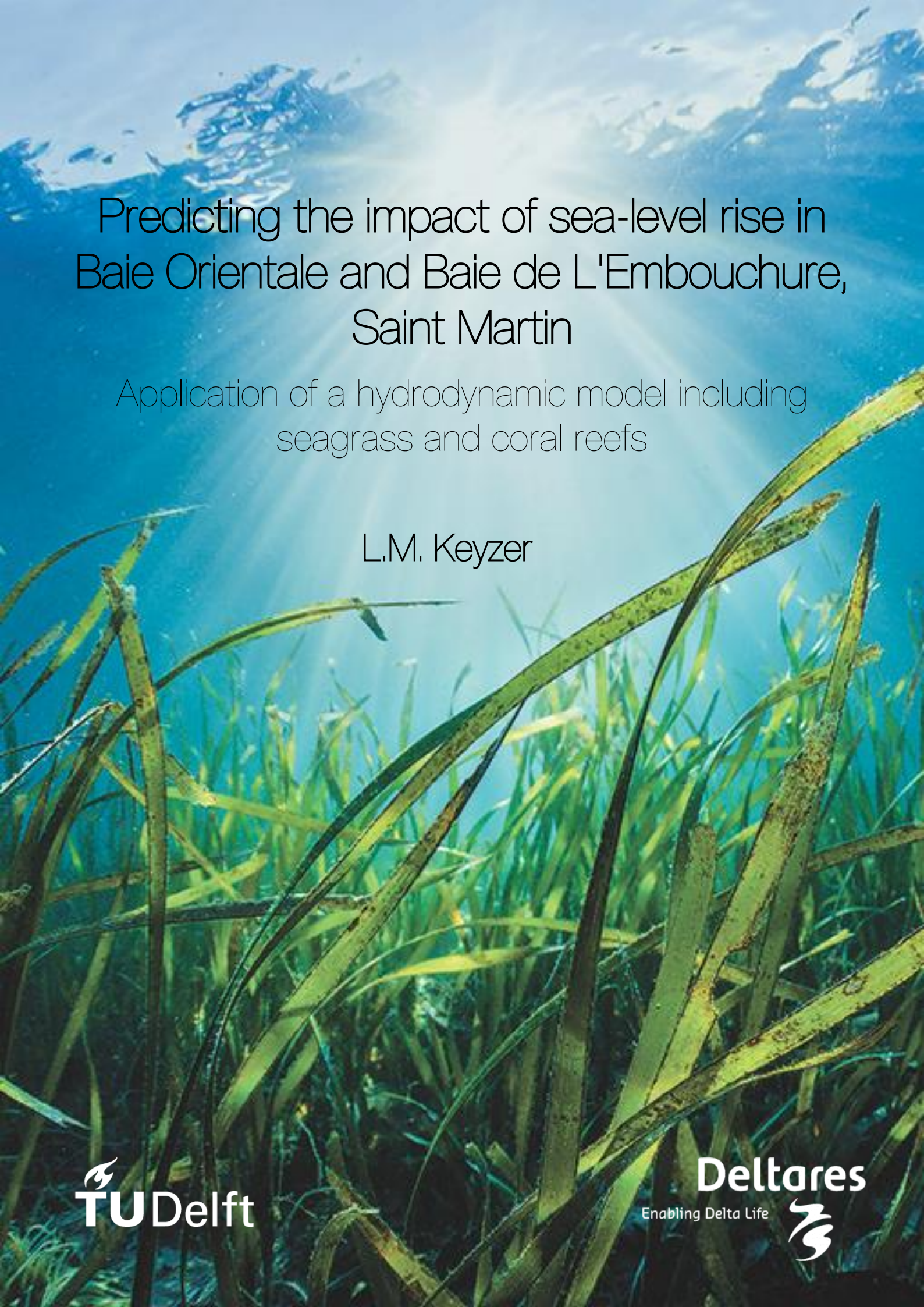

Predicting the impact of sea-level rise in Baie Orientale and Baie de L'Embouchure, Saint Martin

Application of a hydrodynamic model including seagrass and coral reefs

L.M. Keyzer

TU Delft

Deltares
Enabling Delta Life

Predicting the impact of sea-level rise in Baie Orientale and Baie de L'Embouchure, Saint Martin

Application of a hydrodynamic model including seagrass and coral reefs

by

L.M. (Lennart) Keyzer

in partial fulfillment of the requirements of the degree of

Master of Science
in Hydraulic Engineering

at Delft University of Technology,
to be defended publicly October 30, 2018 at 01:30 PM

Student number: 4228456
Project duration: 15/01/2018 - 30/10/2018

Thesis committee

Prof. dr. J.D. Pietrzak (Chair)	TU Delft
Prof. dr. P.M.J. Herman	TU Delft - Deltares
Dr. A.S. Candy	TU Delft
Dr. R.E.M. Riva	TU Delft
Ir. B.P. Smits	Deltares

Delft University of Technology
Faculty of Civil Engineering and Geosciences
Department of Hydraulic Engineering
Section of Environmental Fluid Mechanics

TU Delft Delft University of Technology

Deltares Enabling Delta Life

Preface

This thesis project is my final work in order to complete the Master of Science program *Hydraulic Engineering* at Delft University of Technology (TU Delft). It was carried out at TU Delft and Deltares. The research was part of the project *Stability of Caribbean coastal Ecosystems uNder future Extreme Sea level changes* (NWO SCENES). There are some people who I would like to thank for making this possible.

First, I would express my gratitude to my thesis committee for their feedback during the process. With their professional experience, they were always able to point me in the right direction and provide me with new ideas.

Rebecca James, PhD-student at NIOZ, is the next person I would like to thank. She shared a lot of local knowledge and data which was essential for the result of this study. Her expertise on the local ecosystems and potential threats due to climate change helped me a lot in understanding the situation and defining potential future scenarios.

During the final three months of my project, I was able to work at Deltares a few days per week. I am grateful for the opportunity to work at a very nice location and with the latest versions of Delft3D FM. Especially, I would like to thank Bob, who was always available for helping me out with model-related issues or discussing my work. And Jeffrey and Tim, two fellow students, who I would like to thank for all the motivational coffee and lunch breaks.

Finally, I would like to thank my family and friends. Not only for their support during the last couple of months, but also for making my time as a student in Delft incredible and unforgettable. Because with finishing this project, my time as a student ends.

Enjoy reading my thesis.

L.M. Keyzer
Delft, October 2018

Abstract

Shallow bays in the Caribbean, like Baie Orientale and Baie de L'Embouchure in Saint Martin, are often sheltered by coral reefs and covered by seagrass meadows. They provide valuable services as tourism and coastal protection. The ecosystems are linked through biological, chemical and physical processes. But they are under pressure due to sea-level rise. The response of one of the ecosystems to climate change could impact the other ecosystem.

In order to predict the impact of sea-level rise on the biogeomorphology in Baie Orientale and Baie de L'Embouchure, the hydrodynamic model Delft3D Flexible Mesh is applied. The effect of seagrass meadows and coral reefs on both flow and waves are captured with this model. In this way, the long term change in average hydrodynamic conditions due to sea-level rise is determined depending on the response of the ecosystems.

A wave-driven circulation is found in both bays with flows of 0.5 m/s over the reefs and currents of 0.2 m/s inside the bays. The hydrodynamic conditions are mainly determined by the reef height. Depending on the response of coral reefs to climate change and the amount of sea-level rise, the wave height inside the bays and the wave-induced currents increase. Under the worst-case scenario, where coral reefs degrade and seagrass meadows die, flow velocities increase by more than 100% in Baie de L'Embouchure and by 200% in Baie Orientale under a sea-level rise of 0.87 m. The significant wave height rises to 300% in Baie Orientale and doubles in Baie de L'Embouchure. But this increase of hydrodynamic stresses is not expected to lead to devastating damage to coral reefs and seagrass meadows. Instead, the response of coral reefs will be determined by changing water temperatures and ocean acidification. A shift in seagrass occurrence due to the changed hydrodynamics is expected.

The long term impact of sea-level rise on the biogeomorphology of Baie de L'Embouchure and Baie Orientale seems to be limited. The ability to mitigate the impact of sea-level rise is shown and the resilience of the ecosystems proved, which is very promising for other shallow Caribbean bays that are threatened by sea-level rise.

Contents

List of Figures

List of Tables

Chapter 1

Introduction

1.1 Tropical marine ecosystems in the Caribbean

Shallow bays in the Caribbean contain tropical marine ecosystems providing services as flood protection, tourism and providing habitat for various tropical species such as sea turtles. Indicating the importance of tourism, in 2015 23.9 million tourists visited the Caribbean spending 28.1 billion USD (UNWTO, 2016). The Caribbean marine ecosystems often consist of a combination of coral reefs and seagrass meadows (NWO, 2018). In the seagrass meadows calcifying algae can be found (Van Berlo, James, Van Katwijk, & Van Der Heide, 2016). These algae produce carbonate sediment (Barry, Frazer, & Jacoby, 2013), which is stabilized by the seagrass (Reynolds, Duffy, & Knowlton, 2017). Seagrass also prevents the sediment from resuspension. The coral reefs protect the bays from incoming waves leading to calm conditions where seagrasses are able to flourish. Moreover, the seagrass meadows also attenuate waves and currents further. So, coral reefs, seagrasses and calcifying algae form together an interdependent system with self-maintaining feedbacks that determine the morphology of the bays.

Saint Martin is such an island in the Caribbean Sea that is surrounded by many (shallow) bays. It is one of the Leewards Islands, which are located in the Eastern part of the Caribbean. Most people live close to the coastline and 85% of the inhabitants work in the tourism sector which is centered around the beaches (Central Intelligence Agency, 2018). There is also a small fishing industry. These facts indicate the importance of the bays to the inhabitants.

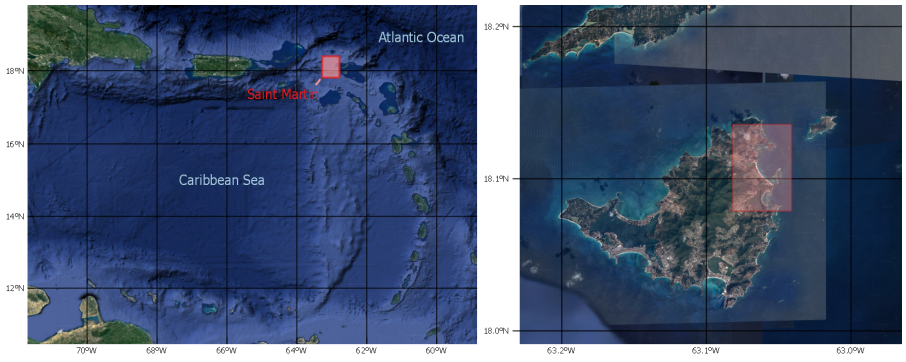

Figure 1.1: Left: Caribbean Sea with Saint Martin indicated Right: Saint Martin with area of interest highlighted (Google Maps, 2018)

Two of these bays are Baie Orientale and Baie de L'Embouchure, both located in the French part on the eastern coast. The eastern coast is exposed to trade winds and the associated swell

waves both coming from the East (Meteorological Department Curaçao, n.d.). These bays are vegetated with seagrass meadows including calcifying algae (Van Berlo et al., 2016) and coral reefs are present in front of the bays. The seagrass meadows and coral reefs are clearly visible on the satellite images in Figure 1.2.

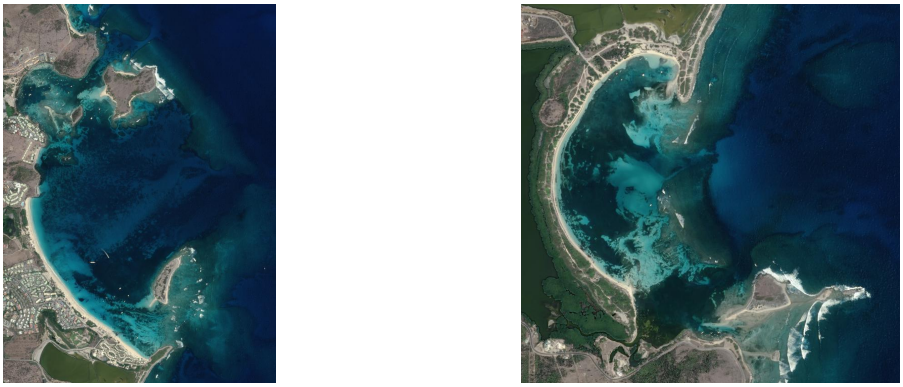

Figure 1.2: Left: Baie Orientale Right: Baie de L'Embouchure (Insitut National de L'Information Geograhique et Forestiere, 2017)

1.2 Problem statement

Tropical marine ecosystems in shallow bays and lagoons around islands in the Caribbean are threatened by changing sea-levels due to global climate change. During the period 1993-2010 a sea-level rise of 1.7 $\pm$ 1.3 mm/year has been observed in the Caribbean Sea. But there are significant spatial variabilities in local sea-level changes. The interdependent ecosystems with self-maintaining feedbacks have to keep up with relatively large sea-level changes and changing wave characteristics (NWO, 2018). The response of one of the elements in the interdependent system to climate change could lead to a negative feedback loop and affect the other ecosystems.

According to Siegle and Costa (2017) the coastal zones protected by coral reefs are the ones that will be affected mostly by sea-level rise. Due to ocean acidification and rising seawater temperatures, it is unlikely that the coral reefs are able to keep up with sea-level rise (Hoegh-Guldberg, 1999; Hoegh-Guldberg et al., 2007; Siegle & Costa, 2017) and reduced sand production by coral reefs may cause coastal erosion (Hoegh-Guldberg et al., 2007). It is thought that wave dissipation by reefs will be reduced due to the larger water depth above the reefs and reduced reef roughness due to coral degradation (Quataert, Storlazzi, van Rooijen, Cheriton, & van Dongeren, 2015). Larger wave-induced currents will occur in the bays and sediment transport will increase. This could affect the seagrass meadows. Resulting erosion and coastal retreat could be harmful to the tourist industry and inhabitants of Saint Martin. So, it is important to understand what the response of the ecosystems to climate change will be and how the hydrodynamics are affected.

The danger of drowning tropical marine ecosystems is also present near Saint Martin. Baie Orientale and Baie de L'Embouchure are two bays near Saint Martin with this typical interdependent system. For the local tourist industry and the inhabitants is it very important to know what the impact of the changing conditions on the marine ecosystems is. For example, will it still be able to function as a natural coastal flood protection?

In order to predict the effect on the coastal hydrodynamics, a hydrodynamic model is necessary. This model needs to take into account the flow and waves, their mutual interaction and the interaction with vegetation. Including biotic factors in the model is essential, because seagrasses, calcifying algae and coral reefs play a crucial role in forming and maintaining the coastal system (Van Berlo et al., 2016) and influence the hydrodynamics.

1.3 Research objective and scope

Based on the problem statement, the main goal of this research project is defined as:

Determining the impact of sea-level change due to global climate change on biogeomorphology in shallow tropical bays through the application of a hydrodynamic model.

As said before, Baie Orientale and Baie de L'Embouchure in Saint Martin will be used as the case study area.

1.3.1 Research questions

The following research questions are formulated to achieve the research objective:

What is the impact of a changing sea-level on the biogeomorphology in Baie Orientale and Baie de L'Embouchure, Saint Martin?

This research question is still very broad. Using the following subquestions, we make sure that each specific aspects of the research question will be explored and answered.

1. What is the spatial variability of flow and waves in the bays?
2. What is the dominant mechanism that forces flow in the bays?
3. What are the effects of seagrass meadows and coral reefs on the hydrodynamics in the bays?
4. What is the impact of a changing sea-level on the seagrass meadows and coral reefs?

1.3.2 Scope

At the moment of writing, there is a larger research project going on, Stability of Coastal Ecosystem uNder future Extreme Sea level changes (SCENES), which is a collaboration between Utrecht University (UU), Delft University of Technology (TUDelft), Royal Netherlands Institute for Sea Research (NIOZ) and Deltares. This research tries to determine the impact of global climate change on local bays in the Caribbean by downscaling from global climate simulations to regional ocean modelling further to biogeomorphic modelling of local bays (NWO, 2018). This thesis project is focused on the hydrodynamic modelling of local bays. Baie Orientale and Baie de L'Embouchure near Saint Martin are used as case study area. In order to prevent overlap with the SCENES project and keep this research feasible considering the amount of available time, some limitations are defined.

Depth-averaged hydrodynamic model By choosing for a depth-averaged hydrodynamic model are important processes such as alongshore currents and wave refraction and diffraction covered while the computational time of the model remains workable.

No density-driven currents Chosen is to force to model only with tide, wind and waves. Density-driven currents are not taken into account. Phenomena that can lead to density differences and induce currents, like freshwater discharges or solar radiation, are therefore excluded from this study.

Effects of global climate change are limited to sea-level rise The SCENES project looks at the local effects of global climate change. Besides rising sea-levels, changing regional currents, wind fields, water temperatures, salinity or pH are a consequence which could affect the hydrodynamics and ecosystems. In order to keep this thesis project feasible, only sea-level rise is considered.Including all effects of global climate change would make the problem more complex and increase the computational expense of the model.

Simplifying vegetation The species, cover and density of seagrasses will be measured by other members of the SCENES project. For this modelling study a seagrass meadow is simplified to one species with a constant density and height.
The growth of vegetation will not be modelled. This will be simplified by assuming that the vegetation survives or dies depending on the scenario.

Considering the long term impact on the average situation The change in hydrodynamics will be different for every circumstance. One base scenario with average wave and wind conditions is set up and used for comparison. In this way, the impact on the average conditions is considered. Single extreme events are not taken into account.

1.4 Thesis outline

After this introduction, the thesis starts with a chapter containing information about Caribbean marine ecosystems, hydrodynamics and (impact of) sea-level rise. Chapter 3 is an extensive area description presenting all relevant, mainly physical aspects of the area of interest. In the following chapter, the methodology is explained. The model description, setup and validation are given is and the setup of future scenarios is described. The current hydrodynamic situation is described in Chapter 5. This will also be the base scenario which is used as reference in order to determine the impact of future scenarios. The next chapter contains the results of future scenarios. This thesis ends with a final discussion, the conclusion and further recommendations.

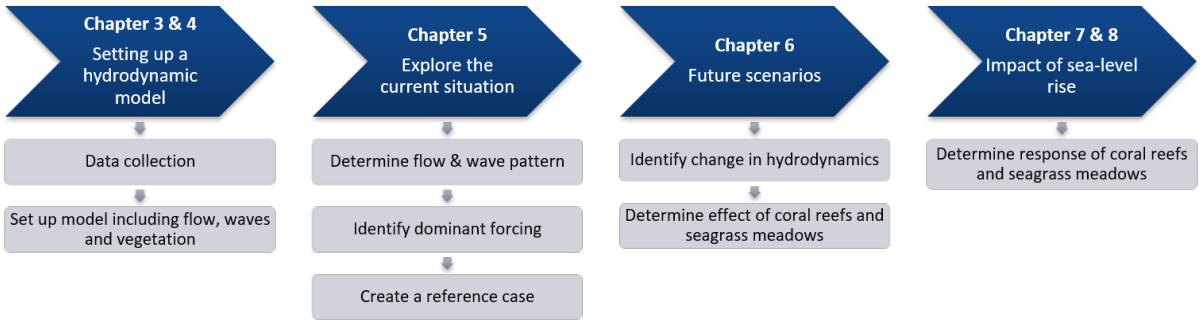

Figure 1.3: Main research objectives per chapter

Chapter 2

Literature study

In this chapter, background information on the ecosystems, the relevant hydrodynamics and their interdependency will be given. This will help understanding the model results and predict the potential impact of sea-level rise on the entire system. This chapter starts with an introduction about the Caribbean coastal ecosystems and their role in coastal protection. Section 2.2 continues with theory about relevant coastal- and reef-hydrodynamics and the interaction with the ecosystem. The final section considers the possible consequences of global climate change.

2.1 Caribbean coastal ecosystems

Baie Orientale and Baie de L'Embouchure contain two typical ecosystems which are found frequently in coastal shallow waters in the Caribbean, namely coral reefs and seagrass meadows. Together, they form a self-maintaining coastal system which is able to alter the hydrodynamics and contains multiple positive feedback loops between coral reefs, seagrass meadows and the hydrodynamics. Both seagrasses and coral reefs play a dominant role in the coastal protection (Duarte, 2002; Elliff & Silva, 2017; Ferrario et al., 2014; Reynolds et al., 2017). The relevant characteristics of the ecosystems and their interdependency are described in this section.

2.1.1 Coral reefs

Coral reefs are a very diverse marine ecosystem which are mainly found in shallow and deep (sub-)tropical waters all over the world (Knowlton, 2017). Reefs are formed by many colonies of coral and provide food and shelter for many organisms. By providing tourism and food, they are also very important to human beings. They also function as submerged breakwater enhancing shoreline protection (Elliff & Silva, 2017).

According to Darwin (1842) three types of coral reefs can be distinguished, (i) fringing reefs which are attached to the land, (ii) barrier reefs which are separated from the land by a lagoon and (iii) atolls which are reefs in open ocean enclosing a lagoon. Saint Martin is surrounded by barrier reefs (DCNA, 2014). The cross section of a barrier reef (Figure 2.1) consists of four zones: the reef front, crest, flat and the lagoon. The reef front is the area between the deep sea and the reef crest. This zone is characterised by high bottom roughness due to spurs and grooves (or buttresses and channels) which are formed by waves and currents. The reef crest is the highest part of the reef. The zone between the reef crest and the lagoon is called the back reef. This is the sheltered part of the reef. Behind the reef the lagoon is filled with carbonate sediments. Here, the wave and flow conditions are relatively calm.

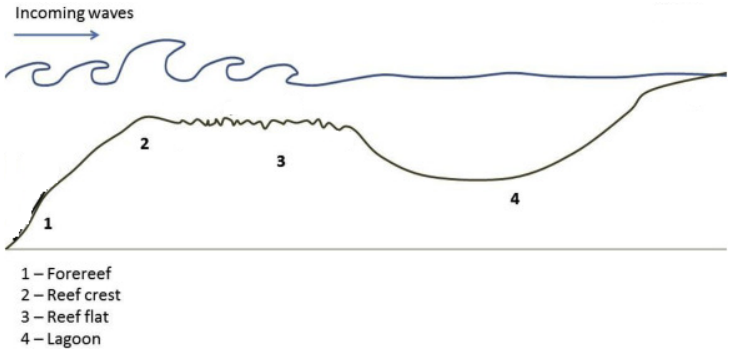

Figure 2.1: Cross-section of barrier reef. Adapted from Elliff and Silva (2017).

2.1.2 Seagrass meadows

In the calm waters behind the reefs, seagrass meadows are found. Seagrasses are rhizomatous plants that live in salty, marine environments worldwide (Duarte, 2002). *Thalassia testudinum* and *Syringodium filiforme* are the seagrass species that grow in the considered bays around Saint Martin (Van Berlo et al., 2016). *Thalassia testudinum* is the most common species of seagrass in the Caribbean (Short, Carruthers, van Tussenbroek, & Zieman, 2010). It forms extensive meadows with dense rhizome mats below the bed. Seagrass has the ability to trap and stabilize sediment and attenuate flow and waves. In this way, seagrass prevents erosion and contributes to coastal protection (Duarte, 2002; Reynolds et al., 2017).

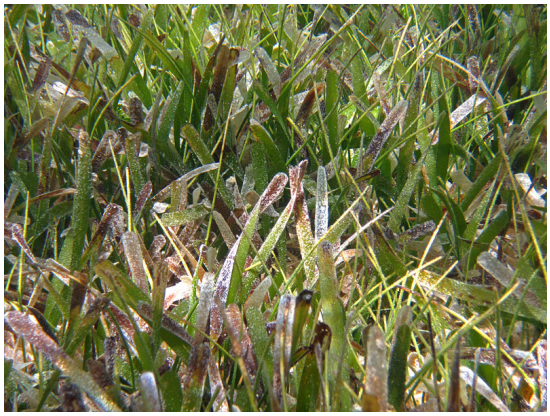

(a) Seagrass: *Thalassia testudinum* (thick) and *Syringodum filiforme* (thin)

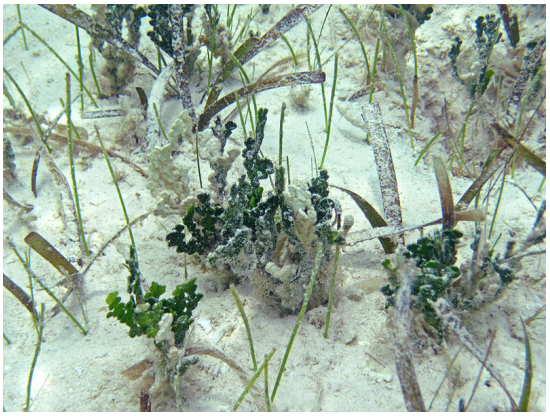

(b) Calcifying algae: *Halimeda incrassata*

Figure 2.2: Vegetation in the bays

The occurrence of seagrass is determined by physical, chemical and geological parameters. The lower limit is in general determined by the light availability, while the upper limit depends on the physical exposure. Although it differs per species, seagrasses require about 11% of the irradiance that is available at the water surface (Duarte, 1991). The irradiance decreases linearly with the water depth and depends on the suspended sediment concentration (Van Duin et al., 2001). Currents, waves and tide determine the upper depth limit (Greve & Binzer, 2004). Due to these physical processes, resuspension and erosion of sediment may occur, which prevent the seagrass from growing. The amount of nutrients, water temperature, salinity, oxygen, sulphide

and biotic factors also affect the growth and distribution of seagrass. The interaction between these parameters makes the seagrass distribution hard to predict.

In the seagrass meadows in the bays surrounding Saint Martin, there are also the calcifying algae *Halimeda* and *Penicillus* present (Van Berlo et al., 2016). Calcifying algae contribute to the formation of reefs and decomposed algae are an important element in the supply of carbonate sediment (Kangwe, Semesi, Beer, Mtolera, & Björk, 2012).

2.1.3 Interdependency of ecosystems

The described tropical marine ecosystems are linked by biological, chemical and physical interactions (Ogden & Gladfelter, 1983; Saunders et al., 2014). Coral reefs provide relatively calm wave conditions in the lagoon, which enables seagrass meadows to grow extensively. In turn, the seagrass meadows stabilize sediment. This prevents the burial of reefs by resuspended sediment during storm events. The seagrasses also provide a buffer against low pH (Unsworth, Collier, Henderson, & McKenzie, 2012) and filters nutrients and sediments, which is beneficial for the coral reefs. Seagrass meadows are also nursery grounds for reef fish.

2.2 Hydrodynamics in a reef-lagoon system

The flow in a reef-lagoon system is a combination of tide-, wind-, wave- and density-driven currents (Lowe et al., 2009b). The significance of each mechanism differs per situation depending on the bathymetry, reef morphology and meteorological and oceanic conditions. During this study, the density-driven currents are excluded from the model. In this section, the generation of currents by tide, wind and waves within a coastal reef-lagoon system is explained. The effect of seagrass meadows on the hydrodynamics is also described.

2.2.1 Tide

Daily water level variations are caused by the tide. This is a long wave generated by the rotation of the Earth, the gravitational attraction of the Moon and to a lesser extent of the Sun (Bosboom & Stive, 2015). The tidal wave can be seen as a combination of different harmonic oscillations (tidal constituents). Each constituent has a specific amplitude, period and phase. The main tidal constituents are M_2 and O_1 (both induced by the Moon) and S_2 and K_1 (both induced by the Sun). Constituents with a subscript 1 represent a diurnal component and subscript 2 represent semi-diurnal components. To classify the tides, the tidal form factor F is used, see Equation 2.1 and Table 2.1.

$$F = (K_1 + O_1)/(M_2 + S_2) \tag{2.1}$$

where the symbols of the tidal constituents represent their amplitudes.

The tide-induced currents in the reef-lagoon system are the result of the rise and fall of the water level in the reef-lagoon system. The tidal ranges and thus tide-induced currents depend on the geographic location and local situation (Bosboom & Stive, 2015).

Table 2.1: Tidal character expressed by the form factor F (Bosboom & Stive, 2015)

Value of F	Category
0-0.25	Semi-diurnal
0.25-1.5	Mixed, mainly semi-diurnal
1.5-3	Mixed, maily diurnal
>3	Diurnal

2.2.2 Wind

Another phenomena that will drive currents is the wind. Wind also generates waves, which will be discussed in the next section. The bays are exposed to onshore directed trade winds. These winds exert a shear stress on the water surface. The shear stress will move the water and thus drive a flow. Another effect is wind set-up. Water is 'pushed' towards the shore leading to a set-up in water level. Because water cannot pile up infinitely against the coastline, a circulation current is driven.

2.2.3 Waves

The eastern coast of Saint Martin is exposed to swell and wind waves. Swell waves are generated by distant storms and have a lower frequency than wind waves, which are locally generated and have a shorter period (Holthuijsen, 2007). In short, the waves will break on the reef and create a wave set-up of the water level above the reef. The pressure gradient of the water level will force a current over the reef through the lagoon back to the ocean. The wave set-up depends on the wave conditions.

Wave transformation

Once the waves approach the coast and enter shallower water, they will transform. The wave height and direction change due to the limited water depth. Generally, four processes of wave transformation are distinguished (Holthuijsen, 2007).

The change in wave height when water depth increases is called *shoaling*. Waves slow down once they enter shallower water leading to an increase of energy and thus an increase of wave height.

Diffraction is the process of a wave bending into a sheltered area behind e.g. a headland or breakwater.

The change of direction of the wave is called *refraction*. If a wave approaches the coast under an angle, it experiences a change in wave length and speed. As the propagation speed depends on the water depth, the wave will bend towards the area with lower propagation speed in order to conserve its energy. As a result, the wave turns towards the coast.

In the end, waves will break. This can be caused by the asymmetry or the limited water depth. When the waves become too steep (wave asymmetry), they break (white-capping). Or when the wave height with respect to the water depth is too large, they break too (depth-induced

breaking). In both cases, a surface roller is generated in which energy is converted into turbulent kinetic energy and dissipated via turbulence (Bosboom & Stive, 2015).

Orbital motions and Stokes drift

Waves set the fluid particles underneath the surface in motion. In deep water these motions are closed circles, but in shallow water become the orbital paths elliptical (Holthuijsen, 2007). The horizontal orbital velocity depends on the water depth. This leads to elliptical paths which are not fully closed. This causes a current in the same direction as the wave propagation and is called *Stokes drift*.

Wave-induced forces, set-up and currents

So far, only the transfer of energy by waves is considered. But waves also transport momentum. According to Newton's second law, the transport of momentum is equivalent to a stress. Variations in the stress will act as a force. The depth-integrated and wave-averaged transport of momentum by waves is called *radiation stress* S_{xx}. Horizontal gradients in radiation stress result in *wave-induced forces*. These forces cause currents and changes in water levels (Bosboom & Stive, 2015; Holthuijsen, 2007).

In the breaker zone, waves are dissipated leading to a decreasing radiation stress. This leads to an onshore-directed wave force which is compensated by a pressure force in offshore direction due to the so-called wave set-up. In the longshore direction will the gradient in radiation stress force a current and is the radiation stress gradient compensated by a time mean shear stress.

Applying this theory to the reef-lagoon system leads to the situation schematized in Figure 2.3. Waves break on the forereef and reef flat leading to an decreasing radiation stress, which results in an onshore directed wave force that is compensated by a wave set-up over the reef. As a result, a current is driven from point A over the reef, through the lagoon via point B and C to the channel back to point D in the ocean.

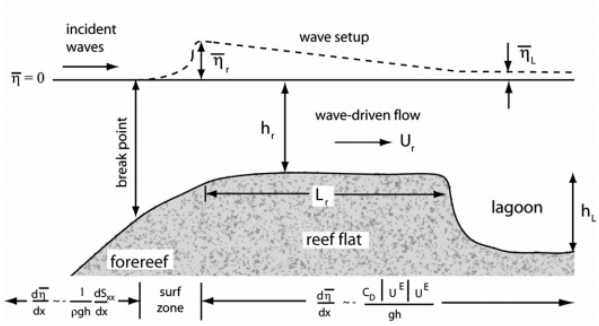

(a) Wave set-up over the reef due to breaking waves

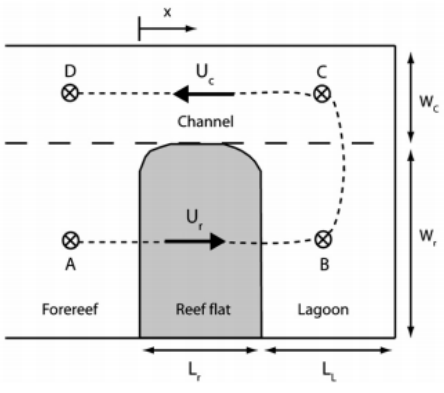

(b) Top view of wave-induced circulation current

Figure 2.3: Schematization of wave-induced set-up and currents around the reef (Lowe et al., 2009b)

2.2.4 Lagoon circulation

So far, the different mechanisms that could drive the flow in the reef-lagoon system are described. The exact circulation depends on many variables like bathymetry, tide, wave height and direction, wind speed and direction, etc. (Roberts & Lugo-Fernández, 2011). The importance of each forcing is still unknown for the considered case study area, but a schematic prediction of the flow pattern can already be made.

The waves will break on the reef leading to a set-up of the water level over the reef. This set-up gives rise to a current over the reef into the lagoon. Also the tide generates a flow over the reef. During flood tide the flow will be directed into the lagoon and opposite during ebb tide. The wind, when coming from the East, will also drive a flow into the lagoon by exerting shear stress on the sea surface. All the water that flows into the lagoon will leave the lagoon through the gully. The seaward directed current increases when nearing the outlet. This will also lead to a deeper channel due to higher flow velocities and thus more erosion.

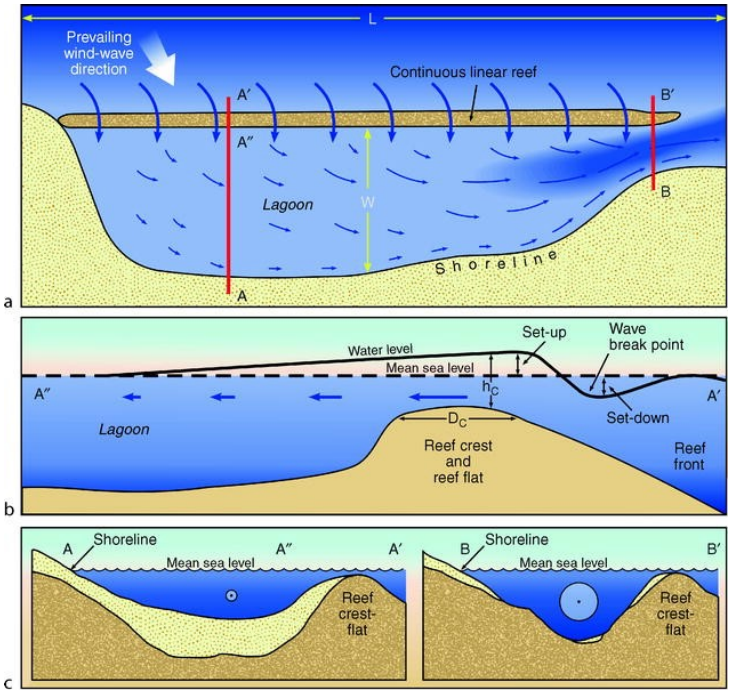

Figure 2.4: Lagoon circulation (Roberts & Lugo-Fernández, 2011)
a) A shallow lagoon is protected by a reef from wind and waves. A current towards and through the outlet develops. b) A cross section (A-A') indicating the set-up above the reef and the resulting current flowing over the reef. c) Two cross sections of the lagoon (A-A' and B-B') with the circles representing the flow velocities. The sediment is stored in the calm and sheltered parts of the lagoon.

2.3 Bed shear stress

The force per unit area exerted on the bed by the flow and waves is called the *bed shear stress* (R. L. Soulsby, 1997). The bed shear stress is used to determine sediment transport and erosion/sedimentation. It can also be used to predict the seagrass distribution. The bed shear stress due to currents only is computed using Eq. 2.2.

$$\tau_c = \frac{g\rho u^2}{C^2} \tag{2.2}$$

where τ_c is the current-induced bed shear stress $[N/m^2]$, g the gravitational constant [m/s^2], ρ the density of water [kg/m^3], u the flow velocity [m/s] and C the Chézy coefficient $[m^{1/2}/s]$. The Chézy coefficient can be expressed using Manning's value (Eq. 2.3). In coastal applications this is preferred, because now the Chézy coefficient depends on water depth.

$$C = \frac{\sqrt[6]{h}}{n} \tag{2.3}$$

where h is the water depth [m] and n Manning's value $[s/m^{1/3}]$.

Bed shear stress is not only generated by currents. Also waves cause bed shear stresses due to the induced oscillatory motion.

$$\tau_w = \frac{1}{2}\rho f_w u_{orb}^2 \tag{2.4}$$

where f_w is the wave friction factor [-] and u_{orb} the peak orbital velocity [m/s].

Again, the induced bed shear stress is dependent on a friction factor. But in this case, also the turbulence in the flow is important. Swart (1974) came up with the following expression of the wave friction factor.

$$f_w = \begin{cases} 0.00251 \exp\left[5.21 \left(\frac{A}{k_s}\right)^{-0.19}\right], & \text{if } \frac{A}{k_s} > \frac{\pi}{2} \\ 0.3, & \text{if } \frac{A}{k_s} \leq \frac{\pi}{2} \end{cases} \tag{2.5}$$

where $A = u_{orb} * T/2\pi$ is the semi-orbital excursion [m] and k_s the Nikuradse roughness [m].

But due to a non-linear interaction between the current and wave boundary layer, the total bed shear stress is not just the sum of the current-induced and wave-induced bed shear stress. The formula of R. Soulsby et al. (1993) is a generally used formula to compute the total mean bed shear stress τ_m.

$$\tau_m = \tau_c \left(1 + 1.2 \left(\frac{\tau_w}{\tau_c + \tau_w}\right)^{3.2}\right) \tag{2.6}$$

The bed shear stress for which sediment particles start moving is called the *critical bed shear stress* τ_{cr}.

$$\tau_{cr} = \theta_{cr}(g(\rho_s - \rho)d) \tag{2.7}$$

where θ_{cr} is the critical Shields parameter [-], ρ_s the density of sediment particles $[kg/m^3]$ and d the grain size [m].

2.4 Effect of seagrass on hydrodynamics

2.4.1 Flow attenuation

For undisturbed flow, the vertical velocity profile can be described using the formulation derived by Prandtl and Von Karman:

$$u(z) = \frac{u_*}{\kappa} \ln\left(\frac{z}{z_0}\right) \tag{2.8}$$

where u_* is the friction velocity [m/s], κ the Von Karman constant [-] and z_0 the roughness length [m].

But in the case of submerged vegetation, two layers can be distinguished (Figure 2.5), one layer with uniform flow trough the vegetation (u_{veg}) and the upper layer where the logarithmic velocity profile is found again. Zone 1 and 3 are respectively a boundary and transitional layer.

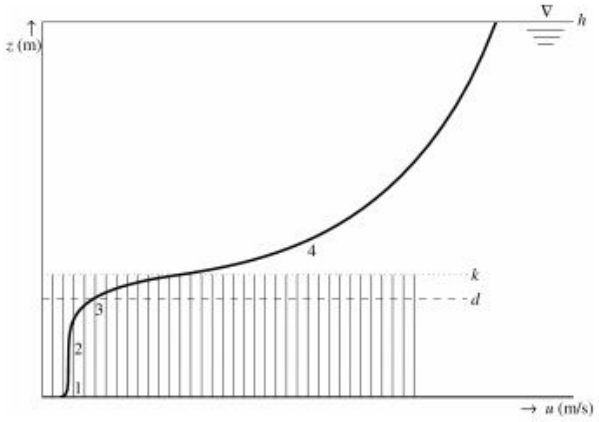

Figure 2.5: Vertical velocity profile (Baptist et al., 2007)

The uniform flow velocity through the vegetation (u_{veg}) follows from the momentum balance where the bed shear stress balances the pressure gradient (Baptist et al., 2007).

$$u_{veg} = \sqrt{\frac{hi}{\frac{1}{C^2} + \frac{C_D N_v b_v h_{veg}}{2g}}} \tag{2.9}$$

$$\tau = \tau_b + \tau_v = \rho g h i \tag{2.10}$$

$$\tau_v = \frac{1}{2}\rho C_D m D h u^2 \tag{2.11}$$

where h is the water depth [m], i the water level slope [m/m], C_D the drag coefficient [-], N_v the number of stems per area [stems/m^2], b_v the stem diameter [m], h_{veg} the vegetation height [m], τ the total shear stress [N/m^2], τ_b the bed shear stress [N/m^2] and τ_v the shear stress due to vegetation [N/m^2].

Above the vegetation the velocity profile becomes again logarithmic and is described by (Baptist et al., 2007):

$$u_0 = \frac{u_*}{\kappa} \ln(\frac{z - h_{veg}}{z_0}) + u_{veg} \tag{2.12}$$

$$u_* = \sqrt{g(h - h_{veg})} \tag{2.13}$$

The drag coefficient is the parameter that cannot be measured properly and should be estimated or can be used for calibration (Baptist et al., 2007). Nepf and Vivoni (2000) suggested a value of 1.0 for the drag coefficient, based on an emergent canopy of flexible vegetation.

2.4.2 Wave attenuation

Waves are also attenuated by seagrass. The wave dissipation depends on plant properties such as geometry, buoyancy, density, stiffness and spatial configuration and wave parameters (Mendez & Losada, 2004). Fonseca and Cahalan (1992) showed that one meter of *Thalassia testudinum* and *Syringodium filiforme* can reduce the wave energy with respectively 44% and 43%.

Based on linear wave theory, considering normal incident waves on a straight coastline with parallel depth contours and assuming the vegetation to be rigid cylinders, the equation for the conservation of energy is reduced to

$$\frac{\partial E c_g}{\partial x} = \varepsilon_v \tag{2.14}$$

$$\varepsilon_v = \int_h^{h+h_{veg}} F_x u dx \tag{2.15}$$

$$F_x = \frac{1}{2} \rho C_D b_v N u |u| \tag{2.16}$$

where E is the energy density [N/m], c_g the group velocity [m/s], ε_v the time-averaged rate of energy dissipation [N/ms], F_x the horizontal force exerted by the seagrass on the fluid [N] and C_D the drag coefficient [-] which needs to account for the ignorance of the swaying leaves (Dalrymple, Kirby, & Hwang, 1984).

This leads to the following formulation of the mean rate energy dissipation per horizontal area due to wave damping by vegetation (Mendez & Losada, 2004).

$$\langle \varepsilon_v \rangle = \frac{1}{2\sqrt{\pi}} \rho \tilde{C}_D b_v N_v \left(\frac{gk}{2\omega} \right)^3 \frac{\sinh^3 kh_{veg} + 3 \sinh kh_{veg}}{3k \cosh^3 kh} H_{RMS}^3 \tag{2.17}$$

where $\langle \varepsilon_v \rangle$ is the mean rate of energy dissipation by vegetation [N/ms], $\tilde{C}_D$ the bulk drag coefficient [-], k the wave number [m^{-1}], ω the radian frequency [s^{-1}] and H_{RMS} the root-mean-squared wave height [m].

According to Bradley and Houser (2009) the bulk drag coefficient of seagrass can most accurately be described using the Reynolds number $Re = \frac{uh}{\nu}$.

$$\tilde{C}_D = 0.1 + \left(\frac{925}{Re} \right)^{-3.16} \tag{2.18}$$

This results in a bulk drag coefficient of 0.1 for the seagrasses found in the bays. Also according Paul and Amos (2011), this is a reasonable bulk drag coefficient.

2.5 Impact of climate change in the Caribbean

2.5.1 Sea-level rise

Sea-level rise is a consequence of global climate change. It is mainly caused by thermal expansion of the oceans and melting of glaciers and the Greenland and Antarctic ice sheets (Church et al., 2013). The Intergovernmental Panel on Climate Change (IPCC) uses different scenarios to predict the sea-level rise. A scenario is called a Representative Concentration Pathway (RCP). These standard RCPs are used to ensure that the same starting conditions are used and that research is comparable. There are four RCPs (RCP2.6, RCP 4.5, RCP6.0, RCP 8.5), each containing a radiative forcing which represents a scenario including economic, technological, demographic and political factors (Moss et al., 2008). RCP8.5 can be seen as a high emission scenario, while RCP2.6 represents a mitigation scenario. Church et al. (2013) determined the global mean sea-level rise for each RCP, see Table 2.2.

Table 2.2: Resulting global mean sea level rise for every RCP (Church et al., 2013)

Scenario	RCP2.6	RCP4.5	RCP6.0	RCP8.5
Global mean sea-level rise [m]	0.44 [0.28-0.61]	0.53 [0.36-0.71]	0.55 [0.38-0.73]	0.74 [0.52-0.98]

A global warming of $2°C$ is widely suggested as a threshold beyond which the consequences become too high (Jevrejeva et al., 2016). For both RCP4.5 and RCP8.5 this threshold is reached between 2040 and 2050. In case of the RCP8.5 global temperatures increase with $4°C$ by 2083 and in 2100 it might even be $5°C$. Jevrejeva et al. (2016) computed the local sea-level rise for these scenarios for different locations worldwide, also taking into account the vertical motion of the land. They have done this also for San Juan, Puerto Rico, which is located within 325 km of Saint Martin. This will be very similar to the expected sea-level rise near Saint Martin. For the different scenarios of global warming, the following intervals of sea-level rise were determined.

Table 2.3: Local sea-level rise (in meters) under the RCP8.5 scenario at San Juan, Puerto Rico (Jevrejeva et al., 2016)

Global warming	Year	Mean SLR [m]	5-95 percentile
$2°C$	2041	0.21	0.13-0.35
$4°C$	2083	0.60	0.35-1.24
$5°C$	2100	0.87	0.47-2.01

2.5.2 Impact of climate change on coral reefs

The coral reefs are under pressure due to climate change. Reef-building corals are very sensitive to changing conditions. Changing temperatures, salinity and light have significant impact on the growth (Hoegh-Guldberg, 1999). Rising water temperatures and ocean acidification, which are direct consequences of climate change, lead to coral bleaching and coral degradation (Elliff & Silva, 2017). Although corals survived more extreme conditions in the past, feared is that the reefs do not have sufficient time to adapt (Hoegh-Guldberg et al., 2007). Currently, coral

bleaching occurs also due to seasonal variations. But due to climate change it is likely that the frequency of bleaching increases such that coral reefs do not have sufficient time to recover. The increase of bleaching events in the Caribbean is among the highest in the world (Hoegh-Guldberg, 1999).

Also sea-level changes will probably affect coral reefs (Saunders et al., 2015). There are three possible scenarios, which are shown in Figure 2.6. The growth rate of reefs equals the rate of sea-level rise and thus the depth above the reef remains constant, the reef will catch up later if the sea-level has stabilized and the reef system is adapted to the changed conditions. or the reef is not able to adapt to the higher sea-level and it will die.

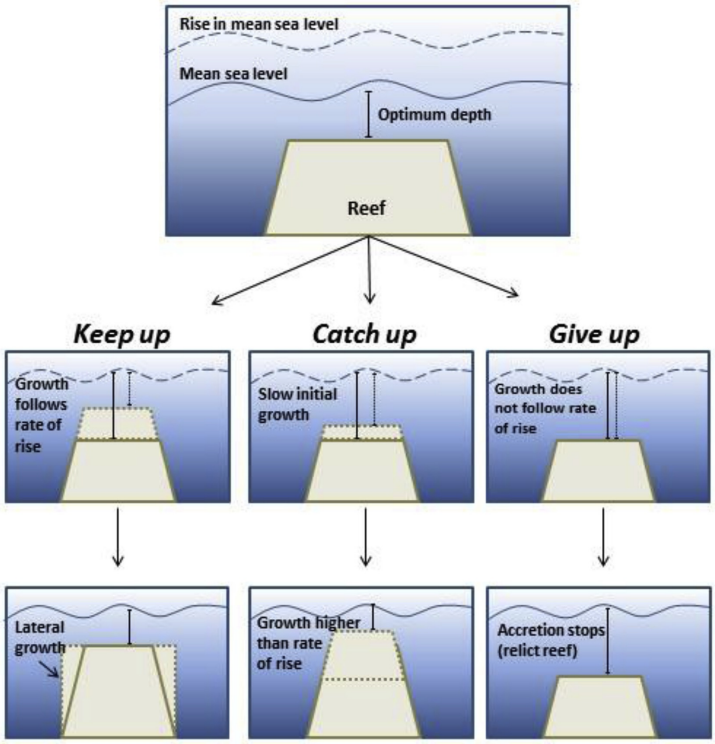

Figure 2.6: Coral reefs under the face of sea-level rise (Elliff & Silva, 2017).

According to Hoegh-Guldberg (1999); Hoegh-Guldberg et al. (2007); Siegle and Costa (2017), it is unlikely that the coral reefs are able to keep up with sea-level rise due to ocean acidification and rising seawater temperatures. van Woesik, Golbuu, and Roff (2015) predicted that reefs in the western Pacific can keep up with sea-level rise for the low-mid RCPs. So, what will happen with reefs under the light of global climate change cannot be said with certainty. But the consequences can be very significant. The reduced sand production by coral reefs may cause coastal erosion Hoegh-Guldberg et al. (2007). Also due to the higher water depth above the reefs, wave attenuation will be less, see Figure 2.7. Coral degradation leads to smoother reefs, which reduces wave dissipation by the waves even more (Quataert et al., 2015). Wave-induced currents will intensify. Due to the increase of wave energy that reaches the shoreline will coastal erosion also increase. Besides, the seagrass meadows will become more vulnerable (Hoegh-Guldberg et al., 2007). But as said, the final effect is dependent on the ability of the reefs to adapt to changing conditions.

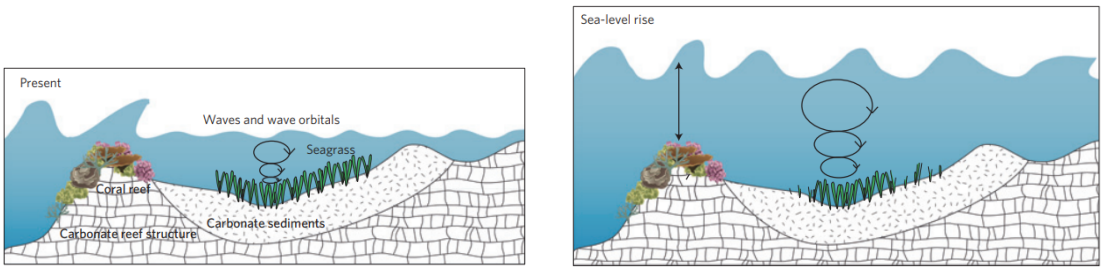

(a) Wave breaking reefs and limited wave orbital motion in lagoon

(b) Increased wave orbital motions due to sea-level rise

Figure 2.7: Impact of sea-level rise due to increased water depth above reefs (Saunders et al., 2015)

2.5.3 Impact of climate change on seagrass

Climate change is also a potential danger for seagrasses (Reynolds et al., 2017). Rising sea-levels reduce the amount of light reaching the leaves, which limit the growth rate of seagrasses. Also the potentially increased wave action, which depend on growth of coral reefs, and water temperatures can lead to less favorable conditions for seagrass meadows. The ability of seagrass meadows to trap and stabilize sediment and attenuate flow and waves will decrease. This leads to stronger currents and increased sediment concentrations, resulting into a further deterioration of the conditions for the remaining seagrass (Duarte, 2002). This will further enhance the risk of coastal erosion and the loss of other services. The calcifying algae will be under pressure too due to increasing water temperatures and pH, which can lead to a decreasing production of carbonate sediment (Hoegh-Guldberg et al., 2007). The combination of requirements for seagrass to grow makes it hard to predict where it will grow and whether it will survive.

2.6 Conclusion

The seagrass meadows and coral reefs form a interdependent system with positive feedbacks in the Caribbean. Together, they provide many services. But due to climate change the ecosystems are under pressure. Changing hydro- and morphodynamics may be threatening to the health of the coral reefs. Due to the interdependency, the response of one of the ecosystems can initiate a domino effect. For example, when the coral reefs are not able to keep up with the sea-level rise, the wave action in the bays will increase. This can damage the seagrass meadows. When seagrasses are not able to prevent sediment from resuspension, the water quality will deteriorate. Living conditions for the coral reefs and seagrasses worsen even more leading to a downward spiral. Therefore, it is very important to understand the positive and negative feedbacks and further investigate the possible impact of global climate change on Caribbean coastal ecosystems like this. Because when these valuable ecosystems are lost, coastal protection and other services will also be threatened.

Chapter 3

Baie Orientale and Baie de L'Embouchure

As stated in the introduction, the focus during this project lays on two shallow bays at the eastern coast of Saint Martin, namely Baie Orientale and Baie de L'Embouchure. Where the previous chapter provided general theory and background information, this chapter introduces the area of interest and the local characteristics.

3.1 Area of interest

Saint Martin is located in the eastern part of the Caribbean Sea around 18.06°N and 63.05°W. It is one of the Leeward islands, an island group which is part of the Lesser Antilles. It is divided into a French (Saint Martin) and a Dutch part (Sint Maarten). Philipsburg is the main city of the Dutch part. The largest city on the French side is Margriot.

This project is focused on Baie Orientale and Baie de L'Embouchure in Saint Martin. The bays are protected by barrier reefs from incoming waves (DCNA, 2014). Behind the reefs are calm and shallow bays formed like Baie Orientale and Baie de L'Embouchure. In these two bays seagrasses are widely spread (Réserve Naturelle Nationale de Saint-Martin, 2009). The seagrass meadows consist of *Thalassia testudinum* mixed with *Syringodium filiforme*. Also *Halimeda incrassata*, which is a specie of calcifying algae, is found throughout the bays (Van Berlo et al., 2016).

Figure 3.1 shows the bathymetry of the area and the names of characteristic locations. There was no single source containing bathymetry data of the whole area available. Therefore, data from GEBCO (Weatherall et al., 2015), sonar charts (Navionics, 2018) and measurements (James & Lynch, 2018) are combined to come up with this final bathymetry. How this is exactly done, is described in Appendix A where also more detailed charts of the bays can be found. Characteristic is the cross-shore profile of the bay-reef-ocean. From the ocean where the water depth is about 20 m or more and the bottom relatively flat, the forereef domes up. Next, the reef crest comes where the water depth is limited. In between the reef crest and the shoreline, a relatively shallow lagoon is found. This is very typical and essential for the functioning of this system, as we already saw in Chapter 2.

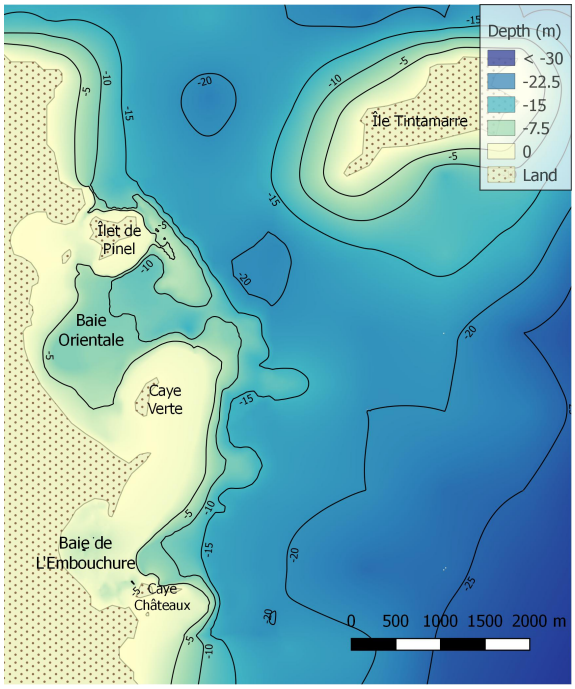

Figure 3.1: Bathymetry of area of interest

3.2 Climate

Saint Martin features a tropical climate with a dry season from January to June and a wet season from July to November (Meteorological Department Curaçao, n.d.). The approximate annual rainfall is 1170 mm. The average daily temperature is 27.2°C (30 year-normal average 1981-2010) (Lawrimore et al., 2011). The monthly average temperature and rainfall are presented in Figure 3.2a. The average wind speed is 9 kts (=4.63 m/s) and coming mainly from the East (Meteorological Department St. Maarten, 2016). Figure 3.2b shows wind rose based on 2016.

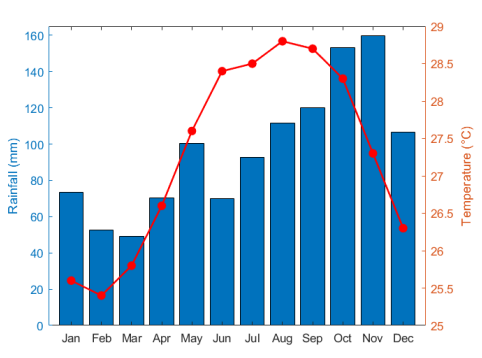

(a) Monthly average rainfall and temperature. Based on Lawrimore et al. (2011)

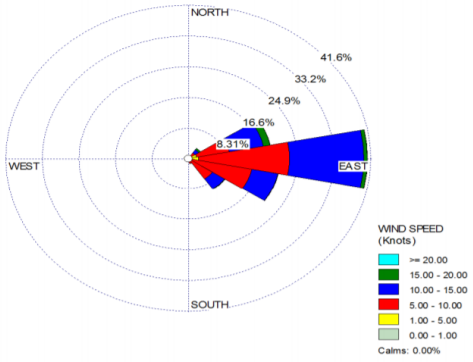

(b) Wind rose Saint Martin (Meteorological Department St. Maarten, 2016)

Figure 3.2: Climate characteristics of area of interest

3.3 Hydrodynamic conditions

3.3.1 Tide

Water level measurements during January - April 2018 from VIZ, UNESCO/IOC (2018) were analysed using UTide (Codiga, 2011) in order to reconstruct the tidal signal. The tidal constituents that follow from the tidal analysis are presented in Table 3.1 (ranked by importance). The form factor is 2.1 (see Eq. 2.1), which indicates a mixed, mainly diurnal tide. In Figure 3.3 the reconstructed tidal signal can be found. It can be clearly seen that the diurnal components dominate. The tidal range varies between 0.30 m (spring tide) and 0.20 m (neap tide). This tidal character and range is also what we could expect according to Kjerfve (1981).

Table 3.1: Tidal constituents

Tidal constituent	Amplitude (m)	Phase (deg)
K_1	0.0649	228
O_1	0.0591	222
M_2	0.0497	357
MM	0.0179	57.7
Q_1	0.0125	211
MSF	0.0115	75.7
NO_1	0.0102	156
S_2	0.00951	25

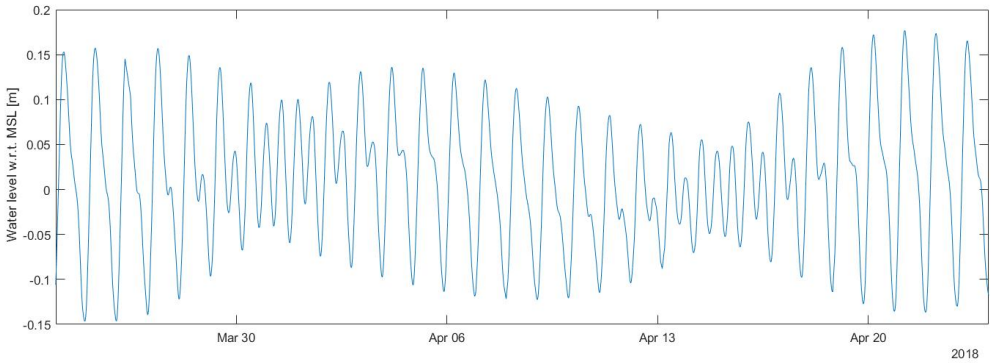

Figure 3.3: Reconstructed tidal signal. Data used from VIZ, UNESCO/IOC (2018).

3.3.2 Waves

No offshore wave data is available in or close to the area of interest. Some measurements are done inside the bays (James, 2015). This indicates that mainly swell occurs. Surf forecasts show most of the time swell waves of 1-1.5 m high with a period of 8-11 s coming from the East (Meteo365, 2018).

3.4 Presence of seagrass and coral reefs

Looking at the aerial images of the bays in Figure 1.2, one can already identify the reefs and seagrass meadows in the clear waters. The map in Figure 3.4, dated from 2009, shows a lot of correspondence with these aerial pictures. Throughout the entire Baie de L'Embouchure and Baie Orientale except in the gullies, seagrass can be found (green). In front of the bays, the reefs (red/pink) are clearly present.

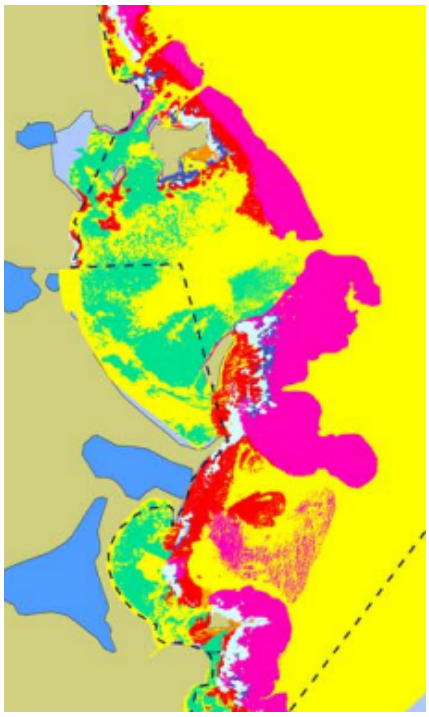

Figure 3.4: Vegetation cover in the area (Réserve Naturelle Nationale de Saint-Martin, 2009). Red/pink: coral reef. Green: seagrass meadows.

No data is available on the roughness and bathymetry of the reefs.

James (2016a) performed a vegetation survey in the area. Table 3.2 gives an overview of the relevant properties of seagrass. Only a few density measurements were done. For *Thalassia testudinum* a density of 800 shoots/m^2 was found.

Table 3.2: Seagrass properties

	Thalassia testudinum		*Syringodium filiforme*
	Deep water (>2.5 m)	Shallow water (<2.5 m)	
Height [mm]	295	89	300
Width [mm]	11	8	2

Chapter 4

Methodology

The research is primarily done with the use of the model Delft3D Flexible Mesh (Delft3D FM). In this chapter, a model description can be found. Next, the model setup and validation are discussed and a sensitivity analysis is performed. How the model is used to predict the impact of sea-level changes is described in the final section.

4.1 Choice of model

As explained before, a hydrodynamic model is needed that is able to simulate flow, waves, their mutual interaction and the interaction with vegetation. Delft3D and Delft3D FM, which is the successor of Delft3D, are both able to do this. The main difference is the use of a structured versus an unstructured grid. The use of an unstructured grid is advantageous as it enables to follow complex topographies and allows locally decreased grid cell size without the number of grid cells becoming too large. Delft3D FM is also able to take into account the wave damping by vegetation, where Delft3D is not. It has to be noted that only the flow module, D-Flow FM, is the only module which is officially released and fully validated. The module for waves (D-Waves) is only available under beta conditions (Deltares, 2018a). Also a module for morphology (D-Morphology) is under development. So, this model can be easily extended for future work regarding sediment transport and morphology.

4.2 Model description

Delft3D Flexible Mesh (Delft3D FM) is the successor of Delft3D (Deltares, 2018a). As said, it is able to simulate two- and three-dimensional flows, waves, sediment transport, morphology and ecology. The model is composed of several modules which are able to interact with each other. At the moment of writing, only the hydrodynamic module (D-Flow) was fully validated (Deltares, 2018a). The wave module was released under beta conditions. In the next paragraphs is a short description of each module given. A more technical description including the governing equations can be found in Appendix B.

4.2.1 Flow module

D-Flow is the hydrodynamic module of Delft3D FM (Deltares, 2018b). This module simulates (non-steady) flow in 1D, 2D or 3D by solving the shallow water equations. Transport phenomena like salinity and temperature can also be solved using this module. Tide and meteorology are used as forcing. The equations are solved for a structured or unstructured grid. The main advantage of a unstructured grid is that one has more flexibility in local resolutions. The

continuity equation is solved implicitly for all points and the time integration of the advection term is done explicitly. Therefore, there is a time step restriction based on the Courant criterion (Deltares, 2018b).

4.2.2 Wave module

The wave module is called D-Waves (Deltares, 2018d). This module is based on the SWAN model which simulates the propagation of random, short-crested waves in coastal regions with deep, intermediate or shallow water. SWAN accounts for wave-current interactions and is therefore based on the spectral action balance.

SWAN takes into account transformation due to shoaling, refraction and diffraction, generation by wind, dissipation by whitecapping, depth-induced breaking and bottom friction and nonlinear wave-wave interactions. Wave setup is not explicitly computed by the wave module. The wave forces are send to the flow module, which again computes the resulting water level.

The wave module is coupled with the hydrodynamic module D-Flow via the communication file (COM-file) (Deltares, 2018b). D-Waves sends the wave forces and Stokes drift to D-Flow, where they are taken into account in the computations. D-Flow sends the bed level, water level, flow velocity and wind field to D-Waves, where this is taken into account during the wave computations.

The process order is as follows. First, the wave module does one computational step and writes its output to the COM-file. Next, D-Flow starts simulating the flow for a certain interval and uses the output of the wave-module as input. At the end of the interval, D-Flow writes its output to the communication file. For the next computational step of the wave module, the Flow-output is used as input again. This goes on and on until the end of the simulation period is reached.

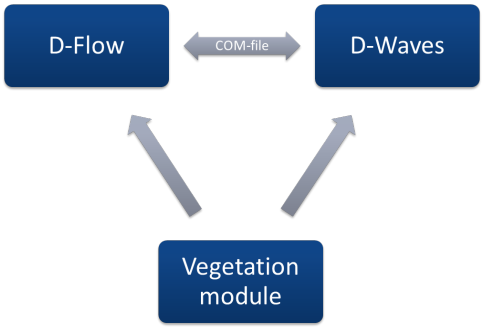

Figure 4.1: Coupling between different modules of Delft3D FM

4.2.3 Vegetation modelling

In order to capture the effect of seagrass on the hydrodynamics, a vegetation module is also included. In D-Flow FM, the effect of vegetation on the flow is modelled using the trachytope approach Deltares (2018b). With this method, the resistance due vegetation is modelled using

a modified bed roughness. The following formula of Baptist is used.

$$C = C_b + \frac{\sqrt{g}}{\kappa} \ln\left(\frac{h}{h_{veg}}\right) + \sqrt{1 + \frac{C_D + N_v h_{veg} C_b^2}{2g}} \tag{4.1}$$

To include wave dissipation by vegetation, the formula proposed by Mendez and Losada (2004) (see Eq. 2.17 in Section 2.4) is implemented in SWAN. The vegetation is modelled as rigid cylinders which exert a force on the fluid. However, seagrass is a form of flexible vegetation. But for a certain range of conditions, flexible vegetation acts similar as rigid plants once the correct deflected height and drag coefficient is chosen (Dijkstra, 2009).

4.3 Model setup

How the model is set up, is presented in this section. The input parameters and processes that are included, are described briefly.

4.3.1 Computational grid and boundaries

The computational domain of the flow module is about 3 km wide and 6.5 km long centered around the area of interest. An unstructured mesh with spherical coordinates is created consisting of triangles. The grid cell size varies from 50 m inside the bays, linearly increasing to 150 m at the offshore boundary. The location of the offshore boundary is chosen such that the flow is more or less unaffected by the bathymetry. However, due to the presence of Île Tintamarre and other complex geometry features, this is hard to achieve. Therefore, it is decided to put the offshore boundary between the 15 m and 20 m contour lines. The lateral boundaries are placed such that boundary effects do not reach the area of interest. Also the requirements regarding orthogonality are met. The final computational grid and the location of the boundaries can be found in Figure 4.2a.

4.3.2 Bathymetry and islands

In Appendix A and Figure 3.1, the bathymetry of the area is composed and presented. This data is used to create the bathymetry in Delft3D FM. The final result is shown in Figure 4.2b. Due to interpolation and a different resolution, not all small-scale features are captured.

Inside the computational domain, some islands can be found. These cells are set as dry areas. The shape of the islands is sometimes slightly altered because of the arrangement of grid cells and to avoid unrealistic angular shorelines. The effect is expected to be small.

4.3.3 Flow boundary conditions

The next step is prescribing the boundary conditions. The landward boundary is a closed boundary. At the seaward boundary the tidal motion of the water level needs to be imposed. This is done by a water level boundary. In order to prevent the model from becoming too complex, it is only forced with the three main tidal constituents (K_1, O_1 and M_2). This results in the tidal signal shown in Figure 4.2c which is imposed at the boundary. At the two lateral boundaries no external forcing is desired. The water should be able to move freely at these boundaries. This is achieved using Neumann boundaries which prescribe a water level gradient. A more detailed description of the water level and Neumann boundary is given in Appendix B.

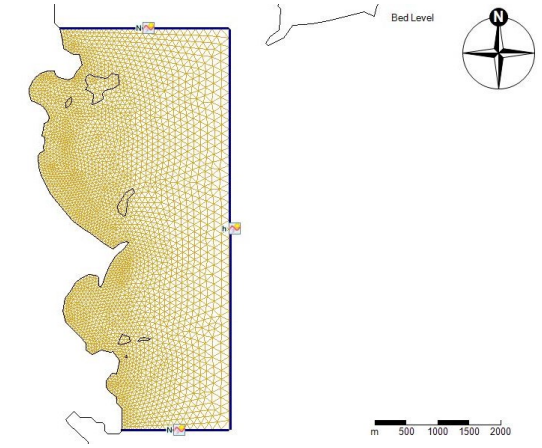

(a) Computational grid and boundaries

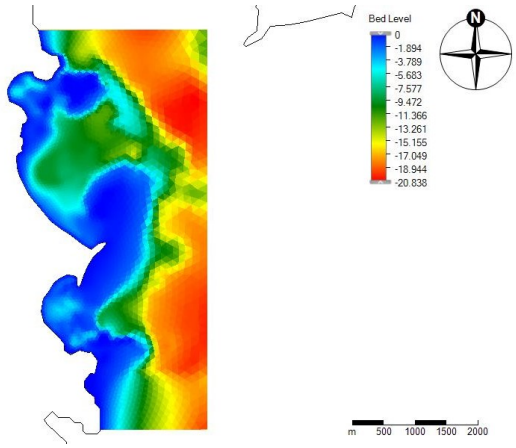

(b) Bathymetry

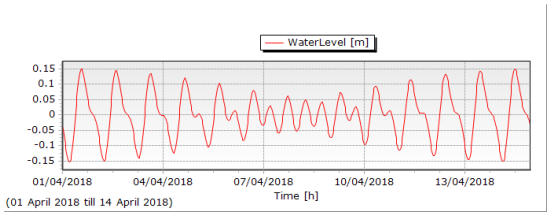

(c) Water level boundary condition at seaward boundary

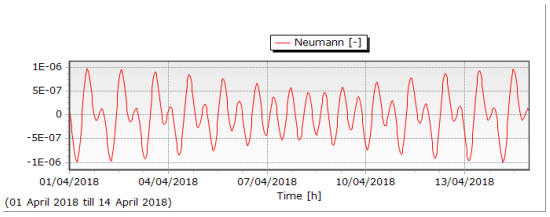

(d) Neumann boundary condition at lateral boundaries

Figure 4.2: Model setup flow module

4.3.4 Model setup waves

The wave module needs its own computational (structured) grid. Again, spherical coordinates are used and a grid size of 0.001 deg ($\approx 110m$) is chosen. The eastern grid boundary is chosen close to the 30m-depth contour. The southern boundary is chosen such that no boundary effects occur in the area of interest, the computational flow domain in this case. The northern boundary is placed further North at the 20m-depth contour making sure that the impact of Île Tintamarre on the waves is captured. Along the whole northern and eastern boundary and at the southern boundary till the 20m-depth contour, a constant boundary condition is applied. The model is forced with waves with a constant height, period and direction. Initially, a constant wave spectra with a significant wave height of 1.5 m, a period of 9 s and coming from the East with a directional spreading of 10 degrees is defined along the boundaries. But different simulations are done in order to investigate the effect of varying wave height, period and direction. The bathymetry is the same as used in the flow model.

4.3.5 Physical parameters

Wind

As shown in Section 3.2, most of time the wind is blowing from the sector Northeast-Southeast. The average wind speed is 9 kts ($\approx$ 5 m/s). In the simulations is a spatially uniform wind field of 5 m/s coming from the East used as forcing. For different simulations is varied with the wind speed and direction to investigate the effect of the wind on the circulation.

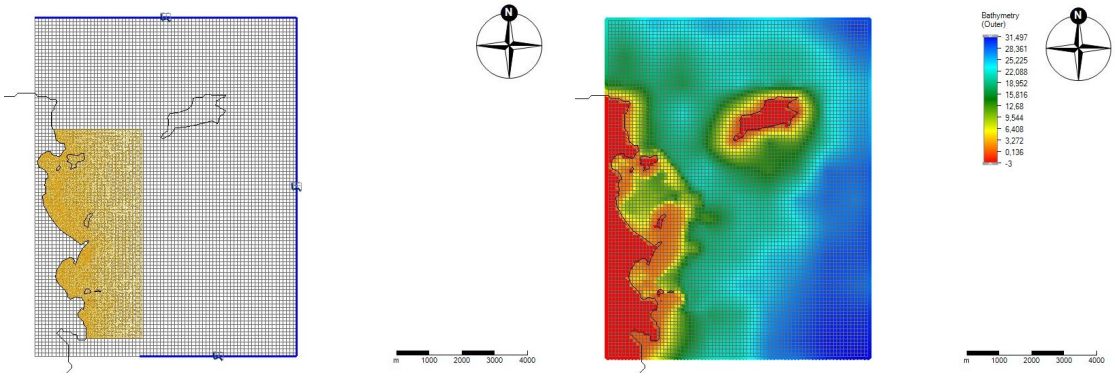

(a) Computational wave grid and boundaries, computational flow grid in yellow

(b) Bathymetry

Figure 4.3: Model setup wave module

Vegetation and bottom roughness

The bottom roughness varies spatially due to the presence of seagrass meadows, coral reefs and rubble, see Figure 4.4a. The presence of seagrass is based on data from James (2016a). The extent of the coral reefs is determined using aerial images and the map presented in Figure 3.4. How the bottom roughness of the seagrass meadows is computed, is explained in paragraph 4.2.3. A Manning value of 0.023 $s/m^1/3$ is chosen. Due to the topographic complexity and different spatial scales within a coral reef, the bottom roughness of a coral reef is hard to define. Literature suggested a friction coefficient c_f that is about 10 times larger than the friction coefficient of a sandy bed and in the range 0.01-0.1 (Lowe et al., 2009b; Pearson, 2016; Quataert et al., 2015; Zawada, 2011). Therefore, a Manning value of 0.07 $s/m^{1/3}$ is chosen, such that the friction coefficient above the reefs is about 10 times as large and varies between 0.01-0.05.

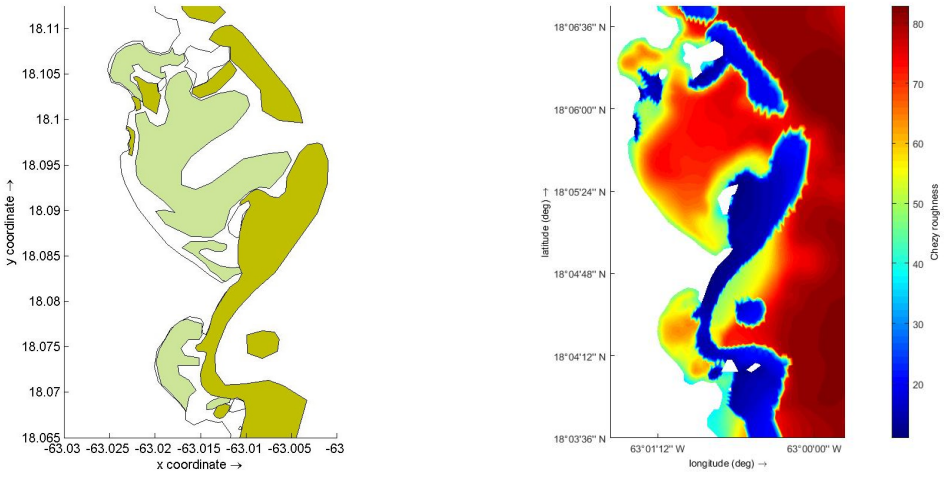

(a) Presence of coral reefs and seagrass meadows

(b) Bottom roughness (Chézy coefficient $[m^{1/2}/s]$)

Figure 4.4: Vegetation cover and bottom roughness

This varying bottom roughness is only applied to the flow module. This is not possible in the wave module, where a constant JONSWAP friction coefficient of $0.038 m^2/s^3$ is applied. In the sensitivity analysis is showed that the consequences of this limitation are limited.

Based on data from James (2016a), two classes of seagrass properties are used, one for the shallow areas (<1.5 m deep) and the other for the deeper area. The meadows are simplified. Assumed is that they only consist of *Thalassia Testudinum*, have a constant height of 88.6 mm in shallow water and everywhere else 295 mm and a width of 8.1 mm in shallow water water or 11.1 mm in deeper water. The density is assumed to be constant everywhere with a value of 800 shoots/m^2, due to lack of additional data.

4.4 Sensitivity analysis

In order to explore the model behaviour, a sensitivity analysis is performed. This is done by varying (increasing or reducing) the value of a single parameter and comparing the output. The sensitivity analysis is limited to physical parameters only. The investigated parameters are listed below. The corresponding results can be found in Appendix C.

Table 4.1: Parameters sensitivity analysis

Module	Parameter
Flow	Bottom roughness - Manning value n
	Reef roughness - Manning value reef n_{reef}
Waves	JONSWAP bottom friction coefficient c_b
	Wave breaking parameter γ
Vegetation	Flow drag coefficient C_D
	Bulk drag coefficient $\tilde{C}_D$
	Seagrass density N_v

The forcing conditions were kept constant during the sensitivity runs. However, in a later stadium of the research is varied with the forcing conditions. The results, which can be found in Chapter 5 and Appendix D, show that mainly the waves and to a lesser extent the wind force the circulation in the bays. Changing the wave or wind conditions results in expected changes in water level set-up, flow velocities and wave height.

These are the main findings following from the sensitivity analysis.

- The reef roughness is more important than the general bottom roughness, as the circulation is mostly determined by the amount of water flowing over the reefs into the bays.
- Given the limited sensitivity to the JONSWAP bottom friction coefficient, the consequences of underestimating the wave dissipation over the reefs will be small.
- The wave conditions in the bays are largely determined by the reef height and to a lesser extent by the reef roughness.
- To calibrate the waves inside the bays, the wave breaking parameter is the most useful parameter.

- Bulk drag coefficient of seagrass is more sensitive than the flow drag coefficient. Via the bulk drag coefficient, wave damping by seagrass is taken into account. The altered wave conditions also affect the flow velocities. The flow drag coefficient only affects the flow directly.
- Seagrass density is a very sensitive parameter. A maximum in flow and wave attenuation is reached between 800 and 1000 shoots/m2.

The sensitivity analysis showed that the parameters which affect the waves directly, are the most sensitive ones. This will later be substantiated when is showed that the waves are the dominant forcing mechanism in the bays. So, the accuracy of the model will mainly depend on the performance of the wave modelling. The wave breaking parameter, bulk drag coefficient and seagrass density turn out to be important parameters regarding the wave modelling. The seagrass density can be measured. The bulk drag coefficient and wave breaking parameter can be used to calibrate the model and improve the model accuracy.

4.5 Model validation

As there is not sufficient data available to validate and calibrate the model completely, other ways of validation are used. First, the use of the model is justified by verifying the assumptions. Next, the model output is validated qualitatively based on expert judgement. Finally, the few data available is compared with model output.

The flow module of Delft3D FM is fully validated (Deltares, 2018a), but some assumptions are done. Its predecessor, Delft3D, is already successfully applied to similar cases (Lowe, Falter, Monismith, & Atkinson, 2009a), implying that Delft3D FM could be suitable for the modelling. Verifying the assumptions is only a first step in justifying the use of the model and validating the results. D-Flow FM solves the 2D shallow water equations. By assuming that the wave length is much longer than the water depth, vertical accelerations can be neglected and the vertical momentum equation reduces to the hydrostatic pressure gradient. In this case, the tidal wave length is indeed much longer than the water depth, so the shallow water equations may be applied. Notice that the propagation of short waves is modelled using the wave module (SWAN) which solves the spectral wave action balance.

Also the model output is inspected carefully. The simplified tide which is imposed at the eastern water level boundary, is reproduced as expected in both bays. Both the water level and velocity shows the corresponding signal in the bays and offshore. The main aspects of flow and wave patterns are represented accurately according to R.K. James and a local park ranger (personal communication, October 9, 2018) the main hydrodynamics aspects of the area are represented accurately. The wave-breaking on the reefs and the sheltered areas are captured correctly and the flow being squeezed around the islands into Baie de L'Embouchure is reproduced. Also areas of low flow velocities in Baie Orientale correspond with locations where a lot of lost items are found. However, the inflow at the South of Baie Orientale might be underestimated.

In Figure 4.5a, the model output is compared with a few measurements. This figure confirms that the inflow at the South of Baie Orientale is underestimated, because the modelled significant wave height is lower than the measured significant wave height in Baie Orientale. In Baie de L'Embouchure, the modelled significant wave height is higher than the measured significant

wave height, as can be seen in Figure 4.5b. It is likely that this is caused by errors in the reef bathymetry due to lacking data. Because the reef height mainly determines the wave height in the bays. Additionally, the bulk drag coefficient and wave breaking parameter can be used to further improve the model accuracy.

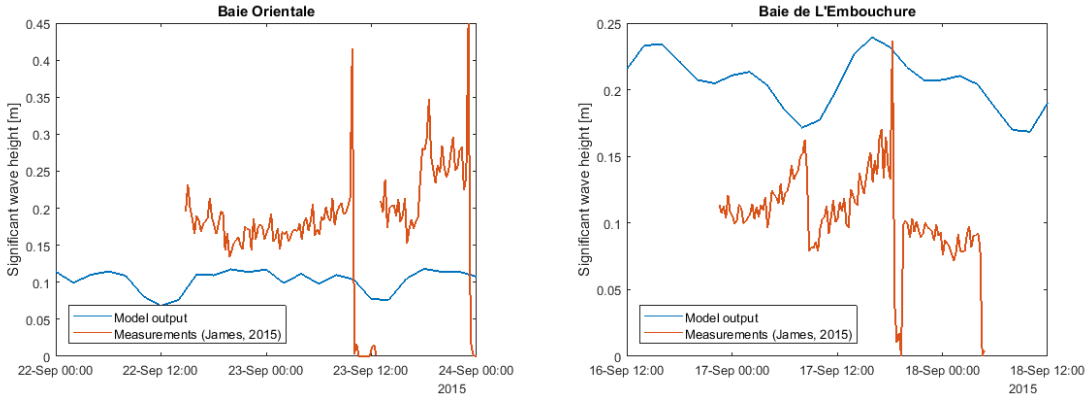

(a) Baie Orientale (b) Baie de L'Embouchure

Figure 4.5: Model validation - significant wave height

Altogether, there is sufficient ground to assume that the use of the model is justified and the results are useful. As the flow and wave patterns are reproduced correctly, this model is a good starting point and definitely fit for qualitative research. But when using it for quantitative analysis, one has to keep in mind that the situation is simplified and the model could not be calibrated with data which leads to mismatches between model output and real conditions.

4.6 Future scenarios

Before, the setup of the base scenario was described, which is mainly used to investigate the current situation. The next step is creating different scenarios to predict the impact of sea-level rise. As explained in Chapter 2, there are a lot of uncertainties regarding climate change. How the ecosystems will respond to changing conditions is unknown. Therefore, different scenarios are created. The potential impact of a certain amount of sea-level rise depends on different factors such as the response of the ecosystems to climate change and the changed hydrodynamics. Whether the coral reefs and seagrass meadows will survive is unknown and the amount of sediment accretion is uncertain. So, in order to identify the impact of a sea-level rise scenario, different simulations are set up. These simulations are based on the following assumptions.

- Three possible scenarios for the coral reefs
  1. Give up
  2. Catch up
  3. Keep up
- Seagrass dies or survives
- When the coral reefs are able to keep up, it is assumed that the conditions remain favorable for the seagrass too, and thus that the seagrass will certainly survive.

- Accretion can only occur if the seagrass is there to trap and stabilize the sediment.
- In case of seagrass survival, sediment accretion happens at the same rate as sea-level rise or not at all.

The principle of give up, catch up or keep up of the coral reefs is based on the theory as explained in Chapter 2 (Figure 2.6). This will be simulated by lowering the reefs by 1 m and reducing the bottom roughness, keeping the bathymetry of the reefs as it is now or increasing the reef height such that the water depth above the reefs remain constant despite the sea-level rise. The death of seagrass meadows will be simulated by turning the vegetation model off or on, such that wave and flow attenuation by the seagrass meadows is excluded. Sediment accretion will happen at the same rate as sea-level rise or not at all. In the case of accretion, the bed level in the bays is raised as much as the sea-level rises. This results in the following set of scenarios shown in Figure 4.6. The most right and left scenarios are the extreme ones, both the seagrass and coral reefs die and degrade versus unaffected, healthy ecosystems. In the end, some additional runs are done with different values for sea-level rise in order to relate the impact to the amount of sea-level rise.

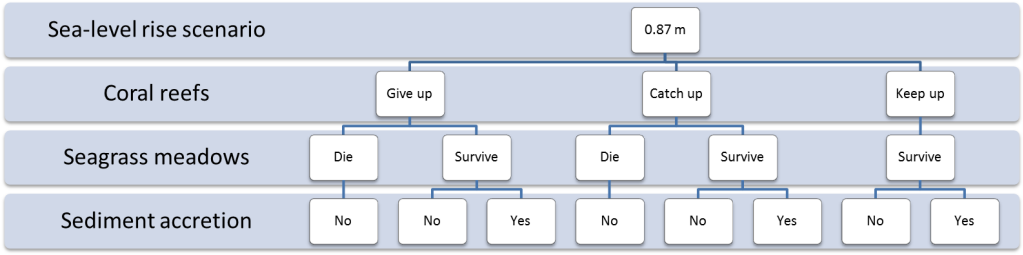

Figure 4.6: Tree of simulations in order to identify the range of impact of a sea-level rise scenario

Chapter 5

Hydrodynamics in the bays

The model, set up as discussed in the previous chapter, is first used to understand and analyse the hydrodynamics in and around the bays in the current situation. This starts by looking at water levels and flow patterns. Subsequently, the waves are considered and finally the effect of the coral reefs and seagrass meadows on the hydrodynamics is examined. The results of this chapter will also be used as reference in order to compare the impact of sea-level rise.

5.1 Water level and flow patterns

In order to discover the flow pattern and identify the dominant flow generating factors, at first the model is only forced with the tide. Subsequently, wind of 5m/s coming from the East and swell waves of 1.5 m also from the East are added as forcing. The results are shown in Figure 5.1 and 5.2.

The maximum tidal range is about 30 cm. The water level variations due to the tide are constant throughout the whole area without a phase lag. But, as can be seen in Figure 5.1a, a set-up of the water level over the reefs (up to 20 cm) and in Baie de L'Embouchure (up to 5 cm) is observed. As explained in Chapter 2, this is likely caused by wind and wave set-up. Figure 5.1b and 5.1c show the setup due to wind and waves separately.

Figure 5.2 shows the flow patterns due to different forcing. The tide sets motion to an alongshore current of 0.1 m/s from North to South. The wind does not affect this longshore current, but gives rise to small currents in the shallower parts of the area, especially over the reefs. But the waves are the dominant factor in forcing the flow. Looking at Figure 5.2c shows that the wave-induced currents overrule the tide-induced current offshore and amplifies the circulation in the bays which was already started by the wind.

Looking at the flow patterns in the bays (Figure 5.3), it is remarkable that the tide generates almost no current ($<$0.01 m/s). Offshore, the tide generates a current of 0.1 m/s which was not affected by the wind. But inside the bays, the wind starts a circulating current in both bays. In Baie Orientale, one can observe a flow over the reefs near Caye Verte and Îlet de Pinel directed into the bays and a small return current through the middle of the bay. The same pattern is observed in Baie de L'Embouchure. Water is pushed over the reefs and flows back via the gully to the ocean. This is exactly the circulation in the bays as was expected according to the theory that was explained in Section 2.2.4. However, the maximum flow velocities remain at $<$0.1 m/s small in both bays. Stronger flows occur when waves are also included as forcing. The flow pattern in both bays remains the same, but the circulation is amplified. Due to wave breaking

on the reefs (see next section), stronger currents up to 0.5 m/s flow over the reefs into Baie Orientale. As a result, the return currents also increase to 0.2 m/s. Baie de L'Embouchure is more sheltered. A strong wave-induced current of 0.5 m/s is observed near the reefs outside the bay. Although, the bathymetry steers this current past the bay, the waves do amplify the circulating current. Flow velocities increase up to 0.2 m/s.

In order to investigate the effect of increased wind speed, changed wind directions, increased wave height and changed wave directions, additional runs are done. The resulting figures can be found in Appendix D. An increased wind speed causes an increased wave height (with 0.15 m) in the bays and as a consequence, increased flow velocities (with 0.1 m/s). The wind direction has very little effect on the flow pattern, velocities or wave height. An increased wave height amplifies the circulation in the bays with 0.3 m/s. The wave direction does not affect the flow in the bays much, but it does affect the currents around the reefs due to a different wave breaking pattern. Around Caye Verte and offshore of Baie de L'Embouchure, the flow direction is opposite for waves coming from the Southeast. From this can be concluded that the flow pattern through and around the bays is determined by the wave direction. The higher the waves, the stronger the resulting currents are. An increased wind speed with the right direction can further amplify the waves and currents, but is not the main factor in determining the flow pattern.

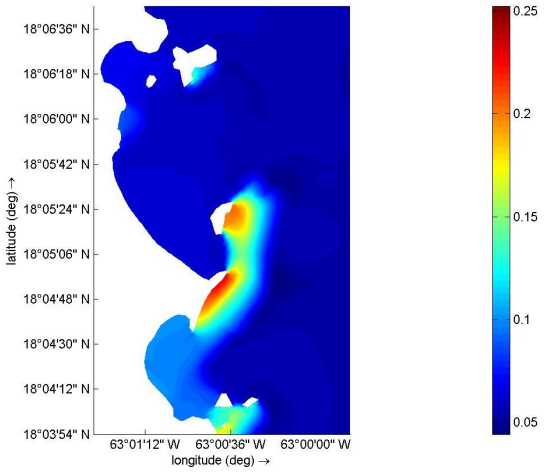

(a) Water level [m]

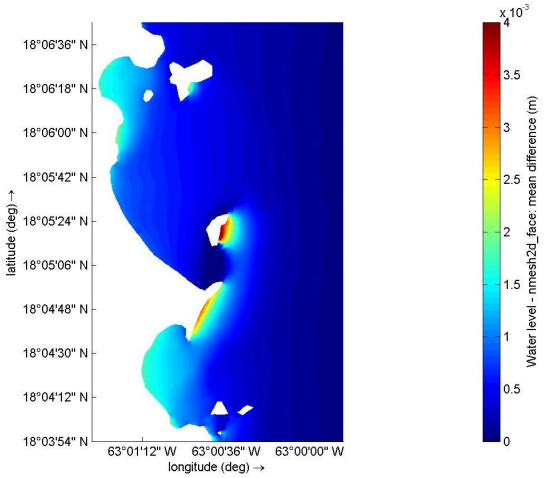

(b) Wind-induced set-up [m]

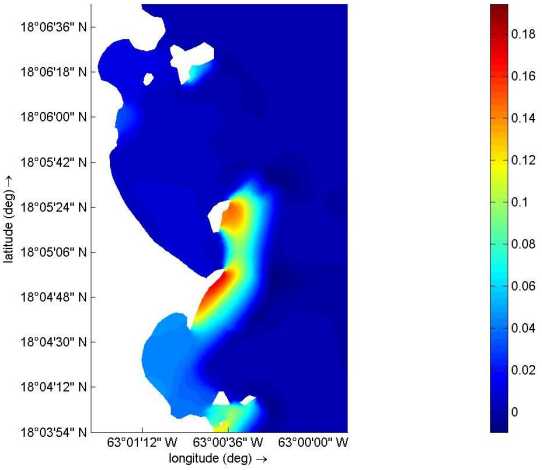

(c) Wave-induced set-up [m]

Figure 5.1: Water level and set-up

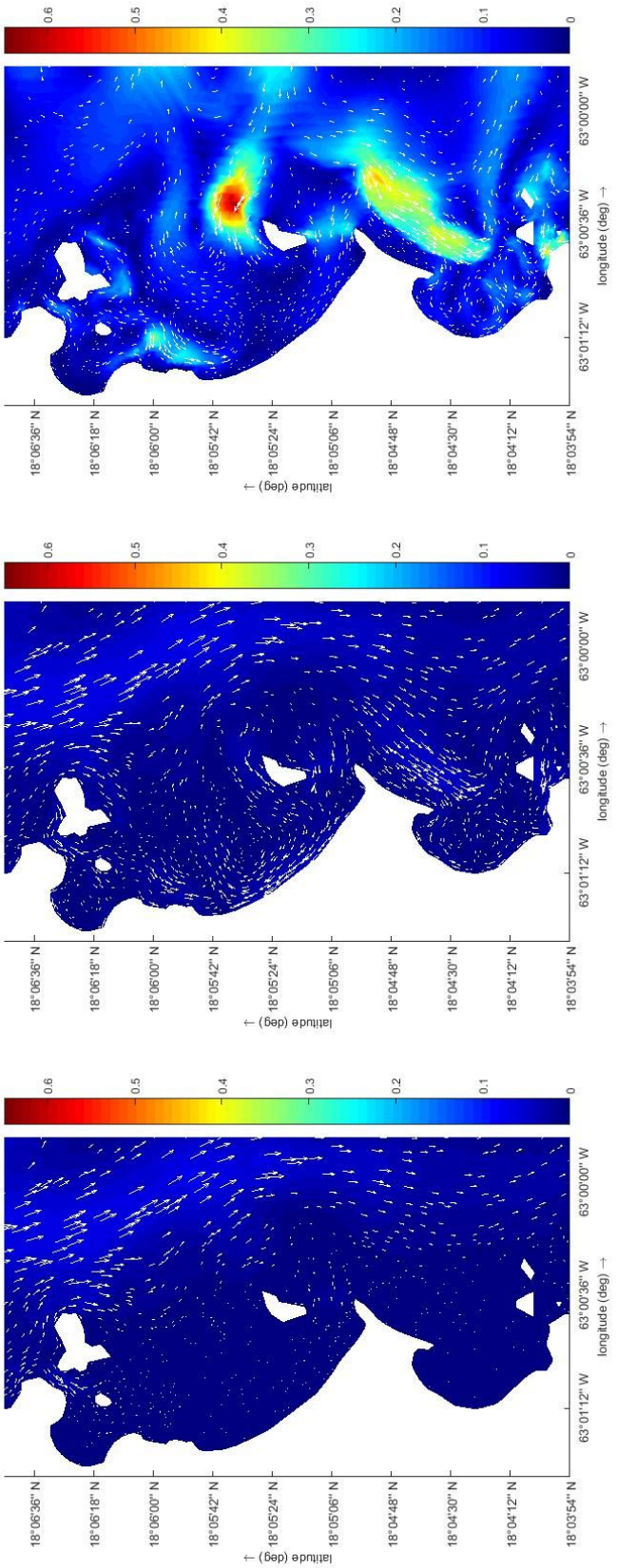

(a) Tide (b) Wind and tide (c) Waves, wind and tide

Figure 5.2: Flow patterns in the bays due to different forcing [m/s]

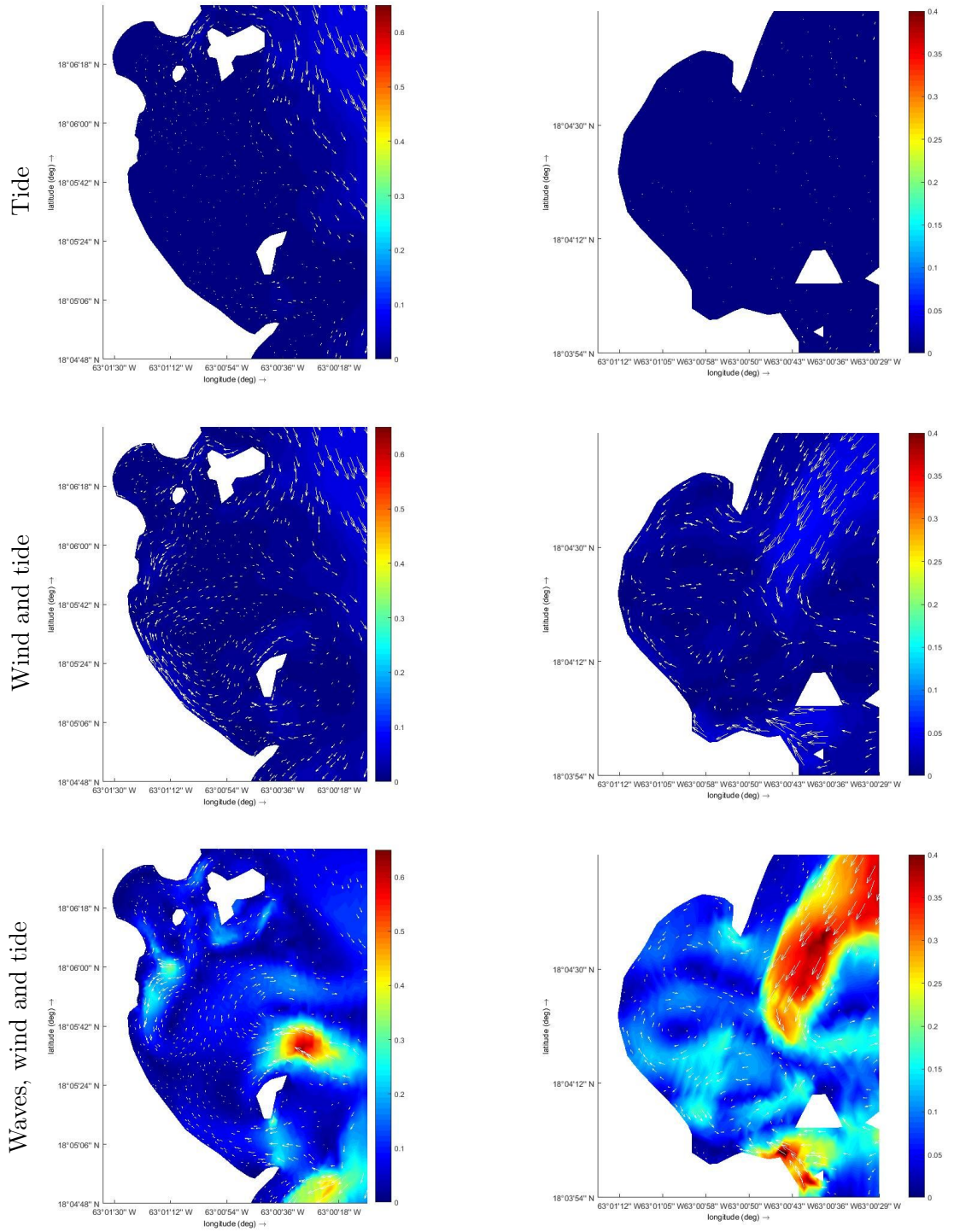

(a) Baie Orientale (b) Baie de L'Embouchure

Figure 5.3: Flow velocities due to different forcing [m/s]

5.2 Waves

The waves are also modelled in and around the bays. In Figure 5.4, the signifcant wave height in the area is shown. In this case, the waves at the boundary come from the East and the significant wave height is 1.5 m. Offshore, the significant wave height remains constant. Towards the reefs in front of the bays shoaling is observed. In between Ile Tintamarre and Pinel Island, a sheltered zone with reduced wave height is found. Ile Tintamarre shelters this area for incoming waves from the East. Due to diffraction, still waves of 0.5 m high enter this part. Looking more closely at the bays in Figure 5.4b, the shoaling towards the reefs and wave breaking on the reefs is clearly visible. Inside Baie de L'Embouchure, the wave environment with a maximum wave height of 0.6 m is calm. Baie Orientale is less sheltered. The northern reef attached to Pinel Island lies deeper and is therefore less efficient in dissipating waves. Here, a significant wave height up to 1.2 m is found. The southern part of this bay is more protected due to Caye Verte and its surrounding reefs. But diffraction leads to waves of 0.3-0.6 m in this zone.

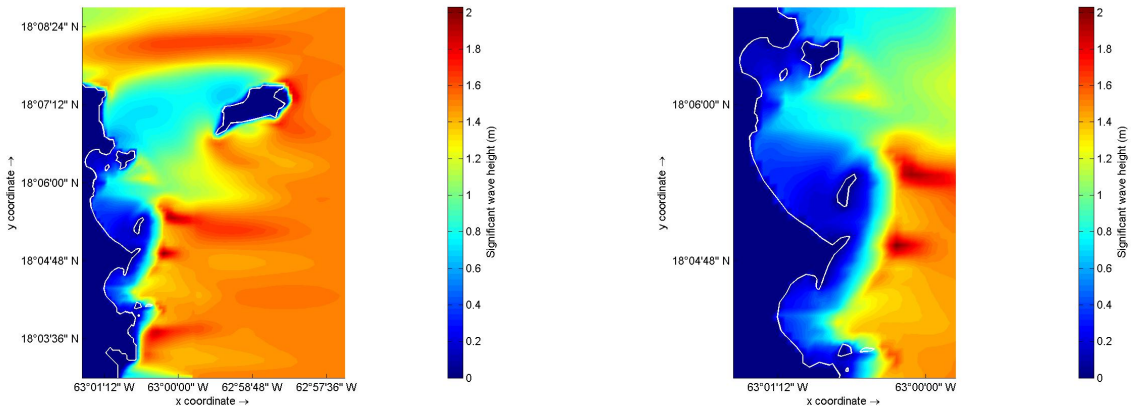

(a) Total wave grid

(b) In the area of interest

Figure 5.4: Significant wave height [m]

5.3 Effect of seagrass

As explained in Chapter 2, seagrass should be able to attenuate flows and dissipate waves. In Figure 5.5, the impact of including seagrass in the hydrodynamic model is shown. The effect is especially clear in Baie Orientale. The return current is pushed northwards. Over the seagrass meadows the flow velocity is reduced and as a result, the flow velocities around the meadows have increased.

Figure 5.5b shows the difference due to the presence of seagrass meadows. The effect of wave dissipation is clearly visible where seagrass is present. The depth-averaged flow velocity is also reduced up to 0.2 m/s by the seagrass and around the meadows some increase in flow velocity is observed. The increase in flow velocity in Baie de L'Embouchure is remarkable. But the presence of seagrass causes a small set-up of the water level in this bay. Although, the RMS wave height is reduced, this resulted in an increase of wave forcing and Stokes drift leading to

the increase of flow velocity.

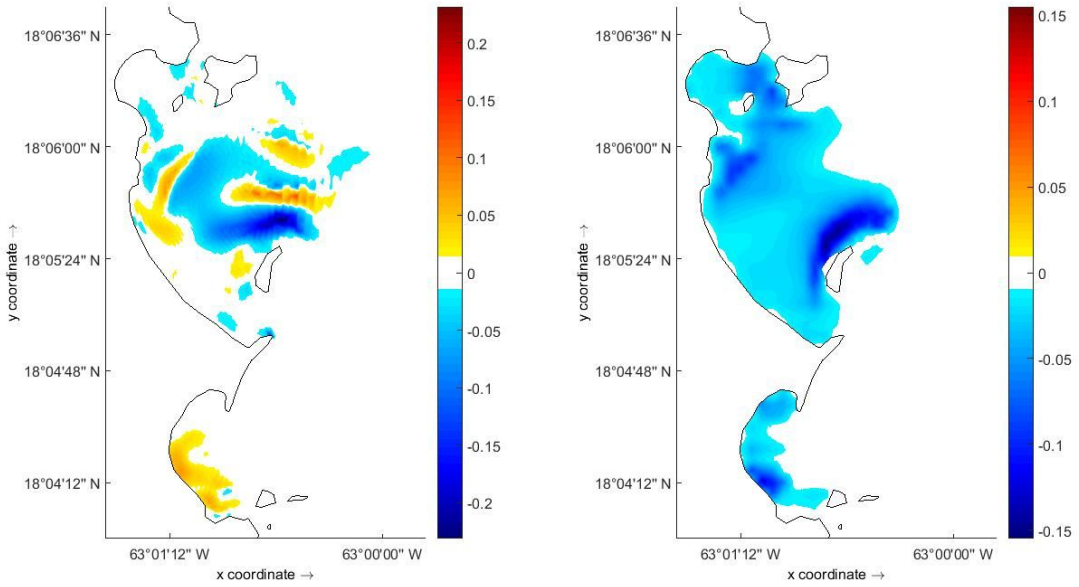

(a) Flow velocity difference [m/s]

(b) RMS wave height difference [m]

Figure 5.5: Effect of seagrass on hydrodynamics

5.4 Effect of reefs

In short, including the roughness of the reefs leads to reduced flow velocities over the reefs due to increased bottom friction. This leads to a small shift of flows. The velocities over the reefs are reduced by 0.5 m/s. At some spots, the flow velocity around the reefs slightly increased by maximum 0.1 m/s. This is most clearly visible in the gully between the two reefs in front of Baie Orientale.

When looking at the difference in wave height due to the increased bottom roughness of the reefs, one has to keep in mind that this is only applied in the flow module, as it is no possible to spatially vary the bottom roughness in the wave module. Theoretically, the reef roughness should lead to more wave dissipation over the reefs and thus a decreased wave height over the reefs and in the bays. However, only a constant wave bottom friction can be applied. Thus, this cannot be reproduced by the model. The observed change in wave height, as shown in Figure 5.6b, is caused by changed wave-current interactions.

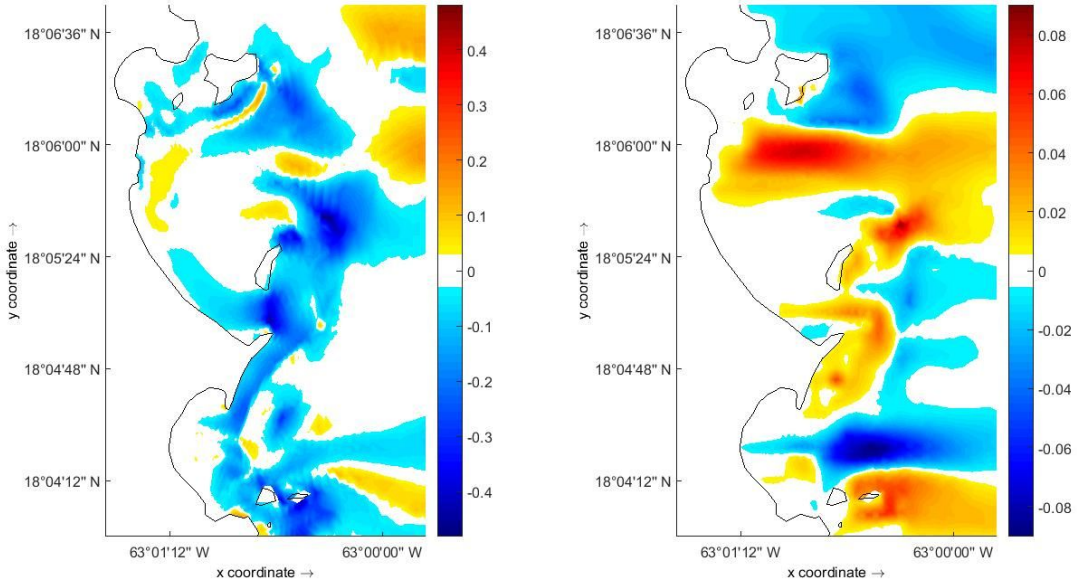

(a) Flow velocity difference [m/s]

(b) RMS wave height difference [m]

Figure 5.6: Effect of reef roughness on hydrodynamics

Chapter 6

Impact of sea-level rise on hydrodynamics

In the previous chapter, the hydrodynamics in the bays under the current conditions were described. Next, scenarios were set up in order to identify the potential impact of sea-level rise under different circumstances. These scenarios were described in Section 4.6. In this chapter, the results of these simulations are presented and analysed. The results are compared at two locations, one in the southern, sheltered part of Baie Orientale and one in Baie de L'Embouchure.

6.1 First scenario

In order to identify the impact of the sea-level rise on the hydrodynamics in the bays, one scenario as starting point is needed. Compared with the reference case presented in the previous chapter, only the water level is risen with 0.87 m. This is the sea-level rise in 2100 under RCP8.5 predicted by Jevrejeva et al. (2016). Assumed is that the coral reefs catch up later and the seagrass meadows are still there. The bathymetry remains unchanged in this scenario compared to the reference case.

The results are shown in Figure 6.1. Wave dissipation over the reefs reduced due to the increased water depth. This leads to an increase in RMS wave height of 0.2 m in the sheltered areas of both bays. Due to the larger waves, also the flow velocities increased with 0.15 m/s to in Baie Orientale and with 0.1 m/s to 0.2 m/s in Baie de L'Embouchure. This implies roughly a doubling of the flow velocity in the sheltered part of Baie Orientale and an increase by a factor of 1.5 in Baie de L'Embouchure. The flow pattern remains unchanged. The reduction in flow velocity North of Orient Beach is remarkable. This is caused by the increased water depth, while the forcing is unaffected here leading to a decrease of the depth-averaged flow velocity.

Due to the increased water level, the importance of the forcing mechanisms might be changed. In Figure 6.2, the results at two locations from runs where respectively waves, wind and tide, wind and tide or tide is used as forcing. The flow velocity has increased for every run due to the sea-level rise. The waves remain the dominant mechanism followed by the wind and tide.

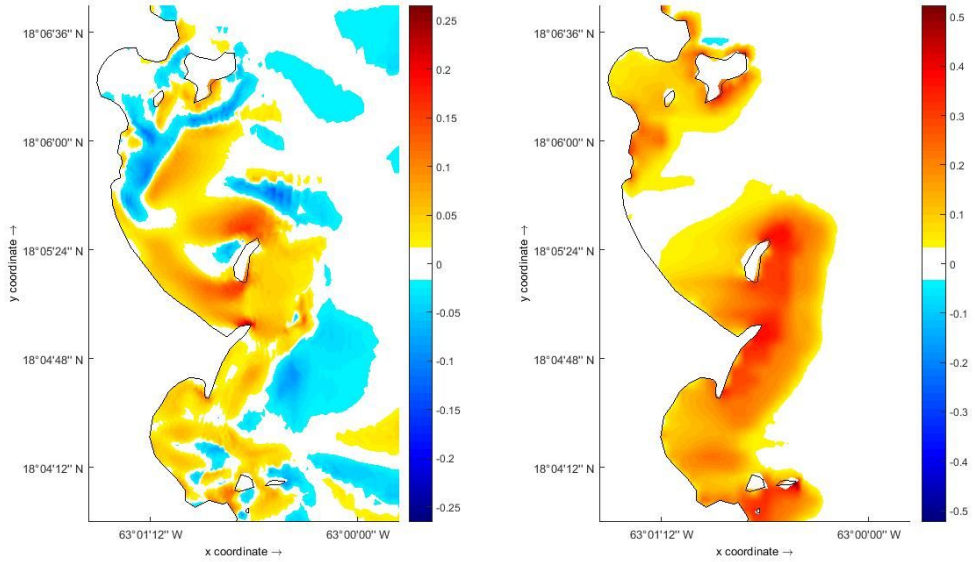

(a) Flow velocity difference [m/s] (b) RMS wave height difference [m]

Figure 6.1: Effect of 0.87 m sea-level rise on hydrodynamics

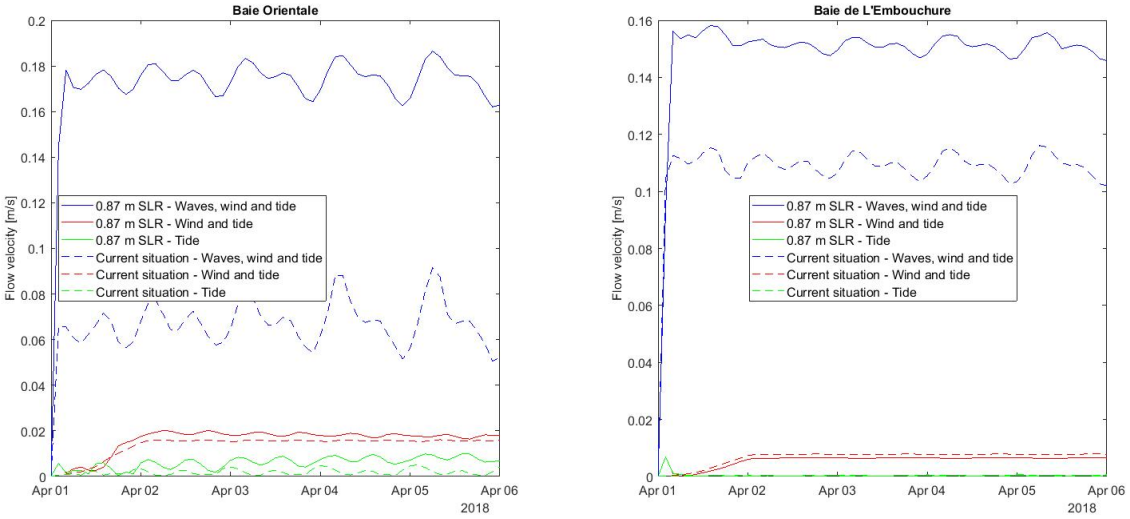

(a) Baie Orientale (b) Baie de L'Embouchure

Figure 6.2: Flow velocity at two locations due to different forcing

6.2 Growth of coral reefs

So, we have seen a first indication of what might be the impact of the sea-level rise. The change in hydrodynamics is mainly determined by the wave dissipation over the coral reefs. But as explained before, the response of the coral reefs to climate change is uncertain. Three scenarios are run in order to identify the impact under different responses of the coral reefs to climate change.

The 'give up'- and 'catch up'-scenario represents situations where the water depth above the reefs increases. For the 'keep up'-scenario, the water depth is exactly the same as in the current situation. Looking at the results shown in Figure 6.3, it can be immediately seen that an increased water depth above the reefs leads to an increased wave height in the bays. Larger waves induce stronger currents over the reefs and through both bays.

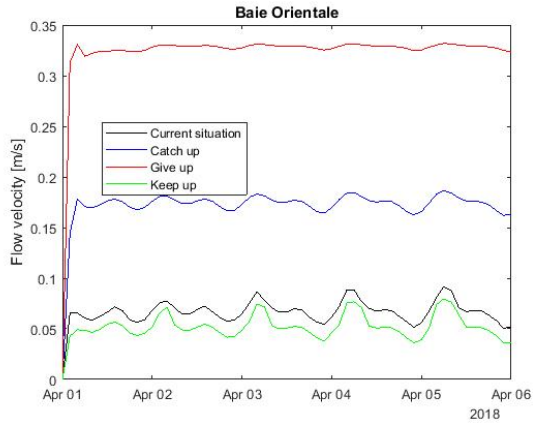

(a) Impact on flow velocity - Baie Orientale

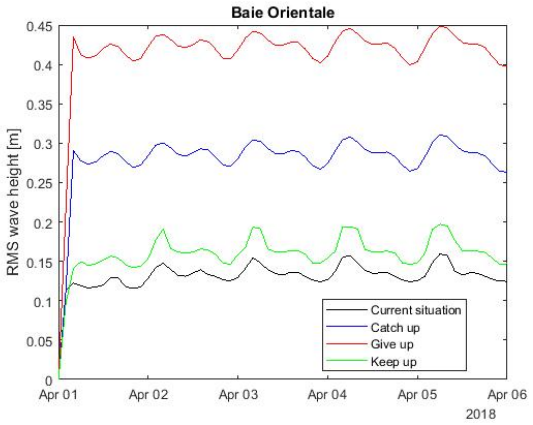

(b) Impact on wave height - Baie Orientale

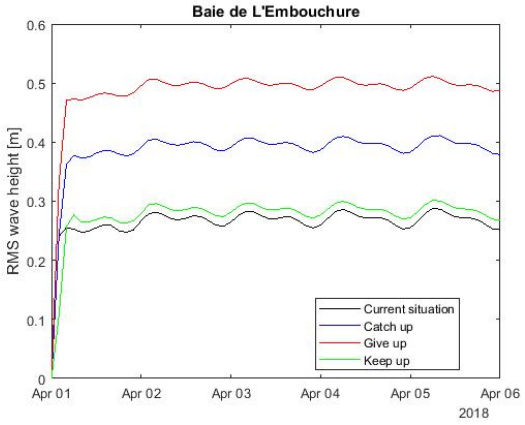

(c) Impact on flow velocity - Baie de L'Embouchure

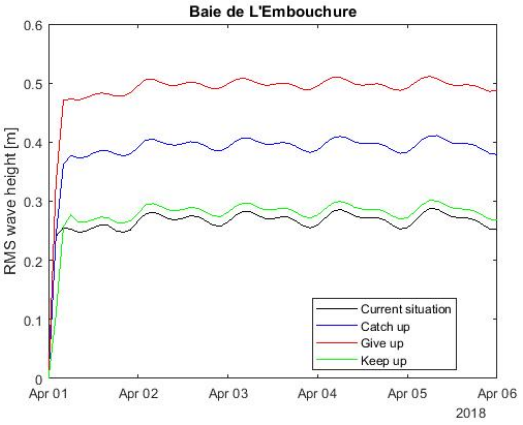

(d) Impact on wave height - Baie de L'Embouchure

Figure 6.3: Impact of different coral growth scenarios

6.3 Death of seagrass meadows

It is likely that the wave height in the bays will increase because of the response of the reefs to climate change. But survival of seagrass can mitigate this effect because of the ability to damp waves and currents. This is shown in Figure 6.4. Compared with the current situation, wave height and flow velocity will increase due to the increased water depth above the reefs. But the death of seagrass seagrass will even lead to a larger increase of flow velocity and wave height. A loss of seagrass will worsen the situation more (dashed versus solid green line) than the difference between the 'give up'- and 'catch up'-scenario for the reefs (red versus green solid line).

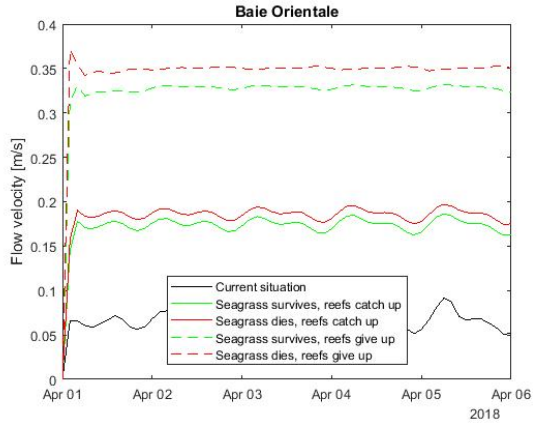

(a) Impact on flow velocity - Baie Orientale

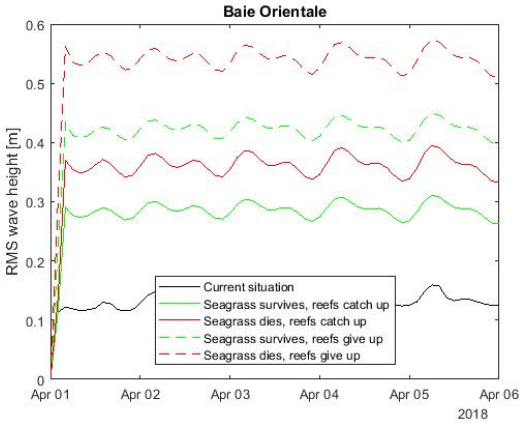

(b) Impact on wave height - Baie orientale

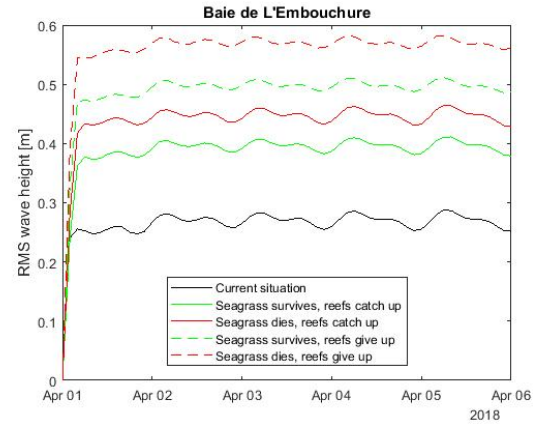

(c) Impact on flow velocity - Baie de L'Embouchure

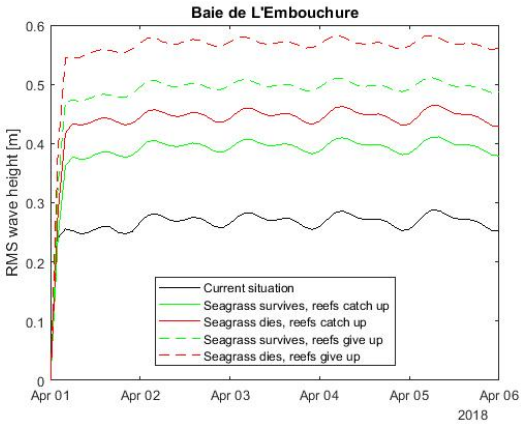

(d) Impact on wave height - Baie de L'Embouchure

Figure 6.4: Impact of death seagrass meadows

6.4 Sediment accretion

Due to sea-level rise, the water depth in the bays increases. But this could be (partly) mitigated by the sediment supply. The calcifying algae form together with the coral reefs an important source of sediment for the bays. If this sediment supply is sufficient to let the bottom level rise with the same rate as the sea-level, the water depth in the bays remains constant. In Figure 6.5, the results are shown of different scenarios with/without accretion. The reduced water depth leads to a lower RMS wave height in the bays. In Baie de L'Embouchure, the flow velocities will reduce too. The effect of the flow velocities in Baie Orientale depends on the response of coral reefs to climate change. In case of the 'catch up'- and 'keep up'-scenario results accretion in an increase of flow velocity. So, accretion could reduce the impact of sea-level rise, but it is dependent on the response of the coral reefs.

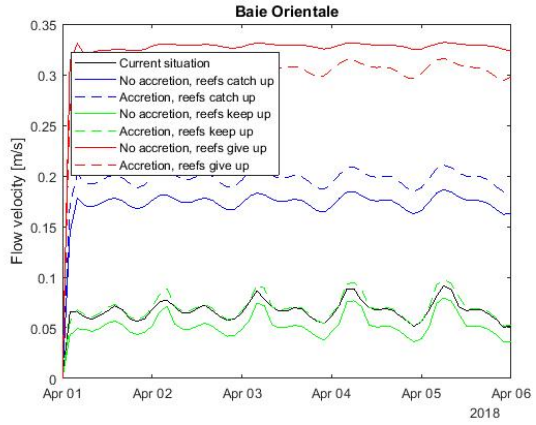

(a) Impact on flow velocity - Baie Orientale

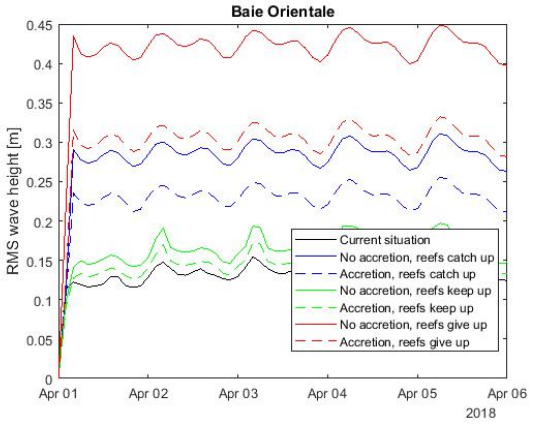

(b) Impact on wave height - Baie orientale

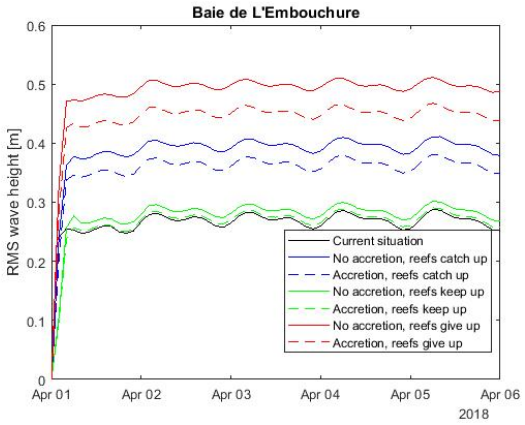

(c) Impact on flow velocity - Baie de L'Embouchure

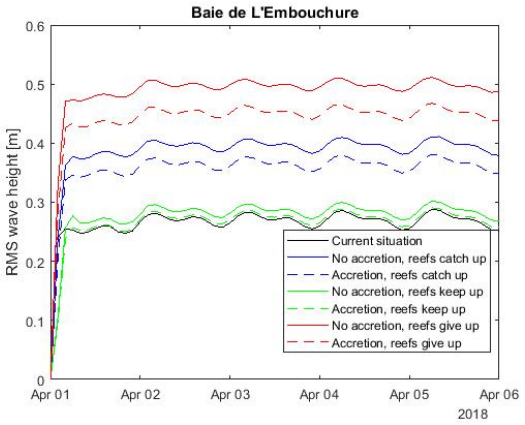

(d) Impact on wave height - Baie de L'Embouchure

Figure 6.5: Impact of sediment accretion

6.5 Extreme scenarios

Insight has been gained on how the different elements affect the impact of sea-level rise on the hydrodynamics, so it is time to look at the most extreme scenarios under a sea-level rise of 0.87 m.

The worst-case scenario is of course when the coral reefs give up and degrade and the seagrass die. The impact is especially large in the sheltered part of Baie Orientale where the flow velocities increase by a factor 6 and the RMS wave height increase from 0.13 m to 0.55 m. In Baie de L'Embouchure, the RMS wave height is doubled and flow velocities have increased by 20%.

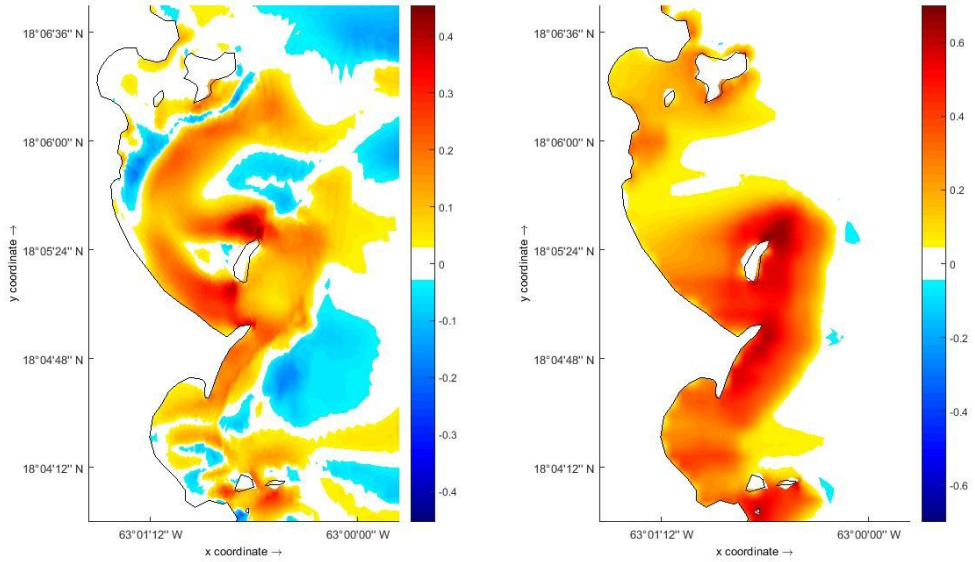

(a) Flow velocity difference [m/s] (b) RMS wave height difference [m]

Figure 6.6: Worst case scenario: death of seagrass meadows and degradation of coral reefs

The better scenario would be if the coral reefs are able to keep up with sea-level rise, the se agrass meadows survive and sediment accretion occurs in the bays such that the water depth does not increase. In this case, the flow velocity remains constant in Baie Orientale and the RMS wave height increases by 0.02 m ($\approx 10\%$). In Baie de L'Embouchure, the RMS wave height remains unchanged, while the flow velocity increases by 0.01 m/s ($\approx 10\%$).

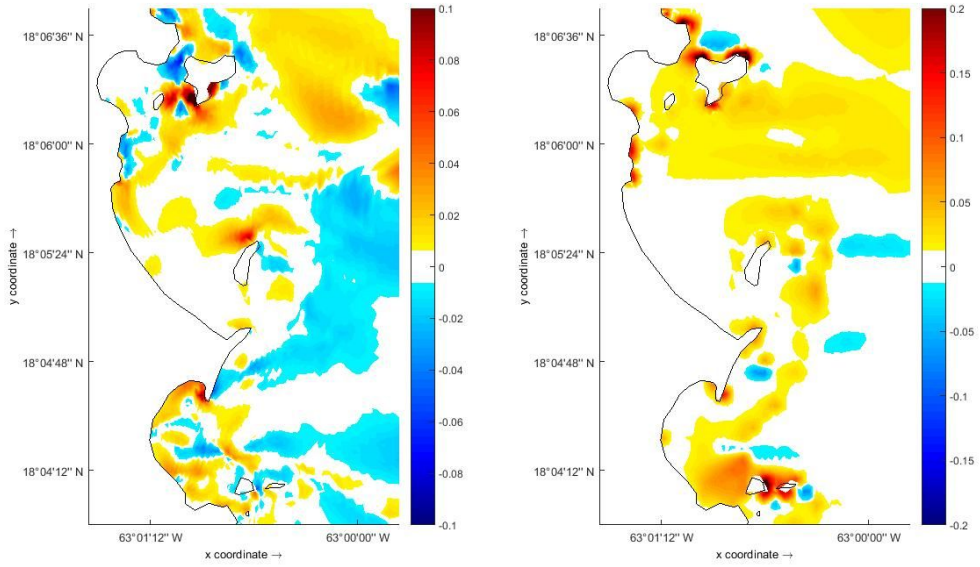

(a) Flow velocity difference [m/s] (b) RMS wave height difference [m]

Figure 6.7: Best-case scenario: coral reefs keep up, seagrass meadows survive and sediment accretion occurs

6.6 Other sea-level rise scenarios

To end with, also simulations are run in order to identify the impact of different sea-level rise scenarios. Three different scenarios are investigated, namely a sea-level rise of respectively 0.21 m, 0.60 m and 0.87 m which correspond with the years 2041, 2083 and 2100. The 'catch up'-scenario for coral reefs and survival of seagrass is assumed. The results are shown in Figure 6.8. The higher the sea-level rise, the larger the increase in flow velocity and RMS wave height will be.

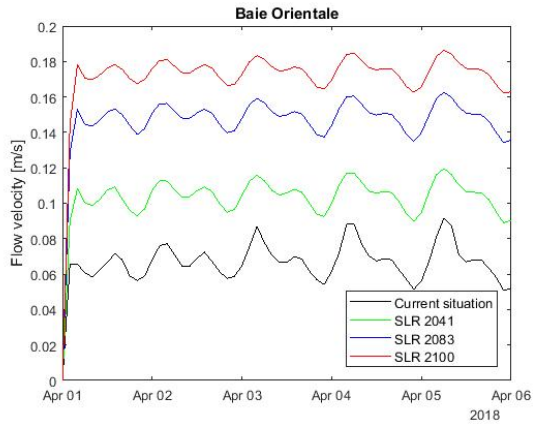

(a) Impact on flow velocity - Baie Orientale

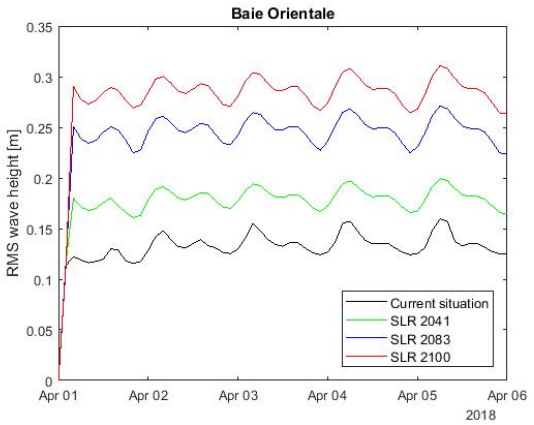

(b) Impact on wave height - Baie Orientale

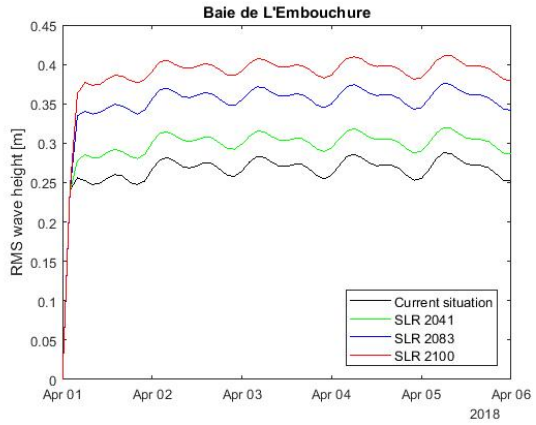

(c) Impact on flow velocity - Baie de L'Embouchure

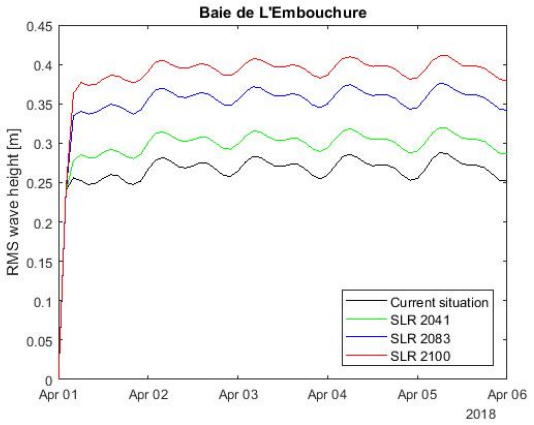

(d) Impact on wave height - Baie de L'Embouchure

Figure 6.8: Impact of different sea-level rise scenarios in combination with the death/survival of seagrass

Chapter 7

Discussion

Before the research questions are answered and main conclusions are drawn, a reflection on the performed research is made. In this way, the value of the research results can be put into perspective leading to a stronger conclusion. The method, the availability of data and finally the results are discussed in this chapter.

7.1 Reflection on methodology

In fact, this research consisted of two parts. The first part was about setting up a hydrodynamic model of the area which is able to include the effect of the seagrass meadows and coral reefs. The next part was about predicting the impact of sea-level rise by running future scenarios with the hydrodynamic model. This section reflects on the model setup and the future scenarios.

7.1.1 Model discussion

Delft3D FM is able to simulate flow and waves. Also the damping by vegetation of flow and waves can be included. Lowe et al. (2009a) showed that Delft3D can be successfully used for a numerical study of a reef-lagoon system similar to what was considered during this thesis project. So, the model is able to take into account the important processes and has been applied successfully in previous studies. During the model validation was showed that the model is able to reproduce the main hydrodynamic aspects of the area. But a complete calibration and validation was not possible due to missing data.

There were also some limitations in the model and model setup. First of all, a two-dimensional depth-averaged model is set up. This implies that vertical variations in velocity are not taken into account. Besides, density-driven currents are excluded as temperature and salinity are taken constant and sediment transport is not included. Coriolis is neglected as forcing. This can be justified with the Rossby number $Ro = \frac{u}{fL}$ ($\frac{L}{u} < f^{-1} \rightarrow \frac{1000}{0.2} < 22272$). At the boundaries of the computational domain, boundary conditions are imposed in order to reproduce the currents inside the basin as accurate as possible. The eastern boundary is a water level boundary representing the (simplified) tide. The lateral boundaries are Neumann boundaries allowing the water to flow freely. Regional large-scale currents are not taken into account. But as the tide-induced currents do not affect the circulation in the bays, the effect is expected to be small.

The sensitivity analysis showed that the wave-related parameters had the biggest influence on the results. The biggest limitation of the wave model for this study is that it is not possible to vary the JONSWAP bottom friction coefficient spatially (Deltares, 2018d). So, a choice was made between applying the friction coefficient for a sandy bottom ($c_b = 0.038 m^2/s^3$) everywhere and

thus, underestimating the wave dissipation due to bottom friction over the reefs and applying the reef friction coefficient ($c_b = 0.05m^2/s^3$ as used by Cialone and Smith (2007)) such that the wave dissipation due to bottom friction is overestimated. In Figure 7.1, the relative difference between the two runs is shown. The difference in flow velocity is less than 0.01 m/s in the bays and the RMS wave height differs about 0.01 m. The choice to apply a wave bottom friction coefficient of $0.038m^2/s^3$ leads to a small underestimation of the wave dissipation due to bottom friction and thus an overestimation of the wave height in bays. But this is less than 10%. Apparently, depth-induced wave-breaking on the reefs is far more important than wave dissipation due to bottom friction when looking at the wave transformation over the reefs. This implies that the reef height, compared with the reef roughness, is more important for the wave conditions behind the reefs. However, the reef roughness still affects the flow over the reefs strongly as was shown in Section 5.4.

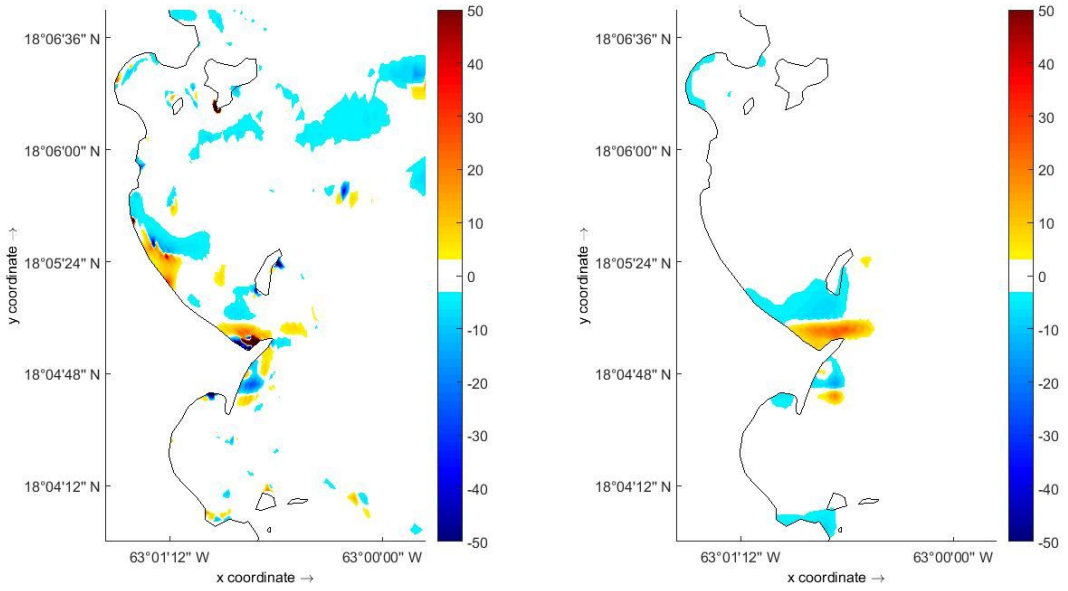

(a) Difference in flow velocity [%]

(b) Difference in RMS wave height [%]

Figure 7.1: Effect of wave bottom friction coefficient ($c_b = 0.05m^2/s^3$ - $c_b = 0.038m^2/s^3$)

7.1.2 Future scenarios

How global climate change will evolve is very uncertain, and thus the response of local tropical ecosystems is even more unpredictable. Each scenario in this study consists of a certain sea-level rise combined with a growth scenario of the coral reefs, the death/survival of seagrass meadows and possible accretion in the bays. Of course, this is a very simplified representation of all potential future scenarios. The growth or degradation of coral reefs will not be constant throughout the whole area. The same applies for the death or survival of seagrass meadows. Also the composition might change. And if accretion occurs, the bed level will certainly not rise with a uniform value, but a spatial pattern of accretion and erosion will be observed. However, simplifying potential consequences enables us to identify the impact of sea-level rise without disregarding all the uncertainties coming with the response of ecosystems to climate change.

7.2 Data availability

As already mentioned shortly in the previous section, sometimes the model input was simplified. This had mainly two reasons. First, it prevented the model from becoming too complex such that linking the impact to the affected processes became complicated. But also lack of data was one of the reasons. The lack of bathymetric and wave data were the major problems as they determine largely the hydrodynamics in the bays. Minor issues came with the lack of wind data and information about the seagrass meadows and coral reefs.

Bathymetry No single bathymetric dataset with sufficient resolution was available for the area of interest. Three sources were combined to create a bathymetry. The reference level of the sonar charts (Navionics, 2018) was unknown. Also no detailed bathymetry data of the reefs was available. These parts were filled using interpolation. Especially, more detailed data about the reef bathymetry would improve the model accuracy, as the sensitivity analysis showed that the reef bathymetry mainly determines the wave and resulting flow conditions in the bays. So, while interpreting the results, one has to keep in mind that here might be a deviation due to the interpolation of reef bathymetry.

Waves Offshore wave data was also missing. The nearest wave buoy is located 600 km away. This requires additional wave modelling, which was outside the scope of this thesis project. Using surf forecasts, impressions of the wave conditions could be obtained. Based on this, the model was forced with a constant wave spectrum during the simulation period. As the waves are the dominant forcing of flow in the bays, this is a shortcoming in this study.

Wind The wind forcing was also simplified. As the interest was understanding the average conditions and not the impact of a single event, the applied wind field was uniform over the domain and constant during the simulation period. Of course, this is not realistic. But due to the dominance of the wave forcing, this limitation is less significant.

Vegetation The reef coverage is estimated using aerial images and maps. Also data is lacking on the reef roughness and bathymetry. The effect of the reefs on the hydrodynamics was still clearly present under the simplified representation of the reefs. But, as said before, the reefs mainly determine the hydrodynamic conditions in the bays, so more detailed data on the reefs would improve the model accuracy. The same holds for the presence and properties of seagrass meadows. By simplifying the seagrass meadows, the effect of seagrass is included. But the sensitivity analysis showed that the density of seagrass does have significant impact. So, more data about the spatial variability in density of seagrass contributes to a correcter representation of the actual flow in the bays.

7.3 Impact of sea-level rise

In the previous sections, the methodology was reflected on and the main shortcomings of this study were discussed. So, now the results can be put into perspective. As shown in Chapter 6, sea-level rise will cause an increase in hydrodynamic stresses. Flow velocity and wave height increase in both bays. However, the results showed that seagrass meadows, coral reefs and to a lesser extent sediment accretion can mitigate the impact. But what is the response of the

ecosystems to the changed hydrodynamics? This response will determine the final impact of sea-level rise.

7.3.1 Impact on bed shear stress

The increased flow velocities and wave height will lead to higher bed shear stresses, as the bed shear stress is directly related to the flow velocity and wave orbital velocity.

$$\tau \propto u^2, \tau \propto u_{orb}^2$$

Higher bed shear stresses could potentially lead to increased suspended sediment concentrations which are unfavourable for both seagrass and corals, and might cause erosion of sediment, seagrass meadows and coral reefs. The model output can be used to determine the change in bed shear stress. Subsequently, this can be used to determine the response of the ecosystems.

A bed shear stress analysis has been performed and is presented in Appendix E. As explained in the appendix, the computed bed shear stress by the model does not look reliable. Therefore, only the current-induced bed shear stress is used, which approximates the actual bed shear stress in the bays where wave action is limited and seagrass is present. Whether sediment particals start moving can be determined with the critical shear stress it can be determined whether sediment particles start moving. Using Eq. 2.7, the critical bed shear stress for carbonate sediments with a median grain size of 0.5 mm as found by James (2016b), is estimated to be 1.4 N/m^2.

In Figure 7.2, the current-induced bed shear stress for the worst case scenario is plotted. In Baie de L'Embouchure the bed shear stress does not exceed 0.3 N/m^2, so no erosion will occur there as the critical bed shear stress is not exceeded. In Baie Orientale, the bed shear stress does is lower than 0.5 N/m^2 almost everywhere. Only just North of Caye Verte, erosion is expected on the transition from seagrass meadow to coral reef.

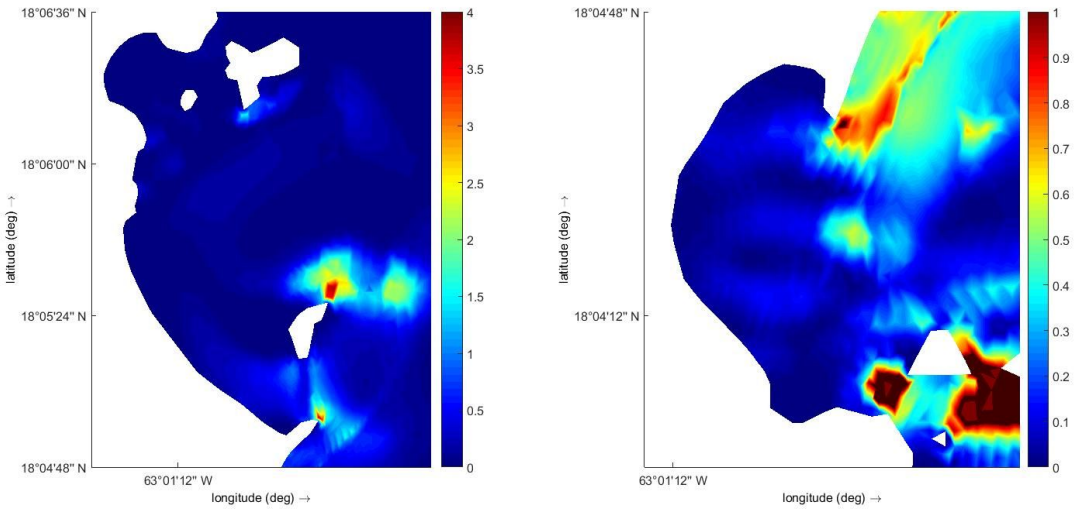

(a) Baie Orientale (b) Baie de L'Embouchure

Figure 7.2: Bed shear stress [N/m^2] in the bays under worst-case scenario in the bays

7.3.2 Response of ecosystems

In the previous paragraph, the impact of sea-level rise on the bed shear stress is determined. This is used to determine the response of ecosystems. The likeliness of the scenarios, and thus the impact, depends on this response.

Coral reefs As coral reefs already occur in the zones with the largest hydrodynamic-induced forces due to wave-breaking, increased bed shear stresses will supposedly not lead to the erosion of coral reefs. The increased water level is a limiting factor if the water depth exceeds 25 m (Lalli & Parsons, 1997). As water depth does not exceed 15 m above the reefs, this will not be the case. Increased sediment concentrations due to the higher bed shear stress could affect the corals due to reduced light penetration or the corals could be smothered with sediment. However, including sediment transport is outside the scope of this thesis project. Thus, as far as considered, the changed hydrodynamic conditions will not determine the response of coral reefs to climate change. This will likely be determined by the rising water temperature and changing pH (Hoegh-Guldberg, 1999).

Seagrass meadows The response of seagrass meadows in the bays will be determined by the currents and waves as the depth limit is not exceeded, which was 10 m for *Thalassia testudinum* (Short et al., 2010). Based on the modelled increase of wave height and flow velocity, it is not expected that the seagrass will disappear completely.

Interesting is the difference in seagrass cover throughout Baie Orientale. In the northern part, where the waves are higher, the seagrass cover is patchy. While in the southern part, which is more sheltered, a dense cover of seagrass is found. Along the coastline where the water depth is limited and in the northeastern corner of the bay where the highest waves occur, seagrass is absent. So, this indicates that the hydrodynamic conditions affect the presence of seagrass. Under future sea-level rise, the stresses acting on the seagrass change, which might lead to a redistribution of the seagrass.

In order to predict this change in seagrass, a logistic regression is performed. Based on the water depth, water depth squared and wave height * water depth, the probability of occurrence of seagrass in the bay is determined for the current conditions. Using the conditions of a future scenario, the change in occurrence can be predicted. A full explanation can be found in Appendix F. It has to be noted that using this approach, the absence of seagrass in the deep central gully cannot be explained.

This approach is applied to the worst-case scenario and the results are presented in Figure 7.3. It is showed that the probability of occurrence increases in the western parts of the bay. Due to the increased water depth, stresses will reduce enabling seagrasses to grow. In the deeper parts, the light availability is reduced, leading to a decrease of seagrass. Also behind the Caye Verte, where the wave height increases, the probability of occurrence reduced due to the increased wave height.

This result shows that it is likely that the seagrass will be affected to changing hydrodynamic conditions and underscores the need for a seagrass distribution model in order to improve the accuracy of the model and future predictions.

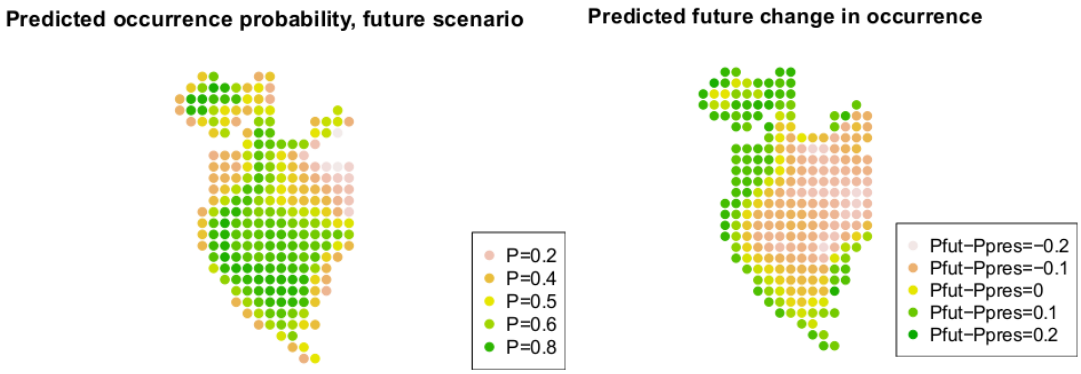

Figure 7.3: Effect on probability of occurrence of seagrass due to sea-level rise

Sediment accretion Sediment accretion was assumed to be constant and uniform. This is very unrealistic. A sedimentation-erosion pattern is more likely, and sedimentation will mainly occur where seagrass is present to stabilize sediment. So, the results indicate that sediment could mitigate the impact of sea-level rise, but this cannot be concluded from this research. A morphological study will be necessary. This morphological study can also reveal what the impact of the changed bed shear stress on the morphology is.

7.3.3 Likeliness scenarios

The scenarios were based on a number of assumptions. Also a worst- and best-case scenario were run. Based on the presumable response of the ecosystems, a relative likeliness of the scenarios can be identified. The best-case scenario assumes that coral reefs are able to keep up with sea-level rise and uniform sediment accretion will occur. However, we have seen that this is not realistic. On the other hand, in the worst-case scenario the total disappearance of seagrass meadows is assumed. But based on the changed hydrodynamics, this is showed to be unlikely. Therefore, a more moderate scenario is more likely. The final scenario will depend on the response of coral reefs to climate change in the first place. This response will mainly determine the change in hydrodynamics. And these change in hydrodynamics will lead to a potential change in seagrass occurrence.

7.3.4 Impact of hurricane Irma

The results indicate that the impact of sea-level rise and the changed hydrodynamics on the ecosystems is limited. But is this realistic? On September 6 2017, Saint Martin was hit by hurricane Irma. The bays were exposed to extreme conditions. Irma caused Wind speeds of 80 m/s (Meteorological Department St. Maarten, 2017). But also during this event, the system showed to be very resilient. The reefs survived and no erosion of seagrass meadows was observed (R.K. James, personal communication, 2018). So, if the bays are able to withstand hurricane conditions, it is reasonable that the increased hydrodynamic stresses due to sea-level rise will not affect the ecosystems directly.

Chapter 8

Conclusion and recommendations

In this final chapter, the answers on the research questions are presented and suggestions for further work are given.

8.1 Conclusion

Coastal ecosystems in shallow bays and lagoons around islands in the Caribbean, like Baie de L'Embouchure and Baie Orientale in Saint Martin, are threatened by rising sea-levels due to global climate change. In these bays, coral reefs are present in front of and seagrass meadows within the bays. Coral reefs and seagrass meadows both influence the hydrodynamics in a positive way. Because of this interdependency, the response of one of the ecosystems could affect the other ecosystem and lead to a negative feedback loop. Resulting erosion and coastal retreat could be harmful to the tourist industry and inhabitants of Saint Martin. So, it is important to understand how the typical coastal ecosystems in the Caribbean will respond to global climate change. This resulted in the following research question of this thesis project.

What is the impact of a changing sea-level on the biogeomorphology in Baie Orientale and Baie de L'Embouchure, Saint Martin?

In order to answer this research question and the subquestions, a hydrodynamic model of Baie de L'Embouchure and Baie Orientale has been set up that includes flow, waves and vegetation. The average conditions were modelled and long term changes were investigated. Single extreme events were not considered.

The model results showed a circulating current of 0.2 m/s in both bays with strong flows of 0.5 m/s over the reefs caused by wave breaking and a return current to the ocean through the gullies between the reefs. The circulating pattern is mainly determined by the wave direction. Increasing wave height and wind speed amplify the flow in the bays. Inside Baie de L'Embouchure, a maximum significant wave height of 0.5 m is found. In the exposed areas of Baie Orientale, the maximum significant wave height is 1.2 m, while in the southern, sheltered part, the significant wave height is less than 0.5 m.

Seagrass meadows slow down the currents and they are slightly steered around. Waves are damped by the vegetation. Coral reefs function as submerged breakwater in front of the bays determining the wave height inside the bays. The reef height turned out to determine the wave height, while the increased bottom roughness reduces the flow velocities over the reefs.

The waves are the dominant forcing mechanism of flow in the area. The tide generates no currents inside the bays, while the wind starts a circulation of 0.1 m/s. Offshore, this is opposite. Here, the tide generates an alongshore current of 0.1 m/s, while the wind does not affect this current.

Under sea-level rise, the waves remain the dominant forcing mechanism. As was seen in the current situation, the wave height is determined by the coral reefs and to a lesser extent by the seagrass meadows. A loss of one of them could theoretically lead to a downward spiral. An increased water depth above the reefs lead to different wave conditions which causes a change in seagrass occurrence. In the worst-case scenario, flow velocities increase by more than 100% in Baie de L'Embouchure and by 200% in Baie Orientale under a sea-level rise of 0.87 m. The significant wave height increases by 300% and is doubled in Baie de L'Embouchure.

But even under these circumstances, the increased bed shear stresses do not form a danger to coral reefs and seagrass meadows. At some locations, erosion will occur. According to literature, other consequences of global climate change like rising water temperatures and ocean acidification will affect the coral reefs. Coral bleaching and degradation will lead to less wave dissipation over the reefs resulting in higher waves in the bays and increased currents. The changed hydrodynamics will cause a shift of seagrass occurrence.

Based on the modelling study presented in this report, the long term impact of sea-level rise on the biogeomorphology of Baie de L'Embouchure and Baie Orientale seems to be limited. Shown is that the system is able to mitigate impact of sea-level rise on the hydrodynamics and that the increased hydrodynamics stresses likely will not lead to devastating degradation of coral reefs or total erosion of seagrass meadows. This emphasizes the resilience of the system, which is a very promising conclusion for other Caribbean bays threatened by sea-level rise.

8.2 Recommendations

The conclusions are largely based on the performed modelling study. In this section, some recommendations are done on improving the current model and research method. Also some suggestions are given for further research. Finally, some advice is given about how to preserve the services provided by the shallow coastal water system under the threat of sea-level rise based on the gained insights.

8.2.1 Methodology

Based on the experience with setting up and working with the model, the following suggestions are done in order to improve the model setup and the obtained results.

Depth measurements Combining different bathymetric sources remains tricky and the developed bathymetry should be validated using measurements. Measurements of the reef bathymetry would improve the model, as the wave conditions are mainly determined by the reef height.

Perform a more detailed wave modelling study As the waves were identified as the dominant force in generating the circulation, improving the wave model would be a very good first step in improving the accuracy of the complete model. Wave measurements outside the

reefs could be done in order to validate the existing wave model or the computational domain should be extended such that a wave buoy is captured.

Bed shear stress In order to do a morphological study, the bed shear stress should be computed correctly. This has to be verified first.

8.2.2 Further research

This thesis project is a first step in order to determine the impact of sea-level rise. A lot more research is needed to cover all the unknowns and uncertainties that are still there. Therefore, the following recommendations are done that should be done as follow up of this project.

Extend to morphodynamic model Including sediment transport will give more insight in the sediment concentrations in the area, which affect the conditions for seagrasses and corals. By modelling the morphodynamics, erosion and accretion are simulated leading to a more accurate prediction of change in flow velocities, wave height and bed shear stress.

Include seagrass distribution model During this study, the survival of a part of the seagrass meadows was not an option. However, the results showed that the total extinction of seagrass is not likely, but the seagrass occurrence can change due to changed hydrodynamics. By adding a seagrass distribution model, the growth and death of seagrass could be predicted.. This leads to a better insight in how the situation will change under sea-level rise.

Investigate the response of coral reefs This study showed that the coral reefs determine mainly the hydrodynamic conditions in the bays. When the development of coral reefs under changing conditions is better understood, the impact can be determined more accurately.

Model a storm event A storm event can determine the long term development of the morphology or cause severe damage to coral reefs or seagrass meadows. Investigating the resilience of the biogeomorphology of the bays to single storm events will lead to an improved long term prediction of the response to sea-level rise.

8.2.3 Applicability

This research showed that coral reefs and seagrass meadows form a natural coastal protection that could mitigate the impact of sea-level rise. A morphological study is needed to identify the erosion/sedimentation in the bays. But the bays show great first signs of resilience against sea-level rise. This implies the conservation of services as tourism and coastal protection, which are important to the inhabitants of Saint Martin. However, the study also showed the mitigating effect of the ecosystems. Conservation of the ecosystems deserves therefore priority. Monitoring the ecosystems and conditions both locally and offshore and keeping the bays and reefs clean in order to optimize reef and seagrass growth are measures that will pay off. In case of reef degradation, artificial reef structures might be an solution. They have proven to improve coastal protection and form a base for coral restoration (Silva, Mendoza, Mariño-Tapia, Martínez, & Escalante, 2016). Reef conservation and restoration can be a cost effective measure and proved to be cheaper than constructing breakwaters in tropical waters (Ferrario et al., 2014). In order to achieve this, close cooperation between ecologists, engineers and oceanographers is required.

References

Baptist, M. J., Babovic, V., Rodríguez Uthurburu, J., Keijzer, M., Uittenbogaard, R. E., Mynett, A., & Verwey, A. (2007). On inducing equations for vegetation resistance. *Journal of Hydraulic Research*, *45*(4), 435–450. doi: 10.1080/00221686.2009.9521996

Barry, S. C., Frazer, T. K., & Jacoby, C. A. (2013). Production and carbonate dynamics of Halimeda incrassata (Ellis) Lamouroux altered by Thalassia testudinum Banks and Soland ex König. *Journal of Experimental Marine Biology and Ecology*, *444*, 73–80.

Bosboom, J., & Stive, M. J. (2015). *Coastal Dynamics I* (.5 ed.). Delft: Delft Academic Press.

Bradley, K., & Houser, C. (2009). Relative velocity of seagrass blades: Implications for wave attenuation in low-energy environments. *Journal of Geophysical Research*, *114*(F01004). doi: 10.1029/2007JF000951

Central Intelligence Agency. (2018). *The World Factbook: Saint Martin.* Retrieved 2018-02-15, from `https://www.cia.gov/library/publications/the-world-factbook/geos/rn.html`

Church, J., Clark, P., Cazenave, A., Gregory, J., Jevrejeva, S., Levermann, A., ... Unnikrishnan, A. (2013). Sea level change. In *Climate change 2013: The physical science basis. contribution of working group i to the fifth assessment report of the intergovernmental panel on climate change* (pp. 1137–1216). Cambridge, United Kingdom and New York, NY, USA: Cambridge University Press.

Cialone, M. A., & Smith, J. M. (2007). Wave Transformation Modeling with Bottom Friction applied to South East Oahu reefs. *10th International workshop on Wave Hindcasting and Forecasting & Coastal Hazard Assessment*, 1–12.

Codiga, D. L. (2011). *Unified Tidal Analysis and Prediction Using the UTide Matlab Functions* (Tech. Rep.). Narragansett, RI: Graduate School of Oceanography, University of Rhode Island. doi: 10.13140/RG.2.1.3761.2008

Dalrymple, R. A., Kirby, J. T., & Hwang, P. A. (1984). Wave diffraction due to areas of energy dissipation. *Journal of Waterway, Port, Coastal, and Ocean Engineering*, *110*(1), 67-79. doi: 10.1061/(ASCE)0733-950X(1984)110:1(67)

Darwin, C. R. (1842). *The structure and distribution of coral reefs. being the first part of the geology of the voyage of the beagle, under the command of capt. fitzroy, r.n. during the years 1832 to 1836.* London: Smith Elder and Co.

DCNA. (2014). *Coral reefs.* Retrieved 2018-05-01, from `http://www.dcnanature.org/nature/ecosystems/coral-reefs/`

Deltares. (2018a). *Delft3D Flexible Mesh Suite.* Retrieved 2018-02-15, from `https://www.deltares.nl/en/software/delft3d-flexible-mesh-suite/`

Deltares. (2018b). *D-Flow Flexible Mesh User Manual.* Delft.

Deltares. (2018c). *D-Flow Flexible Technical Reference Manual.* Delft.

Deltares. (2018d). *D-Waves Flexible Mesh User Manual.* Delft.

Dijkstra, J. T. (2009, 05). How to Account for Flexible Aquatic Vegetation in Large-Scale Morphodynamic Models. In *Coastal engineering 2008* (pp. 2820–2831).

Duarte, C. M. (1991). Seagrass depth limits. *Aquatic Botany*, *40*(4), 363 - 377. doi: https://

doi.org/10.1016/0304-3770(91)90081-F

Duarte, C. M. (2002). The future of seagrass meadows. *Environmental Conservation*, *29*(2), 192–206. doi: 10.1017/S0376892902000127

Elliff, C. I., & Silva, I. R. (2017). Coral reefs as the first line of defense: Shoreline protection in face of climate change. *Marine Environmental Research*, *127*, 148–154.

Ferrario, F., Beck, M. W., Storlazzi, C. D., Micheli, F., Shepard, C. C., & Airoldi, L. (2014). The effectiveness of coral reefs for coastal hazard risk reduction and adaptation. *Nature Communications*, *5*. doi: 10.1038/ncomms4794

Fonseca, M. S., & Cahalan, J. A. (1992). A preliminary evaluation of wave attenuation by four species of seagrass. *Estuarine, Coastal and Shelf Science*, *35*(6), 565–576.

Google Maps. (2018). *Caribbean.* Retrieved 2018-09-19, from `https://www.google.nl/maps/`

Greve, T. M., & Binzer, T. (2004). Which factors regulate seagrass growth and distribution? In *European seagrasses: an introduction to monitoring and management* (pp. 19–23). M&MS project.

Hoegh-Guldberg, O. (1999). Climate change, coral bleaching and the future of the world's coral reefs. *Marine and Freshwater Research*, *50*(8), 839–866.

Hoegh-Guldberg, O., Mumby, P. J., Hooten, A., Steneck, R., Greenfield, P., Gomez, E., ... Hatziolos, M. E. (2007). Coral Reefs Under Rapid Climate Change and Ocean Acidification. *Science*, *318*(5857), 1737–1743.

Holthuijsen, L. H. (2007). *Waves in Oceanic and Coastal Waters.* New York: Cambridge University Press.

Insitut National de L'Information Geograhique et Forestiere. (2017). *Carte ign - geoportail.* Retrieved 2018-09-19, from `https://www.geoportail.gouv.fr/donnees/carte-ign`

James, R. K. (2015). *Sxm wave measurements.* (Unpublished raw data)

James, R. K. (2016a). *Broad vegetation survey.* (Unpublished raw data)

James, R. K. (2016b). *Grain sizes.* (Unpublished data)

James, R. K. (2018). *Observations cul de sac.* (Unpublished raw data)

James, R. K., & Lynch, A. (2018). *Depth measurements baie de l'embouchure.* (Unpublished raw data)

Jevrejeva, S., Jackson, L. P., Riva, R. E. M., Grinsted, A., & Moore, J. C. (2016). Coastal sea level rise with warming above 2 ÂřC. *Proceedings of the National Academy of Sciences*, *113*(47), 13342–13347. Retrieved from `http://www.pnas.org/lookup/doi/10.1073/pnas.1605312113` doi: 10.1073/pnas.1605312113

Kangwe, J., Semesi, S., Beer, S., Mtolera, M., & Björk, M. (2012). Carbonate Production by Calcareous Algae in a Seagrass-Dominated System : The Example of Chwaka Bay. In *People, nature and research in chwaka bay, zanzibar, tanzania* (pp. 143–156). WIOMSA.

Kjerfve, B. (1981). Tides of the Caribbean Sea. *Journal of Geophysical Research*, *86*, 4243–4247.

Knowlton, N. (2017). *Corals and Coral Reefs.* Smithsonian Institution. Retrieved 2018-05-10, from `http://ocean.si.edu/corals-and-coral-reefs`

Lalli, C. M., & Parsons, T. R. (1997). Chapter 8 - benthic communities. In *Biological oceanography: An introduction (second edition)* (Second Edition ed., p. 196 - 246). Oxford: Butterworth-Heinemann. doi: https://doi.org/10.1016/B978-075063384-0/50064-5

Lawrimore, J. H., Menne, M. J., Gleason, B. E., Williams, C. N., Wuertz, D. B., Vose, R. S., & Rennie, J. (2011). An overview of the Global Historical Climatology Network monthly mean temperature data set, version 3. *Journal of Geophysical Research*, *116*. doi: 10.1029/2011JD016187

Lowe, R. J., Falter, J. L., Monismith, S. G., & Atkinson, M. J. (2009a). A numerical study

of circulation in a coastal reef-lagoon system. *Journal of Geophysical Research*, *114*(C6). doi: 10.1029/2008JC005081

Lowe, R. J., Falter, J. L., Monismith, S. G., & Atkinson, M. J. (2009b). Wave-Driven Circulation of a Coastal Reef-Lagoon System. *Journal of Physical Oceanography*, *39*, 873–893. doi: 10.1175/2008JPO3958.1

Mendez, F. J., & Losada, I. J. (2004). An empirical model to estimate the propagation of random breaking and nonbreaking waves over vegetation fields. *Coastal Engineering*, *51*(2), 103–118. doi: 10.1016/j.coastaleng.2003.11.003

Meteo365. (2018). *Netherlands Antilles Saint Martin Surf.* Retrieved 2018-09-03, from `http://www.surf-forecast.com/regions/Netherlands-Antilles-Saint-Martin`

Meteorological Department Curaçao. (n.d.). *Climate Summary.* Retrieved 2018-02-16, from `http://www.meteo.cw/climate.php?Lang=Eng{&}St=TNCC`

Meteorological Department St. Maarten. (2016). *Climatological Summary 2016.* Meteorological Department St. Maarten.

Meteorological Department St. Maarten. (2017). *Climatological Summary 2017.* Meteorological Department St. Maarten.

Moss, R., Babiker, M., Brinkman, S., Calvo, E., Carter, T., Edmonds, J., ... Zurek, M. (2008). *Towards New Scenarios for Analysis of Emissions, Climate Change, Impacts, and Response Strategies*. Geneva: Intergovernmental Panel on Climate Change.

Navionics. (2018). *Navionics ChartViewer.* Retrieved 2018-04-26, from `https://webapp.navionics.com/`

Nepf, H. M., & Vivoni, E. R. (2000). Flow structure in depth-limited, vegetated flow. *Journal of Geophysical Research*, *105*(C12), 28547–28557. Retrieved from `http://doi.wiley.com/10.1029/2000JC900145` doi: 10.1029/2000JC900145

NWO. (2018). *Stability of Caribbean coastal Ecosystems uNder future Extreme Sea level changes (SCENES).* Retrieved 2018-02-15, from `https://www.nwo.nl/onderzoek-en-resultaten/onderzoeksprojecten/i/77/11877.html`

Ogden, J. C., & Gladfelter, E. (1983). *Coral Reefs, Seagrass Beds and Mangroves: Their Interaction in the Coastal Zones of the Caribbean.* UNESCO.

Paul, M., & Amos, C. L. (2011). Spatial and seasonal variation in wave attenuation over zostera noltii. *Journal of Geophysical Research*, *116*(C8). doi: 10.1029/2010JC006797

Pearson, S. G. (2016). *Predicting Wave-Induced Flooding on Low-Lying Tropical Islands* (Master's thesis, Delft University of Technology). doi: uuid:c3988f4b-99f8-4936-9504-261b32bb0cd1

Quataert, E., Storlazzi, C., van Rooijen, A., Cheriton, O., & van Dongeren, A. (2015, jul). The influence of coral reefs and climate change on wave-driven flooding of tropical coastlines. *Geophysical Research Letters*, *42*(15), 6407–6415. doi: 10.1002/2015GL064861

Réserve Naturelle Nationale de Saint-Martin. (2009). *Cartographie des habitats marins et des biocÃĺnoses benthiques de la rÃĺserve naturelle de saint-martin.* (Map)

Reynolds, P. L., Duffy, E. ., & Knowlton, N. (2017). *Seagrass and Seagrass Beds.* Smithsonian Institution. Retrieved 2018-02-16, from `http://ocean.si.edu/seagrass-and-seagrass-beds`

Roberts, H. H., & Lugo-Fernández, A. (2011). Lagoon circulation. In D. Hopley (Ed.), *Encyclopedia of modern coral reefs: Structure, form and process* (pp. 613–617). Dordrecht: Springer Netherlands.

Saunders, M. I., Albert, S., Roelfsema, C. M., Leon, J. X., Woodroffe, C. D., Phinn, S. R., & Mumby, P. J. (2015, oct). Tectonic subsidence provides insight into possible coral reef

futures under rapid sea-level rise. *Coral Reefs*, *35*(1), 155–167. Retrieved from http://link.springer.com/10.1007/s00338-015-1365-0 doi: 10.1007/s00338-015-1365-0

Saunders, M. I., Leon, J. X., Callaghan, D. P., Roelfsema, C. M., Hamylton, S., Brown, C. J., ... Mumby, P. J. (2014). Interdependency of tropical marine ecosystems in response to climate change. *Nature Climate Change*, *4*(8), 724–729. doi: 10.1038/nclimate2274

Short, F., Carruthers, T., van Tussenbroek, B., & Zieman, J. (2010). *Thalassia testudinum.* International Union for Conservation of Nature and Natural Resources. doi: http://dx.doi.org/10.2305/IUCN.UK.2010-3.RLTS.T173346A6995927.en

Siegle, E., & Costa, M. B. (2017, oct). Nearshore Wave Power Increase on Reef-Shaped Coasts Due to Sea-Level Rise. *Earth's Future*, *5*(10), 1054–1065. doi: 10.1002/2017EF000624

Silva, R., Mendoza, E., Mariño-Tapia, I., Martínez, M. L., & Escalante, E. (2016). An artificial reef improves coastal protection and provides a base for coral recovery. *Journal of Coastal Research*, *75*(sp1), 467–471.

Soulsby, R., Hamm, L., Klopman, G., Myrhaug, D., Simons, R., & Thomas, G. (1993). Wave-current interaction within and outside the bottom boundary layer. *Coastal Engineering*, *21*(1), 41 - 69. doi: https://doi.org/10.1016/0378-3839(93)90045-A

Soulsby, R. L. (1997). *Dynamics of marine sands: a manual for practical applications.* New York, NY: Thomas Telford. doi: 10.1680/doms.25844

Swart, D. H. (1974). *Offshore sediment transport and equilibrium beach profiles* (Unpublished doctoral dissertation). Delft University of Technology.

Unsworth, R. K. F., Collier, C. J., Henderson, G. M., & McKenzie, L. J. (2012). Tropical seagrass meadows modify seawater carbon chemistry: implications for coral reefs impacted by ocean acidification. *Environmental Research Letters*, *7*, 9. doi: 10.1088/1748-9326/7/2/024026

UNWTO. (2016). *Tourism highlights 2016.* doi: 10.18111/9789284418145

Van Berlo, V., James, R., Van Katwijk, M., & Van Der Heide, T. (2016). Competition and facilitation between seagrass and calcifying algae (Halimeda and Penicillus) in the Caribbean coastal ecosystem.

Van Duin, E. H., Blom, G., Los, F. J., Maffione, R., Zimmerman, R., Cerco, C. F., ... Best, E. P. (2001, Feb 01). Modeling underwater light climate in relation to sedimentation, resuspension, water quality and autotrophic growth. *Hydrobiologia*, *444*(1), 25–42. Retrieved from https://doi.org/10.1023/A:1017512614680 doi: 10.1023/A:1017512614680

van Woesik, R., Golbuu, Y., & Roff, G. (2015). Keep up or drown: adjustment of western Pacific coral reefs to sea-level rise in the 21st century. *Royal Society Open Science*, *2*(7), 150181.

VIZ, UNESCO/IOC. (2018). *Sealevel at saint martin island station [sea level station monitoring facility].* Retrieved 2018-05-02, from http://www.ioc-sealevelmonitoring.org/station.php?code=stmt

Weatherall, P., Marks, K. M., Jakobsson, M., Schmitt, T., Tani, S., Arndt, J. E., ... Wigley, R. (2015, aug). A new digital bathymetric model of the world's oceans. *Earth and Space Science*, *2*(8), 331–345. doi: 10.1002/2015EA000107

Wessel, P., & Smith, W. H. F. (1996). A global, self-consistent, hierarchical, high-resolution shoreline database. *Journal of Geophysical Research*, *101*, 8741–8743.

Zawada, D. G. (2011). Reef topographic complexity. In D. Hopley (Ed.), *Encyclopedia of modern coral reefs: Structure, form and process* (pp. 902–906). Dordrecht: Springer Netherlands. doi: 10.1007/978-90-481-2639-2_141

Appendices

Appendix A

Bathymetry

There is no bathymetric data with sufficient detail from a single source available for the area of interest. Therefore, different sources are used to create a complete and accurate bathymetry. Some additional adaptations are performed to improve the result and interpolation is used to fill the gaps. But in the end, there remain some points of attention regarding the final bathymetry. This all will be discussed in this appendix.

A.1 Data sources

The General Bathymetric Chart of the Oceans (GEBCO) (Weatherall et al., 2015) combined with the coastline retrieved from the Global Shelf-consistent, Hierarchical, High-resolution Geography Database (GSHHG) (Wessel & Smith, 1996) functioned as the base layer. GEBCO has a resolution of 30 arc sec. This resolution is too coarse for the shallow bays surrounding Saint Martin. The Navionics sonar chart provides contour lines with a 0.5 m interval (Navionics, 2018). The contour lines are used to create a more detailed bathymetry of the area surrounding Baie Orientale and Baie de L'Embouchure. The Navionics chart contains no data of Baie de L'Embouchure, but depth measurements are done is this bay (James & Lynch, 2018). For the northern end of Baie Orientale (Cul de Sac) is also no data available in Navionics. The bathymetry in this area is based on observations of James (2018). These different sources of data are combined to come up with a complete bathymetry map, see Figure A.1.

(a) Extent of different sources

(b) Data points of different sources

Figure A.1: Different sources of bathymetry data

A.2 Adaptations

The original data from the different sources is adapted at some points for several reasons. All GEBCO data inside the land boundary is deleted and the cells located outside the land bound-

ary of which the value is larger than zero are also removed. Difference in resolution leads to local mismatches between Navionics data and GEBCO. Therefore are also all GEBCO points inside the extent of the Navionics chart removed in order to prevent difficulties during interpolation.

The coastline retrieved from GSHHG is slightly adapted. After projecting the coastline on a Google satellite image were some points moved and added around the area of interest. In this way, the level of detail is increased.

The depth measurements (James & Lynch, 2018) were not corrected for the tide yet. As said in section 3.3.1, a tidal analysis using UTide (Codiga, 2011) is done. Subtracting the tidal amplitude from the depth measurements gives the final depth with respect to MSL. This is the same reference level as GEBCO (Weatherall et al., 2015).

There was also a mismatch between the Navionics chart and the actual depth in Baie de L'Embouchure and Cul de Sac. This is corrected manually based on aerial photographs and satellite images and interpolating neighbouring cross sections.

A.3 Interpolation

The last step in creating a complete and accurate bathymetry is predicting the missing data points by means of interpolation. Several interpolation methods are available in QGIS of which the results are compared below.

- Cubic spline: the resulting contour lines and bathymetry look very promising at first sight, but there are new maxima/minima created at unrealistic locations.
- Inversed distance weight: gives a lot of small peaks and pits around data points, which is not desired.
- Natural neighbour: results in a smooth bathymetry that does not create new minima/maxima and the resulting contour lines match.
- Triangulated irregular network: does not give a smooth bathymetry and accurate contour lines.
- Kriging: this statistical interpolation method produces a result which does not pass through the sample points. Because measurements are used, is this not desired.

In the end gave the 'Natural Neighbour method' the most realistic result.

A.4 Final bathymetry map

This resulted in the bathymetry presented in Figure A.2.

Delft3D FM requires a .xyz-file as input for depth samples. So, the interpolated bathymetry is converted into a point layer and subsequently exported as .xyz file. This might cause some differences between the presented bathymetry here and the bathymetry used in the model.

A.5 Points of attention

There remain some points or of attention for this bathymetry. In some areas, especially on the reefs around Caye Verte and ÃÕlet de Pinel, is little data available, see Figure A.1b. One has to be aware that these gaps are filled using interpolation. Another point of attention is a possible difference in reference level. The measurements done by James and Lynch (2018) and GEBCO provide the water depth with respect to MSL. The reference level of the Navionics chart is unknown.

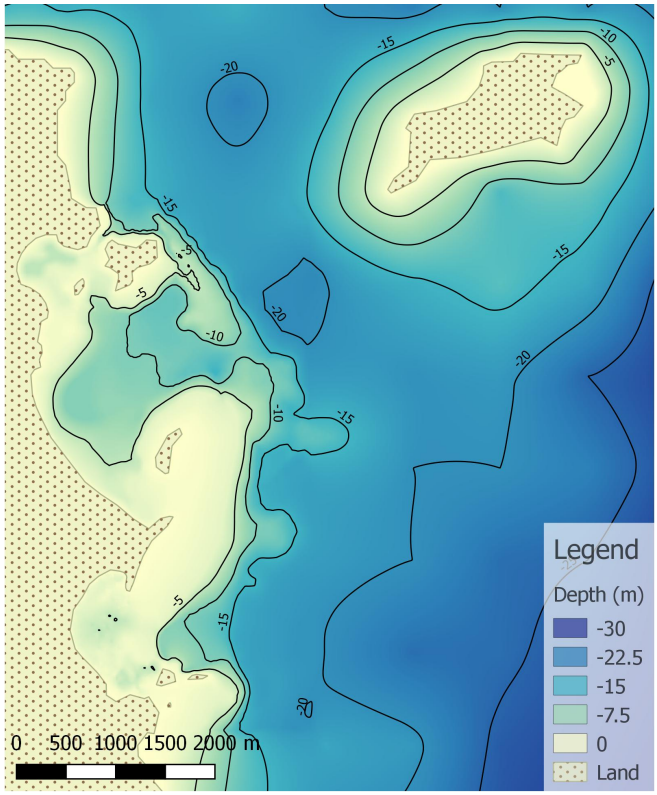

(a) Bathymetry total area of interest

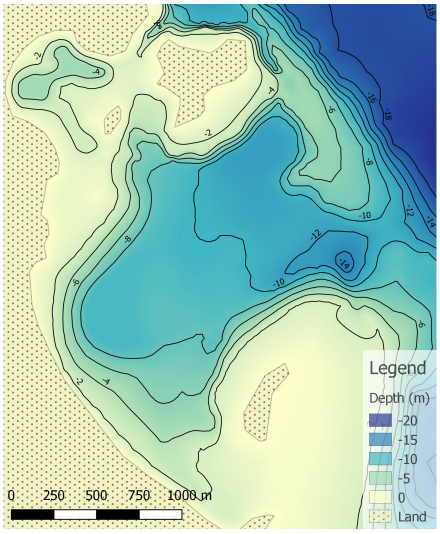

(b) Bathymetry Baie Orientale

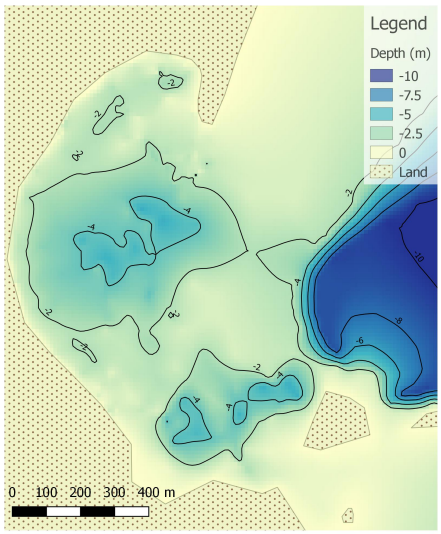

(c) Bathymetry Baie de L'Embouchure

Figure A.2: Final bathymetry

Appendix B

Model description Delft3D FM

This chapter is based on the user manuals and technical reference manuals of D-Flow (Deltares, 2018b, 2018c) and D-Waves (Deltares, 2018d).

B.1 D-Flow

The module D-Flow simulates two- or three-dimensional flow and transport phenomena due to tidal and meteorological forcing. In this thesis is only the two-dimensional depth-averaged situation considered. This is done by solving the shallow water equations (SWE) numerically. The exact equations and how they are solved are described in this section.

Governing equations

The motion of water can be described with the Navier-Stokes equations and the continuity equation. The Navier-Stokes equations are derived from the momentum balance (eqs. (B.1) to (B.3)). The change in momentum is determined by the advective transport and the acting pressure, viscous and body forces.

$$\frac{\partial u_x}{\partial t} + u_x\frac{\partial u_x}{\partial x} + u_y\frac{\partial u_x}{\partial y} + u_z\frac{\partial u_x}{\partial z} = -\frac{1}{\rho}\frac{\partial p}{\partial x} + \nu\left(\frac{\partial^2 u_x}{\partial x^2} + \frac{\partial^2 u_x}{\partial y^2} + \frac{\partial^2 u_z}{\partial z^2}\right) + f_x \tag{B.1}$$

$$\frac{\partial u_y}{\partial t} + u_x\frac{\partial u_y}{\partial x} + u_y\frac{\partial u_y}{\partial y} + u_z\frac{\partial u_y}{\partial z} = -\frac{1}{\rho}\frac{\partial p}{\partial y} + \nu\left(\frac{\partial^2 u_y}{\partial x^2} + \frac{\partial^2 u_y}{\partial y^2} + \frac{\partial^2 u_y}{\partial z^2}\right) + f_y \tag{B.2}$$

$$\frac{\partial u_z}{\partial t} + u_x\frac{\partial u_z}{\partial x} + u_y\frac{\partial u_z}{\partial y} + u_z\frac{\partial u_z}{\partial z} = -\frac{1}{\rho}\frac{\partial p}{\partial z} + \nu\left(\frac{\partial^2 u_z}{\partial x^2} + \frac{\partial^2 u_z}{\partial y^2} + \frac{\partial^2 u_z}{\partial z^2}\right) - g + f_z \tag{B.3}$$

Where u is the flow velocity, p is the pressure, ρ denotes the density, ν is the kinematic viscosity, g is the gravitational constant and f represents the Coriolis force.

The continuity equation (for an incompressible fluid) follows from the mass balance, eq. (B.4).

$$\frac{\partial u_x}{\partial x} + \frac{\partial u_y}{\partial y} + \frac{\partial u_z}{\partial z} = 0 \tag{B.4}$$

In the two-dimensional depth-averaged approach and using some assumptions, the Navier-Stokes equations can be reduced to the two-dimensional SWE. The vertical accelerations are neglected, which reduces the vertical momentum equation to the hydrostatic pressure balance (eq. (B.5)).

$$\frac{\partial p}{\partial z} = -\rho g \tag{B.5}$$

When the density difference with respect to the density is so small ($\Delta\rho << \rho$) that it does not affect the horizontal momentum, a constant density can be assumed. This is the so-called Boussinesq approximation. Furthermore, Reynolds averaging is applied.

The resulting set of equations are the SWE consisting of the depth-averaged continuity equation (eq. (B.6)) and the horizontal momentum equations (eqs. (B.7) and (B.8)) (Holthuijsen, 2007).

$$\frac{\partial \zeta}{\partial t} + \frac{\partial h\bar{u}_x}{\partial x} + \frac{\partial h\bar{u}_y}{\partial y} = 0 \tag{B.6}$$

$$\frac{\partial \overline{u_x}}{\partial t} + \overline{u_x}\frac{\partial \overline{u_x}}{\partial x} + \overline{u_y}\frac{\partial \overline{u_x}}{\partial y} = \frac{F_x}{\rho h} \tag{B.7}$$

$$\frac{\partial \overline{u_y}}{\partial t} + \overline{u_x}\frac{\partial \overline{u_y}}{\partial x} + \overline{u_y}\frac{\partial \overline{u_y}}{\partial y} = \frac{F_y}{\rho h} \tag{B.8}$$

$$\tag{B.9}$$

where F denotes the forcing due to pressure gradients, wind stress, bottom friction, Coriolis, wave-induced forces and more.

The only unknowns are the water level ζ and the velocities u and v which are solved numerically.

Boundary conditions

Water level boundary

At the seaward boundary is a water level boundary condition imposed. This boundary condition is used to represent the tidal forcing. The water level boundary is formulated as the sum of the tidal constituents, see Eq. B.10.

$$\zeta = \sum_{j=1}^{N} \hat{\zeta}_j cos(\omega_j t - \phi_j) \tag{B.10}$$

where ζ is the water level elevation [m], $\hat{\zeta}$ the tidal amplitude of constituent j [m], ω the angular frequency of constituent j[rad/s] and ϕ the phase of component j [rad].

Neumann boundaries

For the northern and southern lateral boundary are Neumann boundaries imposed. Neumann boundaries define the water level gradient perpendicular to the open boundary, so in this case the cross-shore water level gradient. This allows a discharge through the boundary and the water level to move freely along the boundary. The formulation of the Neumann boundary is presented in Eq. B.11.

$$\frac{\partial \zeta}{\partial x} = \sum_{j=1}^{N} k_j \hat{\zeta}_j cos(\omega_j t - (\phi_j + \frac{\pi}{2})) \tag{B.11}$$

where $\hat{\zeta}_j$ is the tidal amplitude of constituent j [m], k_j the wave number of constituent j [-] $= \frac{2\pi}{L}$, ω the angular frequency of constituent j [rad/s] and ϕ the phase of component j [rad].

B.2 D-Waves

D-Waves is the wave module of Delft3D FM. This module can be used to simulate the evolution of short-crested wind-generated waves, which is done by the use of SWAN. SWAN (Simulating WAves Nearshore) is a model developed by the Delft University of Technology. In this section are the equations and numerics of D-Waves shortly discussed.

In SWAN is the evolution of the wave spectrum described by the spectral action balance (eq. (B.12)). Wave action N is conserved and is defined as $N = \frac{E}{\omega}$.

$$\frac{\partial N}{\partial t} + \frac{\partial c_x N}{\partial x} + \frac{\partial c_y N}{\partial y} + \frac{\partial c_\sigma N}{\partial \sigma} + \frac{\partial c_\theta N}{\partial \theta} = \frac{S}{\sigma} \tag{B.12}$$

The first term describes the change of wave action. The second and third term describe the propagation of wave action in horizontal directions. The fourth term describes frequency shifting due to varying depths and currents. Depth-induced and current-induced refraction is accounted for on the last term on the left-hand side of the equation. The source/sink-term on the right-hand side includes generation by wind S_{in}, non-linear wave-wave interactions S_{nl} and dissipation S_{diss}. Dissipation is caused by white-capping S_{wc}, bottom friction S_{bfr} and surf-breaking S_{surf}.

$$S = S_{in} + S_{nl} + S_{diss} \tag{B.13}$$

$$S_{diss} = S_{wc} + S_{bfr} + S_{surf} \tag{B.14}$$

$$S_{wc} = -\mu k E \tag{B.15}$$

$$S_{bfr} = -\frac{C_{bfr}}{g}\left[\frac{\sigma}{\sinh kd}\right]^2 E u_{rms,bottom} \tag{B.16}$$

$$S_{surf} = -\frac{1}{4}\alpha_{BJ}\rho g f_0 H_{br}^2 E/m_0 \tag{B.17}$$

Coupling with D-Flow

In order to include the effect of waves on the flow, the wave-induced forced is added to the horizontal momentum equations. The wave-induced force is defined as the radiation stress tensor, see eqs. (B.18) and (B.19). These radiation stresses are computed by SWAN and written to the communication file.

$$F_x = -\frac{\partial S_{xx}}{\partial x} - \frac{\partial S_{xy}}{y} \tag{B.18}$$

$$F_y = -\frac{\partial S_{yy}}{\partial y} - \frac{\partial S_{yx}}{x} \tag{B.19}$$

As explained in Chapter 2, the water particles beneath a surface wave follow an orbital motion. But due to small differences in velocity below the crest and through of a wave, the particles move in the same direction as the wave propagates. This is called Stokes drift U^s. The wave model computes the mass flux due to the wave M, see eqs. (B.20) and (B.21), and writes it to the communication file. D-Flow calculates the Stokes drift using this mass flux, eqs. (B.22) and (B.23).

$$M_x = \frac{E}{\omega} k_x \tag{B.20}$$

$$M_y = \frac{E}{\omega} k_y \tag{B.21}$$

$$U_x^s = \frac{M_x^s}{\rho_0 h} \tag{B.22}$$

$$U_y^s = \frac{M_y^s}{\rho_0 h} \tag{B.23}$$

Appendix C

Sensitivity analysis

The sensitivity of different physical parameters in the flow, wave and vegetation module are tested by varying the value of that single parameter. The results are presented in this appendix. The value of the parameter as used in further simulations is in bold.

C.1 Flow

Bottom roughness - Manning value n

An increase of the bottom roughness leads to a reduction of flow velocities due to higher bottom resistance. The reduction of bottom roughness to 0.02 $s/m^{1/3}$, as suggested by (Deltares, 2018b), leads to an increase in flow velocity in the order of 10% in both bays. The RMS wave height is unaffected (<1%). Notice that the changes in RMS wave height are caused by changed wave-current interactions. The wave dissipation due to bottom friction is not affected. Increasing the bottom roughness has a similar but opposite effect.

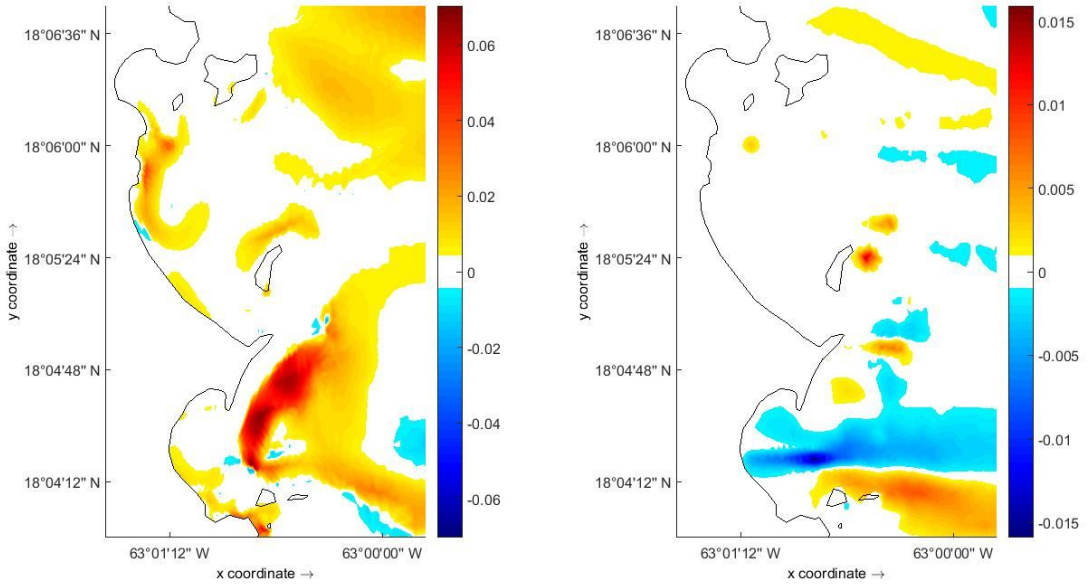

(a) Difference in flow velocity [m/s]

(b) Difference in RMS wave height [m]

Figure C.1: Sensitivity to bottom roughness
($n = 0.02$ $s/m^{1/3}$ - $\boldsymbol{n = 0.023}$ $\boldsymbol{s/m^{1/3}}$)

Reef roughness - Manning value reef n_{reef}

The lower the reef roughness, the stronger the flows over the reefs due to the reduced bottom friction. Due to the reduced reef roughness of 0.05 s/m$^{1/3}$, flows over the reefs increase up to 50%. This also affects the flow in the bays where also change in flow velocity up to 50% is observed. Notice that the changes in RMS wave height are caused by changed wave-current interactions. The wave dissipation due to bottom friction is not affected. This affects the RMS wave height especially in the exposed areas, but the relative change is not bigger than 10%.

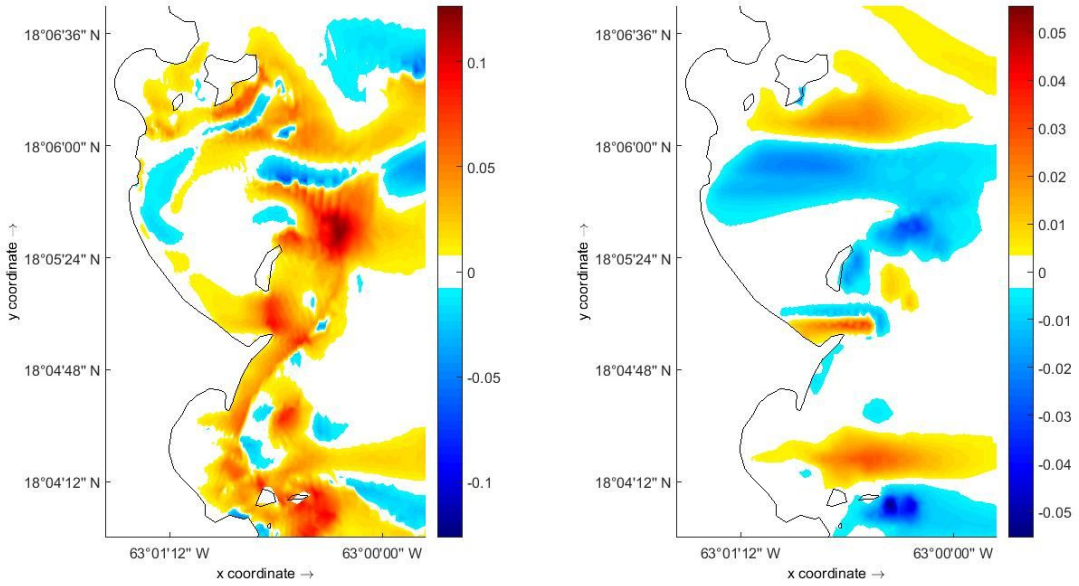

(a) Difference in flow velocity [m/s] (b) Difference in RMS wave height [m]

Figure C.2: Sensitivity to reef roughness ($n_{reef} = 0.05\ s/m^{1/3}$ - $\boldsymbol{n_{reef} = 0.07\ s/m^{1/3}}$)

C.2 Waves

JONSWAP bottom friction coefficient c_b

Increasing the spatially uniform JONSWAP bottom friction coefficient leads to more wave dissipation due to bottom friction. Increasing the uniform JONSWAP bottom friction coefficient to 0.05 m^2/s^3, which corresponds to a reef (Cialone & Smith, 2007), leads to a small reduction in the wave height which is less than 2% and reduced wave-induced currents. The largest differences just South of Caye Verte, but still relatively small, are caused by a numerical error.

Wave breaking parameter γ

The wave breaking parameter is defined as $\gamma = H_m/d$, where H_m is the maximum wave height [m] and d the water depth [m] and is used to include depth-induced breaking in SWAN. Lowering γ to 0.64, as used by Lowe et al. (2009a) in a similar numerical study, leads to a decrease of 10% in the sheltered parts of the bays due to the lower waves that come over the reefs. Subsequently, the flow velocity are also reduced by 10-20%.

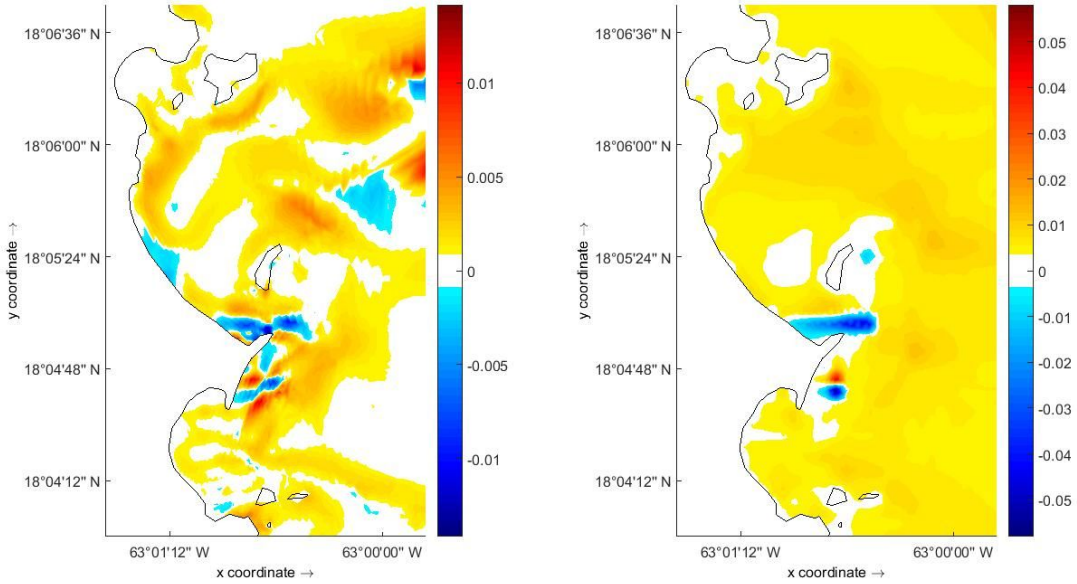

(a) Difference in flow velocity [m/s] (b) Difference in RMS wave height [m]

Figure C.3: Sensitivity to JONSWAP bottom friction coefficient
($\boldsymbol{c_b = 0.038\ m^2/s^3}$ - $c_b = 0.05\ m^2/s^3$)

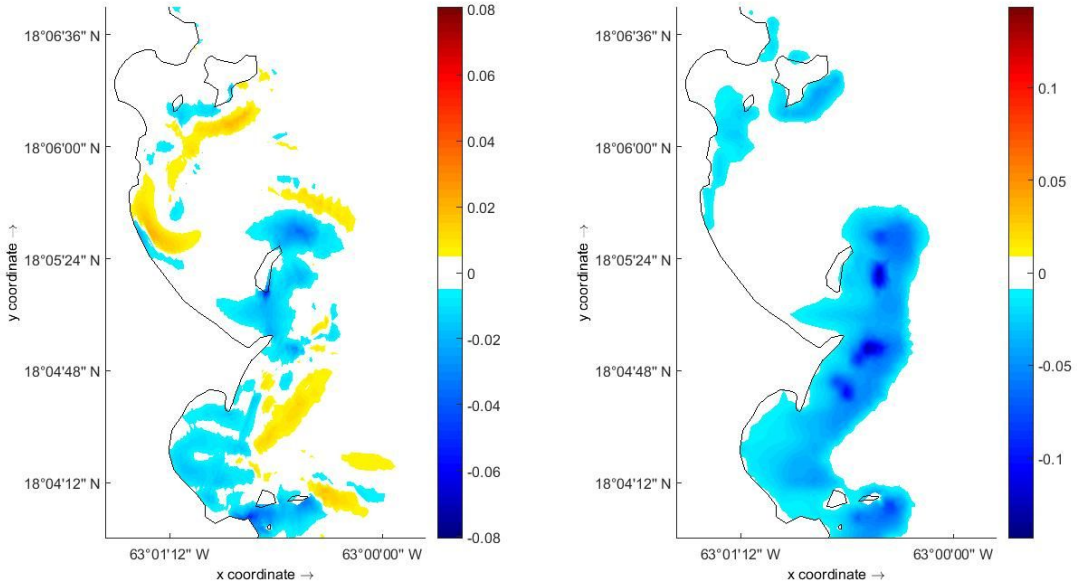

(a) Difference in flow velocity [m/s] (b) Difference in RMS wave height [m]

Figure C.4: Sensitivity to wave breaking parameter
($\gamma = 0.64$ - $\boldsymbol{\gamma = 0.73}$)

C.3 Vegetation

Flow drag coefficient C_D

A lower drag coefficient implies less resistance of the seagrass to the water. So, reducing the flow drag coefficient leads to an increase of flow velocities. Notice that the changes in RMS wave height are caused by changed wave-current interactions. The wave damping due to vegetation is not affected. The decreased drag coefficient of 0.6, which was the default value of Delft3D FM (Deltares, 2018b), leads to reduction of flow velocity up to 10%. The RMS wave height remains unaffected (<1%).

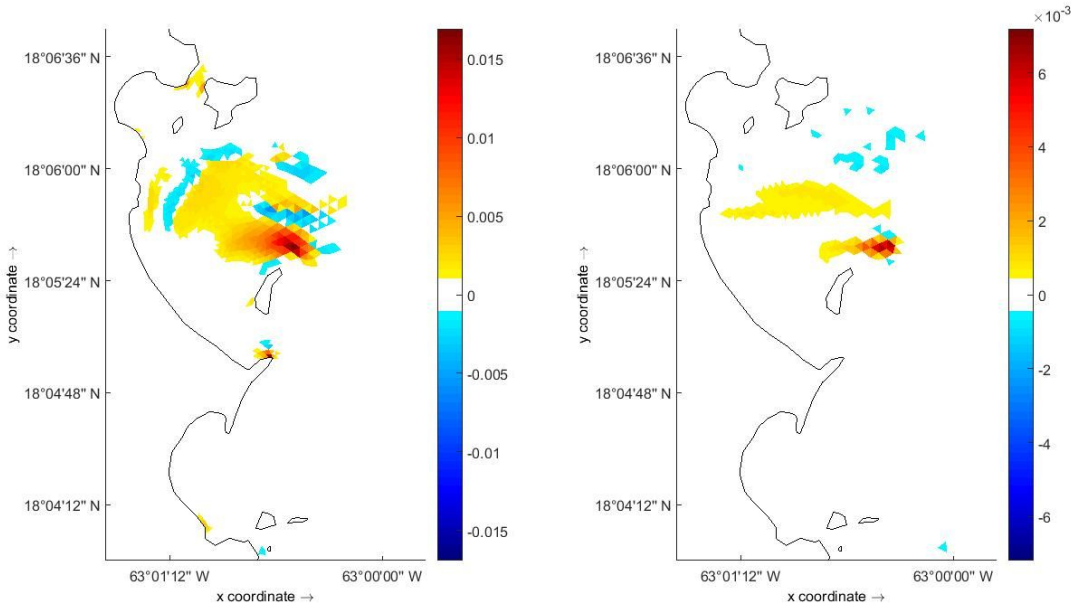

(a) Difference in flow velocity [m/s] (b) Difference in RMS wave height [m]

Figure C.5: Sensitivity to flow drag coefficient
($C_D = 0.6$ - $\boldsymbol{C_D = 1.0}$)

Bulk drag coefficient $\tilde{C}_D$

Increasing the bulk drag coefficient results in more wave damping by the seagrass. Lower wave heights occur and the change in wave height leads to a reduction of wave-induced currents. Doubling the bulk drag coefficient causes the RMS wave height to reduce by 10%.

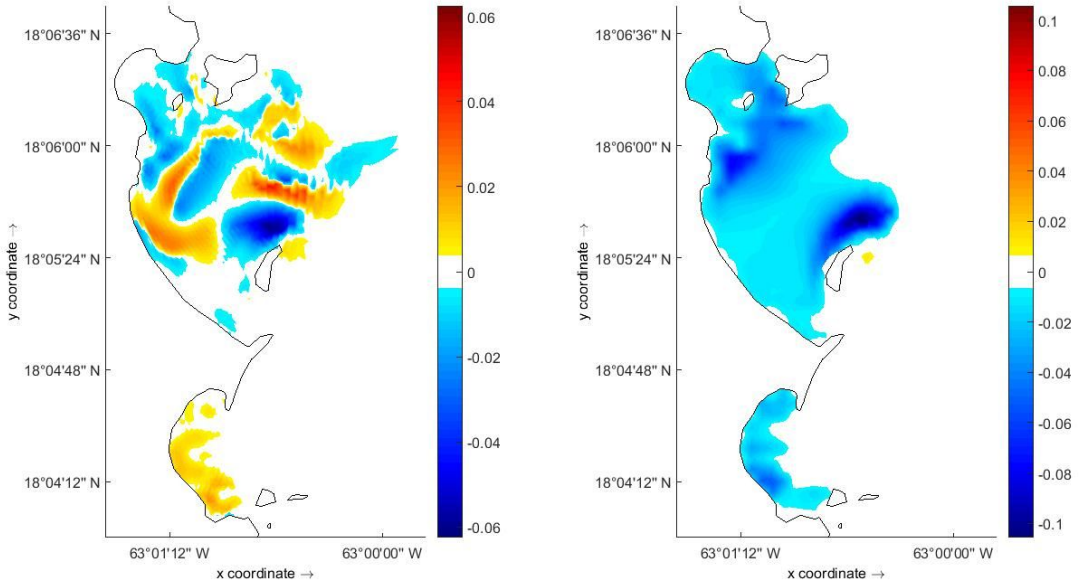

(a) Difference in flow velocity [m/s] (b) Difference in RMS wave height [m]

Figure C.6: Sensitivity to bulk drag coefficient
($\tilde{C}_D = 0.2$ - $\boldsymbol{\tilde{C}_D = 0.1}$)

Seagrass density N_v

A decrease of the density of seagrass meadows leads to less flow and wave attenuation. The changed wave conditions also reduce the wave-induced currents. Decreasing the seagrass density by 25% results locally in an increase in RMS wave height up to 50%. As a consequence, the local flow velocities increase by more than 300%. Remarkable is that increasing the seagrass density by 25% has hardly any effect on the flow and wave conditions (<1%), compared with the decrease of density. Apparently, the maximum flow and wave attenuation is reached for this kind of seagrass in these conditions by a density between 800 and 1000 shoots/m^2.

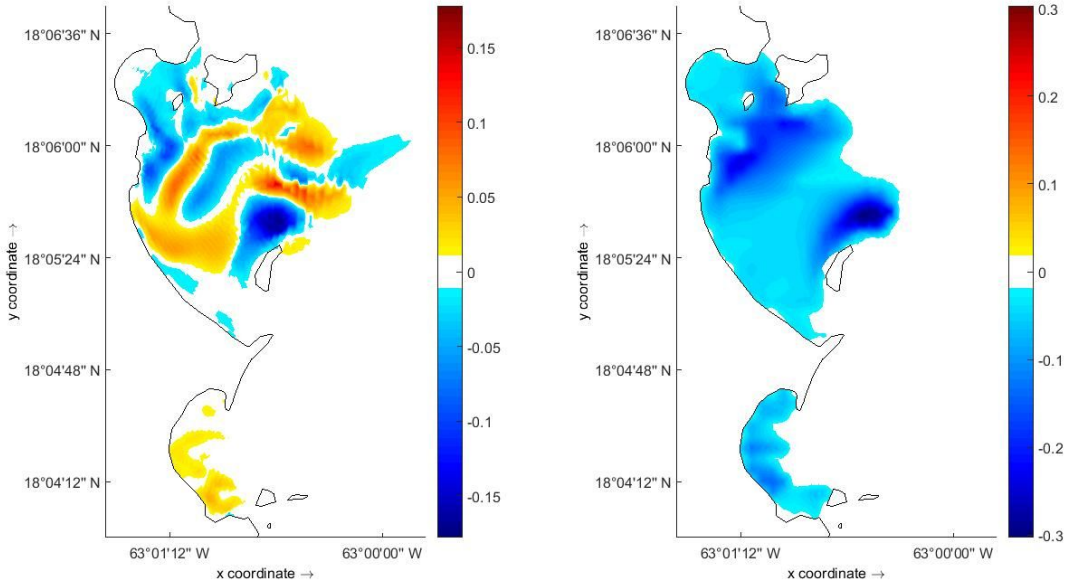

(a) Difference in flow velocity [m/s] (b) Difference in RMS wave height [m]

Figure C.7: Sensitivity to seagrass density
($N_v = 600$ shoots/m^2 - $\boldsymbol{N_v = 800}$ **shoots/**$\boldsymbol{m^2}$)

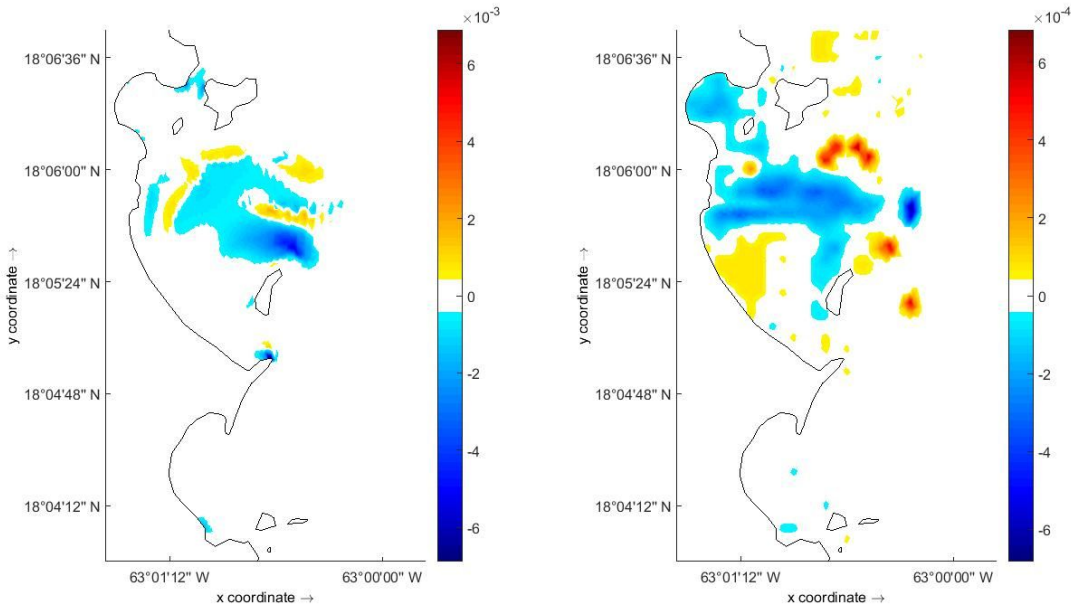

(a) Difference in flow velocity [m/s] (b) Difference in RMS wave height [m]

Figure C.8: Sensitivity to seagrass density
($N_v = 1000$ shoots/m^2 - $\boldsymbol{N_v = 800}$ **shoots/**$\boldsymbol{m^2}$)

Appendix D

Additional modelling results

In this appendix are some additional modelling results shown. Different runs are done in order to explore the flow and wave patterns under different forcing. Varied is with the wind speed and direction and the wave height and direction.

- Wind speed (10 m/s)
- Wind direction - East-northeast
- Wind direction - Southeast
- Significant wave height - 2.5 m
- Wave direction - Northeast
- Wave direction - Southeast

In case of a figure shows the difference in flow velocity or wave height, it is compared with the base run as presented in Chapter 5. This reference run was forced with the tide, a uniform, eastern wind of 5 m/s and swell waves with a significant wave height of 1.5 m also coming from the East.

D.1 Wind

Wind speed - 10 m/s

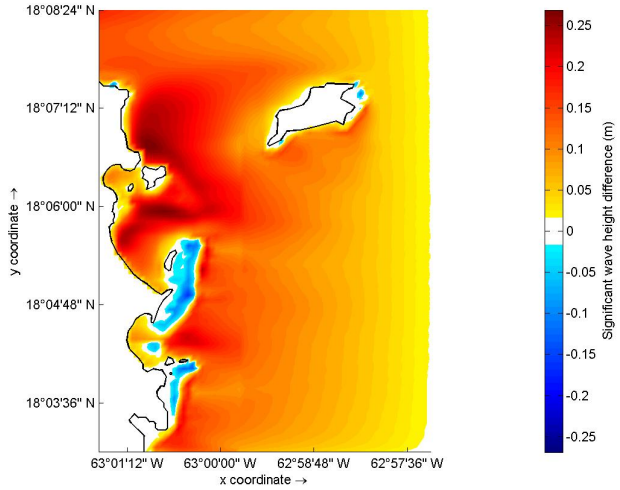

Figure D.1: Change in significant wave height [m] due to increased wind speed

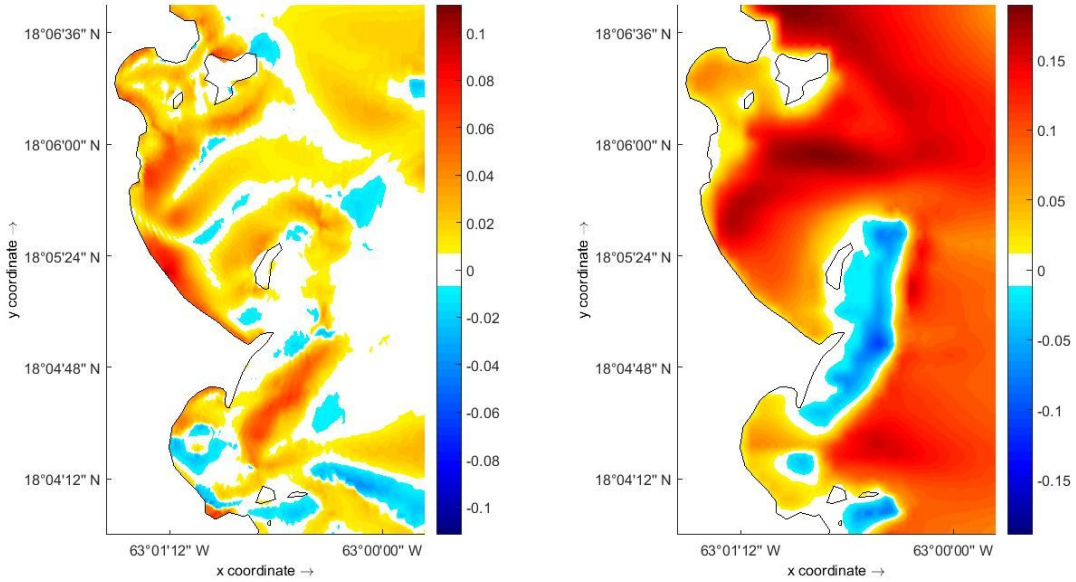

(a) Difference in flow velocity [m/s]

(b) Difference in RMS wave height [m]

Figure D.2: Effect of increased wind speed

Wind directions - ENE, SE

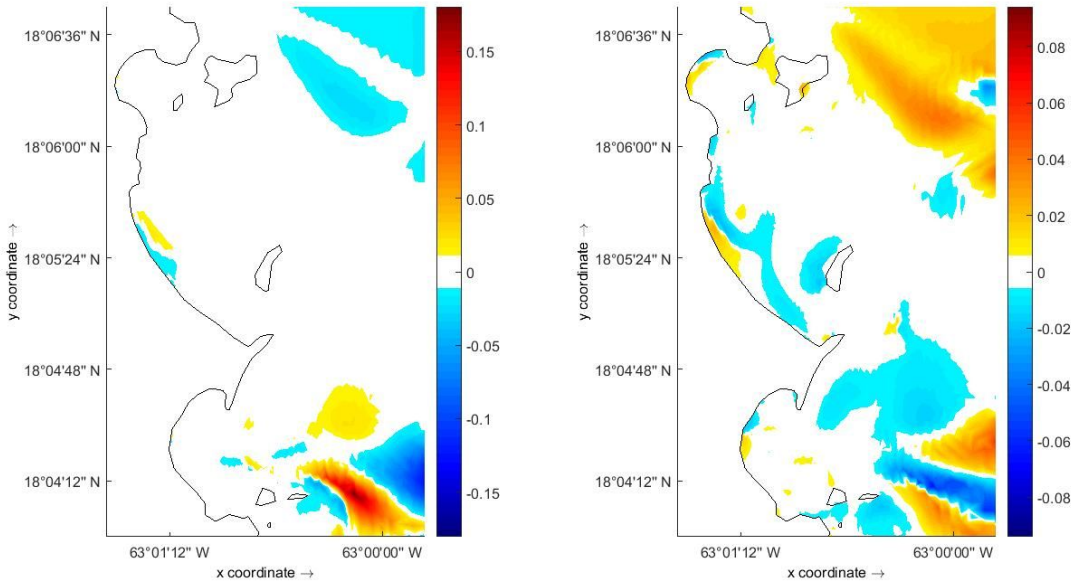

(a) East-northeast (b) Southeast

Figure D.3: Difference in flow velocity [m/s] due to changed wind direction

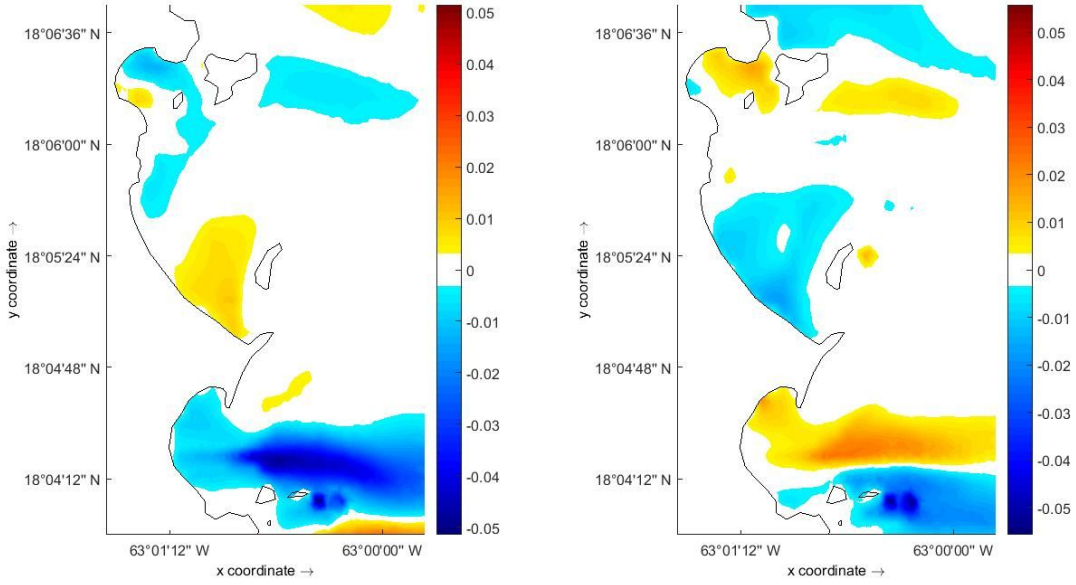

(a) East-northeast (b) Southeast

Figure D.4: Difference in RMS wave height [m] due to changed wind direction

D.2 Waves

Wave height - 2.5 m

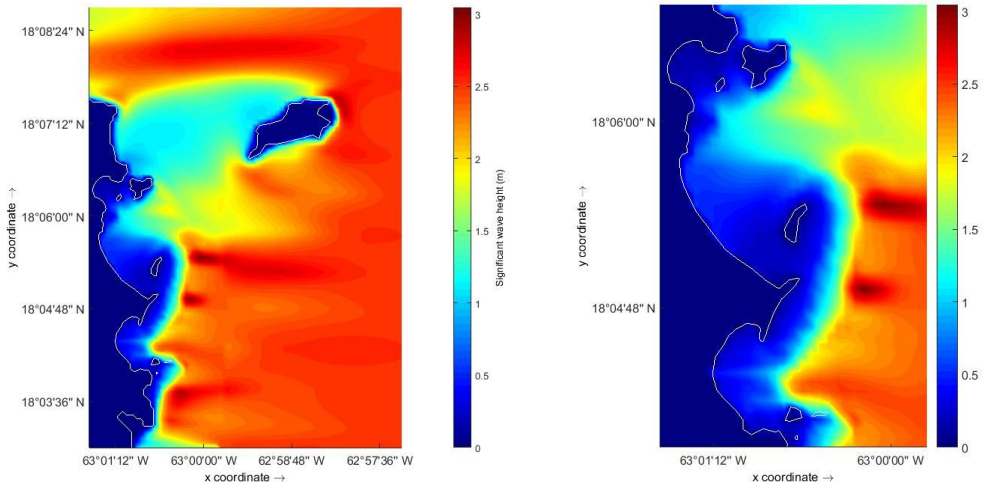

(a) Total area (b) Area of interest

Figure D.5: Significant wave height [m]

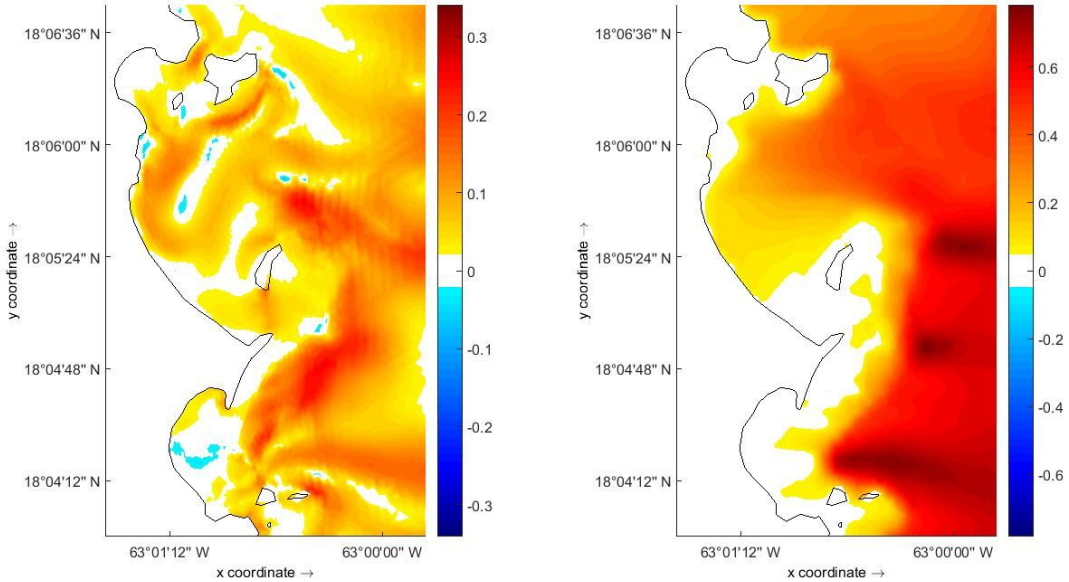

(a) Difference in flow velocity [m/s] (b) Difference in RMS wave height [m]

Figure D.6: Effect of increased wave height

Wave directions - NE, SE

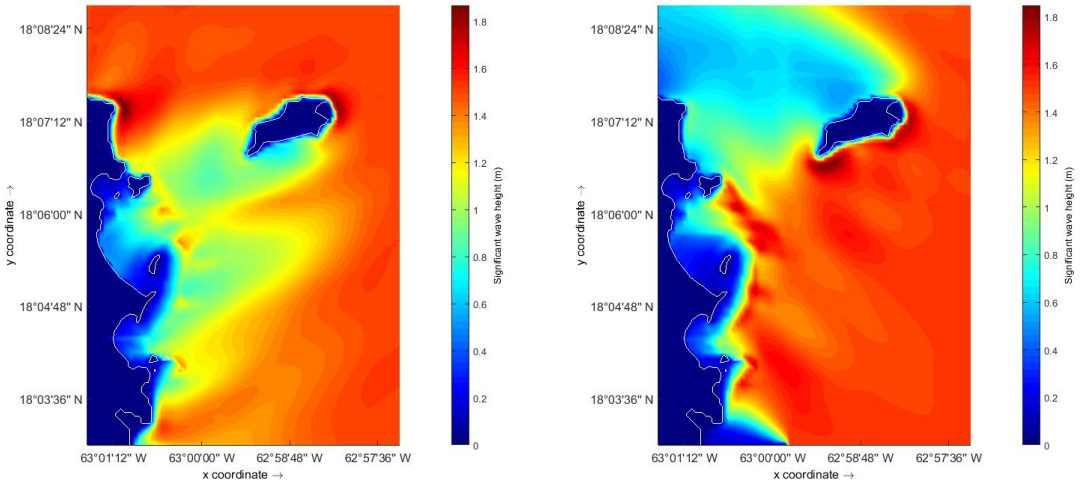

(a) Northeast (b) Southeast

Figure D.7: Significant wave height [m] for different wave directions

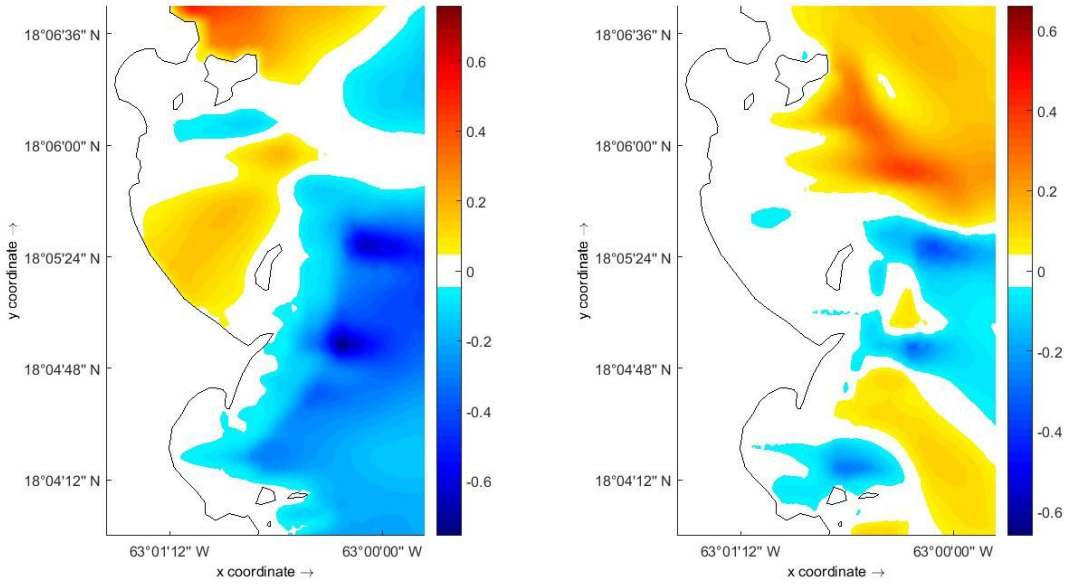

(a) Northeast (b) Southeast

Figure D.8: Difference in RMS wave height [m] due to changed wave direction

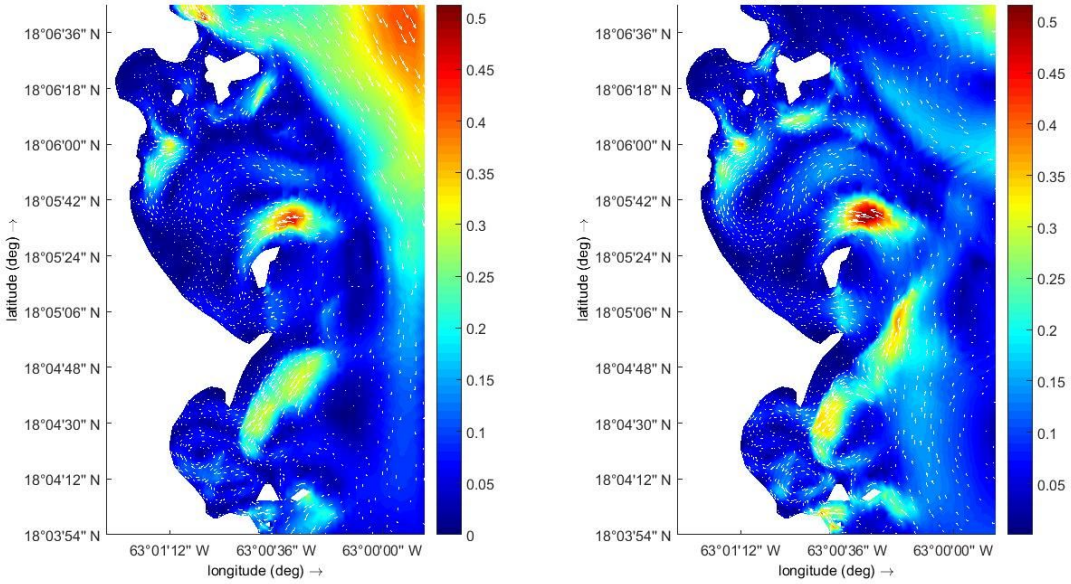

(a) Flow velocity [m/s]

(b) Difference in flow direction compared to base run (red)

Figure D.9: Flow patterns under different wave directions

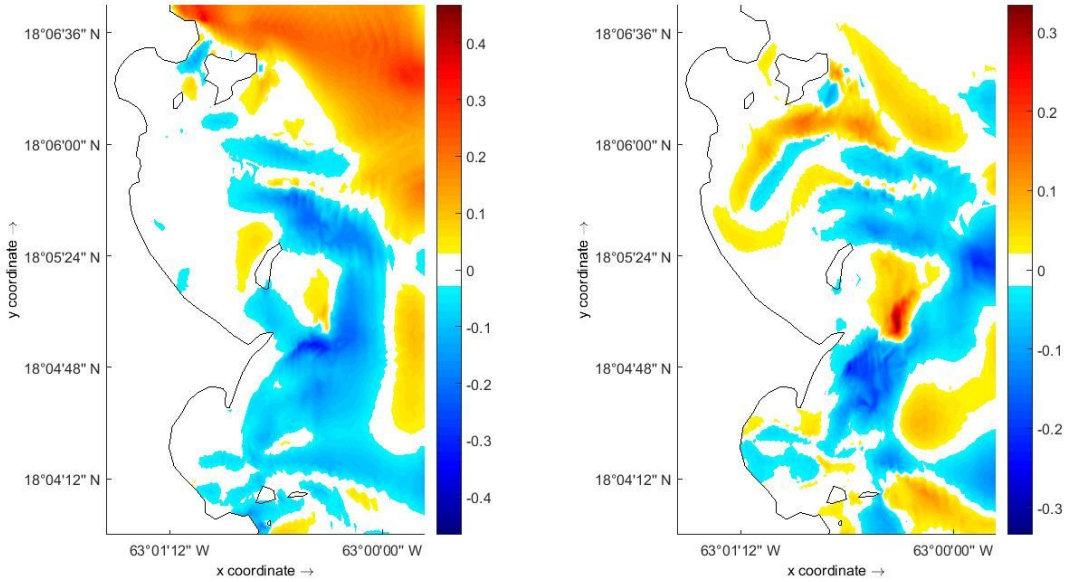

(a) Northeast

(b) Southeast

Figure D.10: Difference in flow velocity [m/s] due to changed wave direction

Appendix E

Bed shear stress analysis

The bed shear stress is the frictional force per unit area exerted by the waves and currents on the bed (R. L. Soulsby, 1997). As already explained, the bed shear stress is an indicator where erosion might occur and seagrass meadows might be removed. Before the bed shear stress is used to predict the response of seagrass meadows and potential erosion, it is analysed carefully in this appendix.

The total bed shear stress is determined by the current- and wave-induced bed shear stress and a non-linear factor. Those components and the total bed shear stress are computed using the formulas described in Section 2.3 and compared with the model output.

E.1 Validation model-calculated bed shear stress

First, a scenario is taken were waves and seagrass are excluded. As there is no wave component, and thus no non-linear factor, the total bed shear stress should equal the current-induced bed shear stress. In Figure E.1, the bed shear stress due to wind- and tide-induced currents is shown. The model output corresponds to the hand calculated current-induced be shear stress.

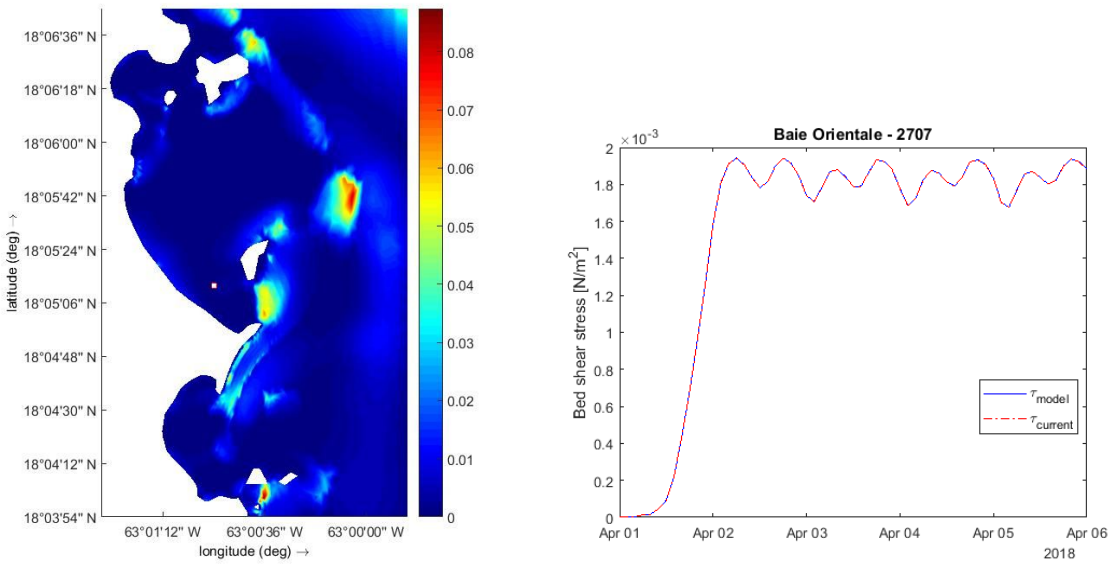

(a) Model output

(b) Comparison with hand calculations

Figure E.1: Current-induced bed shear stress due to wind and tide only. Seagrass excluded

Next, the seagrass is included but the waves are still excluded. According to the theory, a reduction of the bed shear stress is expected due to the presence of seagrass. Looking at the results in Figure E.2, the bed shear stress indeed reduced and the model output corresponds with the hand calculations. However, the reduction is caused solely by a lower depth-average velocity, because the Chézy coefficients are exactly the same. But according to the user manual of D-Flow FM (Deltares, 2018b), the formula 4.1 should be used leading to a reduced bed shear stress.

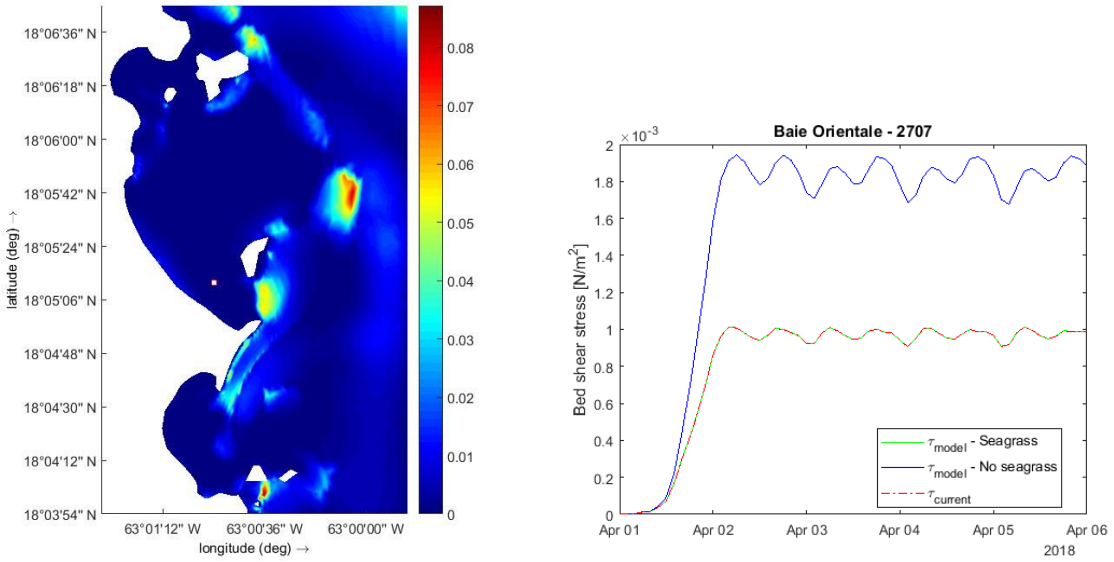

(a) Model output

(b) Comparison with hand calculations

Figure E.2: Current-induced bed shear stress due to wind and tide only. Seagrass included

Now, the waves are included and the seagrass is excluded again. So, the total bed shear stress is determined by all three components. The results are shown in Figure E.3. Extremely high bed shear stresses are observed above the reefs, which could be caused by the local high reef roughness and increased velocities due to wave-breaking. But also behind the reefs, the difference between the model output and hand calculations is about a factor of 10. As is shown before, the current-induced bed shear stress is computed correctly in the case without seagrass. So, the error should be caused by the wave component of the bed shear stress or the non-linear factor.

So, based on the previous presented results, it is not expected that the modelled bed shear stress is useful, as both seagrass and waves are an important part of the model. This is also confirmed by looking at the results of a simulation including waves and seagrass in Figure E.4. However, another error shows up. If the seagrass is included again, the bed shear stress is equal to the hand-calculated current-induced bed shear stress. As we have seen, this is incorrect because of two reasons, the wave component and non-linear factor are not taken into account and the wrong bottom roughness is used.

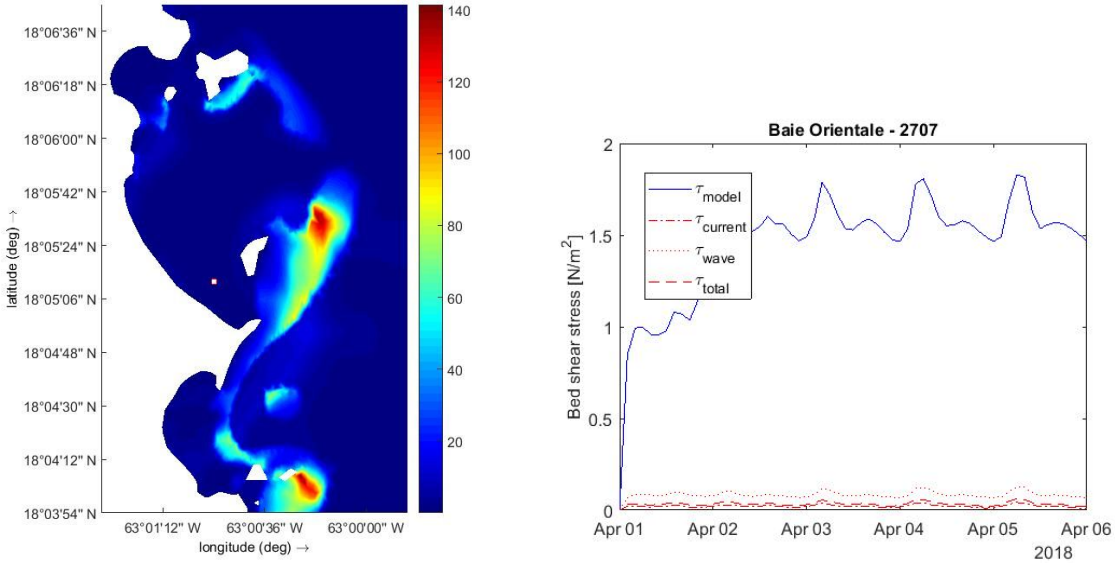

(a) Model output (b) Comparison with hand calculations

Figure E.3: Total bed shear stress. Seagrass excluded

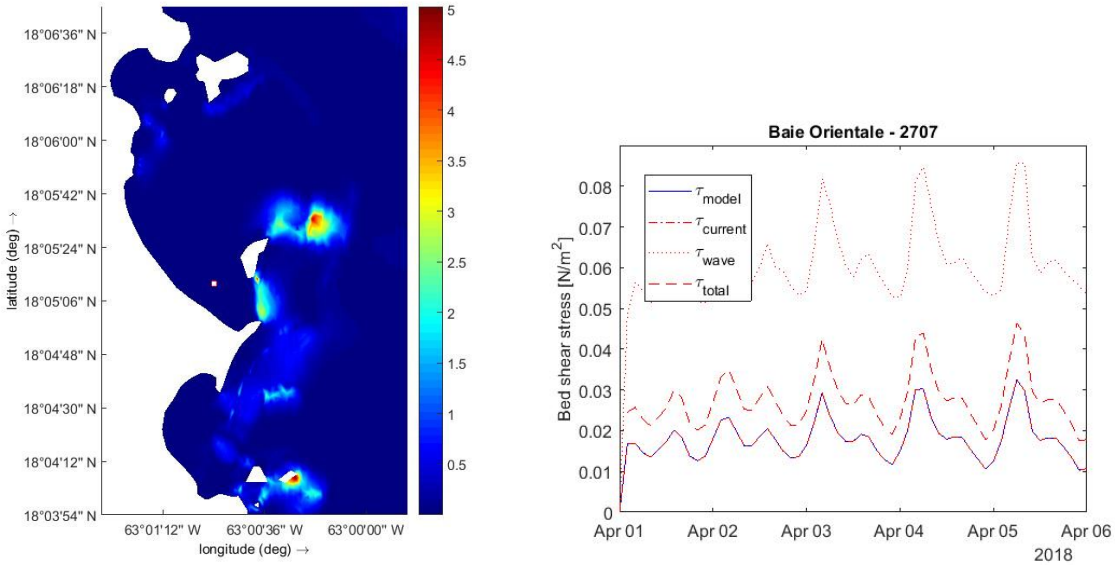

(a) Model output (b) Comparison with hand calculations

Figure E.4: Total bed shear stress. Seagrass is included

E.2 Applicability modelled bed shear stress

In the previous section is shown that the modelled bed shear stress is not reliable. In which case the bed shear stress is correct, is summarized in the table below.

Table E.1: Validation modelled bed shear stress

	No seagrass	Seagrass
Currents only	Correct	Invalid
Waves & currents	Invalid	Invalid

However, in order to say something about the impact of the changed hydrodynamics on the ecosystems, an indication of the change in bed shear stress is desired. Looking at the hand calculation of the situation including waves and seagrass (Figure E.4b), the total bed shear stress is about 1.5 times as large as the current-induced bed shear stress. But the reduction due to the presence of vegetation is not taken into account in the hand calculations. So, the actual bed shear stress will be lower than the hand-calculated bed shear stress. Therefore, it is assumed that the current-induced bed shear stress gives a good indication of the actual bed shear stress. But this is only true inside the bays, where the wave action is limited and seagrass is present.

Appendix F

Statistical analysis of relation between waves, depth and seagrass occurrence

Created by P.M.J. Herman based on supplied data from this study

Appendix: Statistical analysis of relation between waves, depth and seagrass occurrence

Read data

Data have been prepared as two .csv file with x and y coordinates. The first file gives the present situation, and contains presence/absence of seagrass coded as 1, resp. 0, significant wave heigth, water depth, ratio of wave height over water depth, and type of substrate.The second file gives future scenario predictions for wave height and water depth. Both files were merged, and only points that have 'sediment' as substrate type were used in subsequent analyses.

Basic data plots

Spatial plots of the data allow inspecting the relation of wave intensity and depth with seagrass presence/absence.

Fig. 1 indicates that in a number of points, in particular in the NE corner of the bay, high waves correlate with absence of seagrass. However, there are also points where waves are relatively small while seagrass is absent. This is the case along the western coast of the bay. One should take into account that the wave height in this part is high in comparison with the limited water depth, thus potentially still leading to high wave impact on the bottom. This is a reason to consider the interaction between wave height and depth in the statistical model.

Fig. 2 illustrates the relation between depth and seagrass occurrence. Very deep sites (around 10m) tend to have no seagrass, and the same is true for many shallow sites. The probability of seagrass to occur seems to increase with depth up to approximately 6-8 m, but to decrease again afterwards. This is a reason to include a nonlinear (quadratic) expression in the statistical model, while the absence in shallow areas may be explained rather by interaction between wave height and depth.

Based on the basic plots, we propose as a statistical model for seagrass occurrence a logistic regression on depth, depth squared and depth:wave interaction.

Logistic regression

The basic logistic regression using depth, depth squared and the interaction term wave*depth as independent variables, was compared to a number of alternative models including, e.g., also independent contributions from wave and wave squared. However, based on the AIC criterion, the basic model proved to be the best. All terms in this model are significant ($p<0.05$), with the interaction term being least significant.

```
glmnow1<-glm(sg~dep+wave:dep+I(dep^2),sg,family=binomial(link="logit"))
summary(glmnow1)
```

```
##
## Call:
## glm(formula = sg ~ dep + wave:dep + I(dep^2), family = binomial(link = "logit"),
##     data = sg)
##
## Deviance Residuals:
##     Min       1Q   Median       3Q      Max
## -1.9787  -0.8831   0.5335   0.8257   1.9024
##
## Coefficients:
##             Estimate Std. Error z value Pr(>|z|)
## (Intercept) -2.11197    0.42927  -4.920 8.66e-07 ***
```

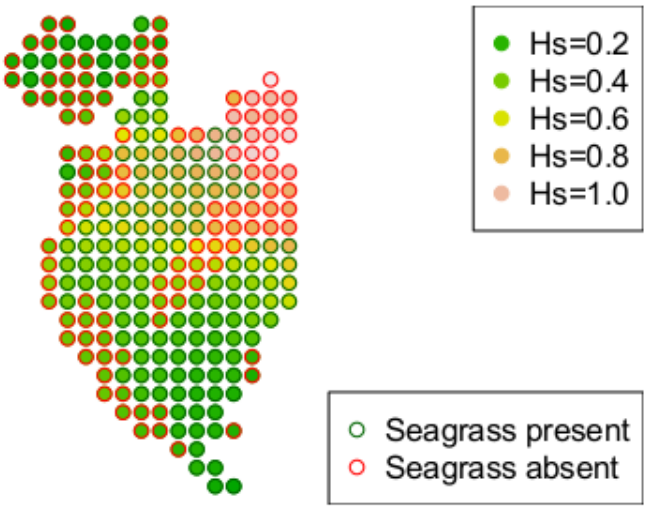

Figure 1: Spatial map of significant wave height Hs (m). Red circles around the points indicate seagrass absence, green circles indicate presence

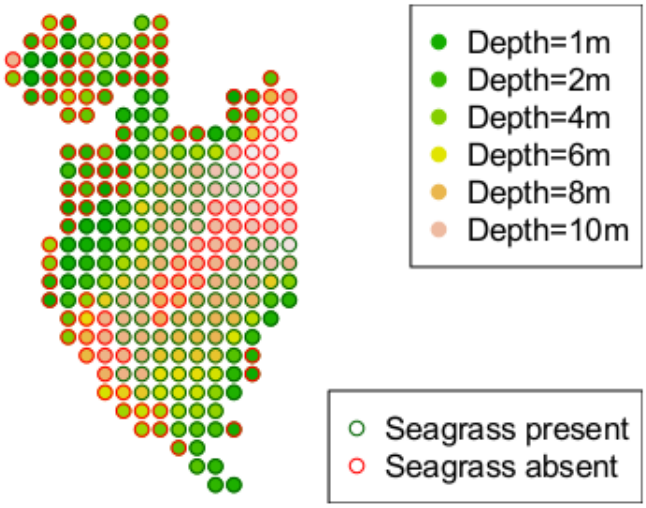

Figure 2: Spatial map of water depth (m). Red circles around the points indicate seagrass absence, green circles indicate presence

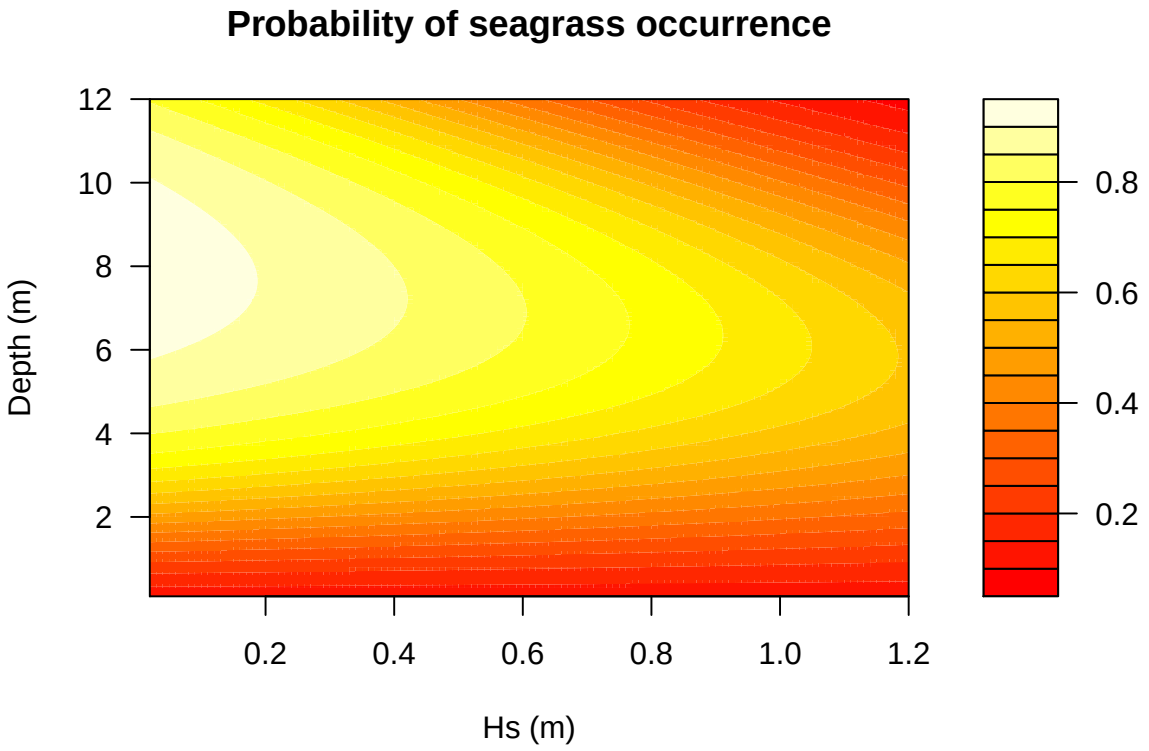

Figure 3: Response landscape of probability of seagrass occurrence versus depth (m) and significant wave height (m). This landscape illustrates the results of the fitted logistic regression model.

```
## dep          1.17758    0.19725   5.970 2.37e-09 ***
## I(dep^2)    -0.07376    0.02071  -3.561 0.000369 ***
## dep:wave    -0.26669    0.12795  -2.084 0.037127 *
## ---
## Signif. codes:  0 '***' 0.001 '**' 0.01 '*' 0.05 '.' 0.1 ' ' 1
##
## (Dispersion parameter for binomial family taken to be 1)
##
##     Null deviance: 341.80  on 248  degrees of freedom
## Residual deviance: 280.35  on 245  degrees of freedom
## AIC: 288.35
##
## Number of Fisher Scoring iterations: 4
```

The response curve, as a function of wave height and depth, is plotted as a filled contour plot in Fig. 3. It shows how both independent variables affect the probability of occurrence of seagrass in the bay.

Based on this statistical model, we compute predicted values for all points in the present situation in 4. The colour coding in this graph illustrates the probability, calculated from the logistic regression model, to find seagrass at the location. It can be seen from this figure that the prediction captures the main patterns in the data, except for the central deep gully in the bay, where presence is predicted but no seagrass occurs. It is unclear what other factors may explain this pattern.

Fig. 5 shows the consequences of future changes for seagrass presence. In the scenario run, water height

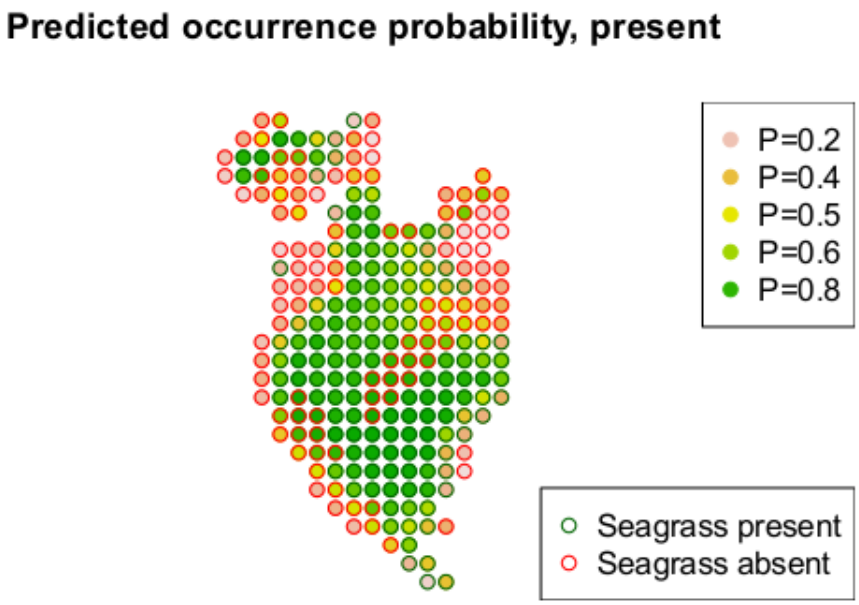

Figure 4: Spatial map of water depth (m). Red circles around the points indicate seagrass absence, green circles indicate presence

is increased due to sea level rise, and the consequences of these changes for the wave climate have been calculated in the simulation model. As a consequence, all points in the bay have a changed depth and wave climate, and the logistic regression model predicts the consequences for the probability that seagrass will occur in these points. It can be seen that the predicted futures spatial distribution of seagrass differs from the present distribution.

These differences are highlighted in Fig. 6. Seagrass is lost in the seaward, deeper parts of the bay, but conditions for seagrass occurrence are predicted to improve in the western coastal part of the bay. Rather than a uniform loss or gain of seagrass, a shift in spatial distribution without much change in the overall occurrence is predicted by the model.

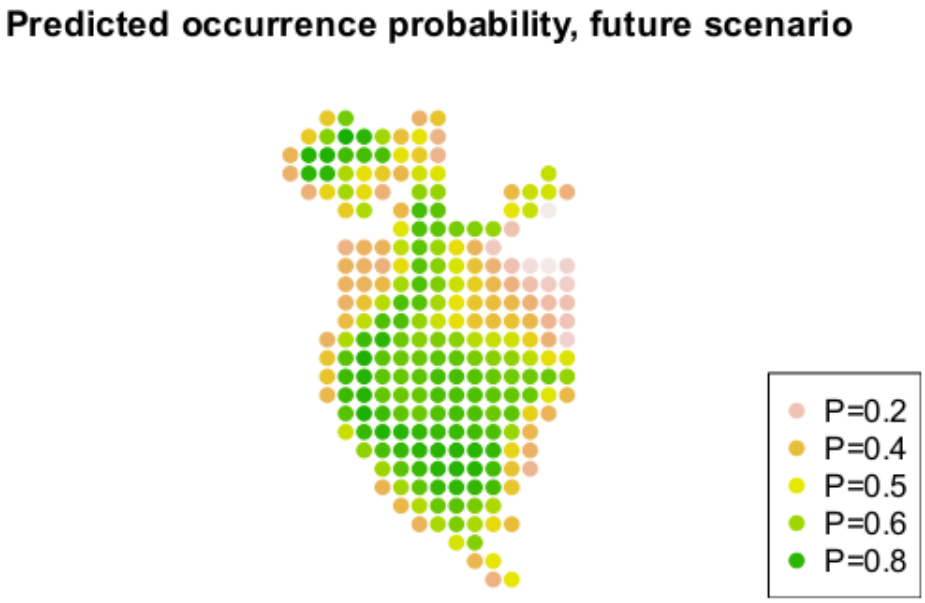

Figure 5: Spatial map of water depth (m). Red circles around the points indicate seagrass absence, green circles indicate presence

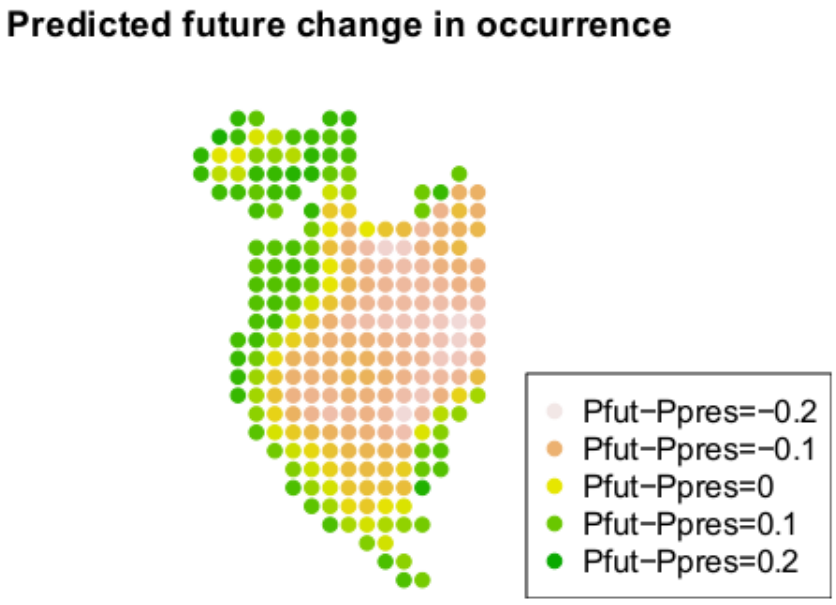

Figure 6: Spatial map of water depth (m). Red circles around the points indicate seagrass absence, green circles indicate presence